UNIVERSITY OF UDINE

Department of Electrical, Management and Mechanical Engineering

PhD in Industrial and Information Engineering

CYCLE XXVIII

PHD THESIS

MODELING AND CONTROL OF FLEXIBLE MECHATRONIC SYSTEMS

Supervisor:

Professor Alessandro Gasparetto

By:

Erfan Shojaei Barjuei

December-2015

MODELING AND CONTROL OF FLEXIBLE MECHATRONIC SYSTEMS

TO ALL WHOM WE LIKE

Acknowledgement

I would like to thank the people at department of electrical, mechanical and managerial engineering of the University of Udine especially my supervisor, Prof. Alessandro Gasparetto, for his help, support and interest in my works.

It is difficult to overstate my gratitude to Dr. Renato Vidoni and Dr. Paolo Boscariol. With their enthusiasm, their inspiration, and their great efforts to explain things clearly and simply, throughout my thesis-writing period, they provided encouragement, sound advice, good teaching, good company, and lots of good ideas. I would have been lost without them.

Lastly, and most importantly, I wish to thank my parents and my brother. They bore me, raised me, supported me, taught me, and loved me. To them I dedicate this thesis.

CONTENTS

Abstract viii

1 Introduction 1

1.1 Introduction 2

1.2 Contribution 8

2 Complaint Manipulator Dynamics 10

2.1 Introduction 11

2.2 Nonlinear Dynamic Model 11

2.2.1 Kinematics 12

2.2.2 Dynamics 14

2.2.3 Linearized Model 16

2.2 Reference Mechanism 17

2.4 Accuracy of the Linearized Model 19

2.5 State Observer 21

3 Linear Quadratic Optimal Control 24

3.1 Introduction 25

3.2 Synthesis of the Optimal Control 25

3.3 Results 28

3.4 Conclusion 30

4 Model Predictive Control 32

4.1 Introduction 33

4.2 General Concept of MPC 33

4.3 Prediction and Control Horizons 34

4.4 Model Prediction and Cost Function 34

4.5 Result of Model Predictive Control with Constraint 36

4.5.1 Effects of fc on the Closed-loop System 36

4.5.2 Effects of H_C and H_P on the Closed-loop System 38

4.6 Robustness 39
4.7 MPC Controller vs. PID Controller 42
4.8 Conclusion 42

5 Robust Control 44
5.1 Introduction 45
5.2 Sensitivity of the Linearized Model 45
5.3 Linear Model Reduction 49
5.4 Synthesis of Robust Controller 53
5.4.1 H_∞ Loop Shaping 53
5.4.2 μ-synthesis 55
5.5 Results 57
5.5.1 Design of H_∞ Loop Shaping Controller 58
5.5.1.2 Response of H_∞ Loop shaping to Disturbance 60
5.5.2 Design of the μ-Synthesis Controller 61
5.5.2.1 Response of the μ-Synthesis to Disturbance 64
5.6 Comparison between Controllers 65
5.6.1 Comparison through μ-analysis 65
5.6.2 Comparison through Frequency Response 66
5.7 Conclusion 67

6 Hybrid Position/Force Control 68
6.1 Introduction 69
6.2 External Force Estimation 69
6.3 Hybrid Position/Force Control 73
6.4 Results 74
6.5 Conclusion 76

7 Linear Quadratic Optimal Control of Cable-Driven Parallel Robots 77
7.1 Cable Robots 77
7.2 Dynamics of the System 78

7.3 Synthesis of the Optimal Controller 80
7.4 Experimental Results 82
7.5 Conclusion 87

8 Conclusion 88

Bibliography 92

Abstract

This thesis deals with modelling and control of flexible mechatronic systems. The flexible mechatronic systems under consideration are a spatial L-shape flexible mechanism and a cable driven parallel robot. Deformation of these mechatronic systems, which contain flexible parts, effect the behaviour of the whole mechatronic system. A finite element model, based on the equivalent rigid link system (ERLS) theory, is used in order to describe accurately the dynamic behaviour of the flexible mechanism. The Feriba-3 which is 3-DOF planar robot for description of cable driven robot is considered as a benchmark.

The model of the flexible mechanism has been validated through the experimental tests in order to apply the linear quadratic (LQ) optimal controller, the constrained model predictive control (MPC), the robust control based on H_∞ loop shaping and μ-Synthesis and the hybrid position/force control for both position control and vibration damping in a spatial flexible L-shape mechanism and to regulate the external force applied to the mechanism as well with taking gravity force into account. In the purpose of applying linear quadratic (LQ) optimal controller on cable-driven parallel robots the kinematic equations of the system are developed.

The synthesis of the controllers, used in this work for both spatial L-shape flexible mechanism and cable driven parallel robot, are described and the most important experimental results are presented and discussed.

CHAPTER 1

Introduction

1.1 Introduction

A mechatronic system usually consist of a precise mechanical system, actuators, sensors and control system. The special software is used for traditional development of individual subsystems and the simulation modelling of the whole system goes several development cycles where the results of individual models from different software are connected with feedback of the system. The behaviour of several mechatronic systems, especially in machine tools [1], robotics [2], application of precision mechanics [3], etc., is affected by deformation of several components and flexible parts [4]. A spatial flexible L-shape mechanism and a cable driven parallel robot are the systems which are investigated in this thesis.

Developing lightweight manipulators leads to improvement of industrial robots performance and operation speed. Given the increase of link elasticity caused by weight reduction, modelling and control of the flexible manipulators become a difficult and complicated issue. Consequently, this research area, especially in the 3D system and their control, is still an open field of investigation [5]–[10].

Flexible link robots have an important role in automated manufacturing systems and industrial robots due to their speed and capabilities. The majority of employed industrial robots work with simple position-controlled manipulators that use joint position feedback to close the control loops. The application of position control is in the tasks where the robot is not constrained by objects in the workspace. Spray painting [11] and pick-and-place [12] tasks are examples of position control in industrial robot applications.

Modelling and control of flexible mechanisms has a variety of applications appearing, from micro-nano flexible devices [13] to medical needle steering [14] and large structures in space [15]. Real-time dynamic simulation is still a challenge for multi-body flexible systems [16], as well as the combination of distributed flexibility with closed kinematic chains. From the control point of view, stabilization with distributed actuators and sensing is still a hot topic, whereas rest-to-rest manoeuvres in finite, assigned time (and no residual vibration), time or energy optimal feedback control, and perfect tracking of output trajectories in case of non-minimum phase input-output characteristics remain all challenging topics, especially in the presence of truly nonlinear dynamics (e.g., for robots with multiple actuated joints and flexible links).

Vibration control of flexible mechanisms as a subset of robot motion control is still an open issue in scientific researches [6]. A mount of work has been carried out in the field of flexible mechanism modelling, analysis, and control since the early 1970s. The consequence of accurate modelling and controlling the vibration phenomenon in the flexible mechanisms is designing and building lighter robot manipulator that is desired criteria in robots performance. For multi-body rigid flexible-link robotic systems, many dynamics models and methods have been proposed so far. Most researchers have concentrated their investigation on the describing of accurate mathematical models both for single body and multi-body system [6], [8], [17], [18].

In multibody dynamics, the classical approach is based on the rigid body dynamical model of the mechanism, then the elastic deformation are introduced to take the flexibility into account. The elastic deformation of the bodies are influenced by the rigid gross motion and vice versa. The resultant complete dynamic formulation is a highly nonlinear and coupled set of partial differential equations.

In modelling flexible link manipulators, the most widely used methods to generate spatially discrete models are the Assumed-Mode Method (AMM), and the Finite Element Method (FEM). The accuracy of the dynamical model derived from the analytical formulation is highly dependent upon the adopted mode shapes of the link deformation and their number.

In the AMM, the shape functions are typically Eigen functions of a closely related simpler problem with standard boundary conditions (BCs). For example, the Euler-Bernoulli beam in one of the following configurations [19]: clamped-free, pinned-free, clamped mass, or pinned-mass. In the FEM, the shape functions, known as interpolation functions, are simple polynomials that verify the continuity conditions between two adjacent elements or nodes. Examples of interpolation functions are Hermite cubics [20], cubic splines [21] and cubic B-splines [22]

The classical approaches applied in flexible multi-body systems deal with mechanisms featuring large displacement and small deformations. Two main technique have been adopted in literature [8], [23]–[27]: the finite element method (nodal approach) and the assumed mode method (modal approach). Rigid body and elastic motion coupling effects have been considered in different works and approaches, firstly by considering only the effect of the rigid body motion on the elastic deformation [23] and then by considering also the effect of the elastic deformation on the rigid body motion [24]. Floating Frame of Reference (FFR) formulation [28]is the consequence

of these works. In the FFR formulation a first set of coordinate expresses the location and orientation of a local reference attached to each link, and a second set describes the deformation of the body with respect to its coordinate system. With this description a system of coupled differential equations is obtained being no separation between the rigid body motion and the elastic deformation of the flexible body. A possible drawback of this approach is that the constraint conditions, i.e. the connection between different deformable bodies, are defined in the global coordinate system: the resulting constraint equations are coupled and do not have an immediate and easy formulation. Moreover, they are usually introduced into the dynamics equations, which depend both on the elastic deformation and on the reference rigid motion of the deformable bodies (e.g. through a vector of Lagrange multipliers).

The problem of control of mechanisms includes on finding an approach to compute the generalized forces that the actuator should apply in the purpose of performing with prescribed accuracy and precision a pre-defined task. This task is very important in modern robotics, where high-speed motion, precision, low power consumption and safety are ever crucial aims. As it should be clear, the design of proper control techniques are even more important for mechanisms with deformable elements (links and/or joints), since their non-minimum phase behaviour [29] and their being in most cases under actuated system [30] make their control issue a challenge if high performance is needed.

In most cases the tasks for mechanical systems are specified in the operative space, i.e. using a set of kinematic quantities (position, velocity, and acceleration) referred to the end-effector of the manipulator. On the other hand, the motion of the mechanisms is implemented using the actuators, which are mounted often on the joints of the mechanisms. The two tasks are completely different, because in the two cases different problems must be surpassed [31]. Hence in the literature the two problems are studied and investigated as control in the operative space and control in the joint space [32].

A control system for flexible systems manipulators should be able to effectively afford with the adverse effects of transient of vibrations and link deflections due to external loads. Both nodal and modal techniques of flexible systems have been applied to design the appropriate control scheme. Generally, the control of flexible link manipulator may be divided in four control objectives [33]:

- End-effector position regulation.
- Rest to rest end-effector motion in fixed time.
- Trajectory tracking in the joint space (tracking of a desired angular trajectory).
- Trajectory tracking in the operational space (tracking of a desired end-effector trajectory).

Many control schemes have been used and adapted to flexible robots from above objectives: Input/output linearization via static state feedback [34], proportional-derivative regulator [35], adaptive control [36], neural network [37], lead-lag controller [38], sliding mode control [39], optimal and robust control [40], optimal trajectory planning [41].

Model Predictive Control (MPC) is a class of computer control algorithms that is based on constructing controllers that are able to adjust the control action before a variation in the occurrence of the output set point. At each control interval the MPC algorithm attempts to optimize future plant performance by computing a sequence of future manipulated variable adjustment. An MPC algorithm can be tuned according to a cost function, constraints on controlled and control variables and to a model of the process to be controlled.

MPC is gaining a lot of usages in different industrial applications, an interesting report about this specific case can be found in [42]. This kind of control has been first employed in large chemical factories, but in recent years has experienced a wider diffusion to other industrial fields. For examples Chen [43] has proposed the application of MPC control in a ball mill grinding process, while Perez in [44] deals with controlling of a rudder roll stabilization control for ships. Other interesting results on MPC control of high-bandwidth systems can be found in [45], [46] and [47]. An experimental validation of MPC as position and vibration control for flexible mechanism is available in [20]. Also several works have proposed the use of Model Predictive Control (MPC) as an effective and suitable solution to the problem of damping vibration in flexible link mechanisms and structure [48]–[50].

Robustness is one of the most important factor in control systems design because of difference between real systems and mathematical models. Modelling of flexible link mechanisms causes difficulty in controlling due to distributed parameters in the plant. The mathematical models have various uncertain parameters, each on affecting the system performance. Moreover, high-level performance as well as robustness of the closed loop system is influenced by the inherent non

minimum phase behaviour of the plant; hence, the importance of synthesis of the robust controller for flexible manipulators is quite evident. As a result, some researchers have developed in recent years in order to design and apply robust controller to flexible link mechanisms and manipulators. For example, Caracciolo introduced a mixed H_2/H_∞ controller for a planar flexible mechanism without taking into account the gravity force effects in [40], robust H_∞ vibration control in [51] and in [52], design of robust controller based on μ-synthesis in [53], [54] and other types of robust controllers such as Lyapunov based [55] and neural network [56]. Lyapunov's second method in [17] and neural networks in [18] are also used to improve the robustness of position control of flexible-link manipulators.

The work in this area is of paramount importance, considering that gravity can be neglected only in space applications and in the limited cases of a planar mechanism moving along a horizontal plane. In all, a spatial flexible-link mechanism can swing in 3D environment in terms of generalized coordinates and elastic displacements such as mechanisms studied in [57], [58]. It is also worth to mention that the majority of works in this area, not only for testing robust controllers, but also other tasks such trajectory planning, [21] and model predictive control[61] have been developed with reference to planar mechanisms, often moving in the horizontal plane, thus without considering gravity.

Moreover, many controllers designed for this class of mechanisms are based on linearized and reduced-order models [40]: in this cases the improved robustness brought by a specifically designed robust control can solve the problem of the additional plant-model mismatch introduced by a linearized model, whose accuracy can be guaranteed only in the neighbourhood of the linearization point [19].

The research on force control of rigid link-manipulators started as early as 1960's but the algorithm was developed over 1970's to 1980's. The approaches systemized are basically divided into hybrid position/force control schemes and impedance control schemes [48], [62]. So far force control of rigid manipulators has been one of the striking research issues, however, the same for flexible manipulators just initiated in 1985 by Fukuda [63]. Chiou and Shahinpoor have mentioned that the link flexibility is the main reason of dynamic instability. They have extended their research from one-link flexible manipulator in planar environment to two-link manipulator through analysing their stability by applying hybrid position/force control approach

[64]. Matsuno and Yamamoto presented a quasi-static hybrid position/force control approach and dynamic hybrid position/force control technique for a planar two-DOF manipulator with flexible second link [65]. For force control of flexible manipulators, the inverse kinematic dynamics is principal, and has been proposed by Svinin and Uchiyama in [66].

So far several force control solutions for flexible link mechanisms have been proposed and for example, Payo introduces a force control approach for a flexible link manipulator based on coupling torque feedback in [67], while a force control for a two link rigid-flexible manipulator using neural network technique has been developed by Borowiec in [68]. Liu in [69] has proposed the use of a feedback an parallel linear compensation, with the re-definition of the output to overcome the non-minimum phase behaviour of flexible manipulators, while a feed forward solution obtained form an inverse dynamic model has been proposed in [12].

Since the majority of investigation of controlling of flexible systems has been done in the plane with neglecting the gravity effect due to dealing with nonlinear terms and inertia coupling between rigid-body motion and vibration phenomena, accurate modelling and controlling of these systems in spatial environment with consideration of gravity effect is still an open issue for studying.

Cable robots are also recognized as a kind of flexible mechatronic systems. In fact, the majority of cables are flexible. A major challenge is the nonlinear behavior of the cables. Cables are usually flexible and have to encounter some unavoidable situations such as elongation because of the cable driven robot character. This flexibility may lead to position and orientation errors. Moreover, the system might be exposed to undesirable disturbances which may lead to vibration, and cause the whole system to be uncontrollable. In recent years, many investigations have been done on cable-driven parallel robots due to their advantages over serial and conventional parallel kinematics. High structural stiffness, payload, good precision, vast workspace and high speed performance are some examples of these benefits; however, low stiffness of the robots due to cable application may decrease the accuracy of motion. On the other hand, optimal linear quadratic regulator (LQR) controller provides all the states of the system for the feedback such as position and velocity. Application of such optimal controller in cable-driven parallel robots can result in more efficient and accurate motion of the system. One of the aim of this thesis is to present an approach to apply optimal linear quadratic regulator (LQR) controller on cable-driven

parallel robots. In this thesis, the kinematic model of the system is briefly explained. In order to employ the classical optimal control theory, the kinematic equations of the system are developed.

The chapter 3 of this thesis is about developing a linear quadratic regulator for a spatial L-shape flexible mechanism. In the chapter 4, a model predictive control (MPC) with constrains is proposed to control the position and minimize the amplitude the mechanical vibration during the motion of a 3D flexible L-shape mechanism. There are some motivating reasons for choosing this controller: first, the prediction ability based on an internal model can be a very effective advantages in fast-dynamic systems. Then MPC is well applicable to MIMO plants, because the outputs are calculated by solving a minimization problem which can take in consideration of several variables. Another remarkable advantages of this control scheme is its competences to perform constrains on both control and controlled variables [70]. The aim of chapter 5 is to design two types of robust controllers based on H_∞ loop shaping and μ-Synthesis for position control and vibration damping for a spatial flexible mechanism to provide a feasible solution that can deal with the uncertainties in the model parameters and nonlinearities imposed by the presence of the gravity force. The main goal of chapter 6 is to present a dynamic hybrid position/force control approach for a spatial flexible L-shape mechanism, with consideration of gravity force into dynamic modelling formulation of the mechanism. Consequently, the main objective is to allow the tip of the mechanism to safety contact objects in an uncertain environment. Finally, the aim of the chapter 7 is to design a linear quadratic optimal controller (LQR) for a planar cable-driven parallel robot. The dynamic model of the system is presented in terms of state space equation form. From control point of view, a classical optimal controller is applied. The defined performance index accounts for the position and velocity of the end effector as well as applied torques by electric motors during the trajectory tracking. In order to minimize the performance index of the controller.

1.2 Contribution

This thesis builds upon and adds to the general body of knowledge surrounding flexible mechatronic systems, focusing on dynamic modelling and control of spatial flexible mechanisms and cable-driven robots. Specifically, this thesis contributes to the following:

- Provides a simulation framework for the development of the linear quadratic regulator optimal controller (LQR) for the flexible link mechanisms in 3D environment.

- Provides a simulation framework for the development of the model predictive controller (MPC) for the flexible link mechanisms in 3D environment.
- Provides a simulation framework for the development of the robust controller based on H_∞ and μ-synthesis for the flexible link mechanisms in 3D environment.

- Provides a simulation framework for the development of the hybrid force/position control for the flexible link mechanisms in 3D environment.

- Provides a simulation framework and an experimental validation for the development of the linear quadratic optimal controller (LQR) for the cable-driven robots.

CHAPTER 2

Complaint Manipulator Dynamics

2.1 Introduction

The high productivity, high-technology system required by the modern mechanical industry need high performance speeds, robust reliability, appropriate performance, light weights and high-precision machinery. In the purpose of obtaining high speed operation and increase efficiency, weights of many components in industrial robots and various machines are reduced. As operating speed grows up and weights of components reduced, a rigid-body model is not suitable anymore. Hence, these components cannot be considered as rigid links, they become flexible. High speed-lightweight link-manipulators can be an example of flexible multibody system.

Accurate modelling of flexible mechanisms is an open issue to investigate, and different approaches have been presented since the 1970s. In this chapter, an approach for modelling of three-dimensional flexible mechanisms is presented, based on an equivalent rigid-link system, based on which elastic deformations are defined and computed. Concepts of three-dimensional kinematics are used in order to define an effective relationship between the rigid body and the elastic motion. The model is based on a compact kinematic formulation and, there is no requirement for customizing the formulation. By using the principle of virtual work, a coupled dynamic formulation is found. An important advantage of this method is that it is not necessary to explicitly formulate the compatibility equations expressing the link connections, because they are included in the matrices of the system dynamics.

2.2 Nonlinear Dynamic Model

One of the most studied topics in flexible multi-body systems is dynamic modelling which is still an open issue to investigate. In comparison with rigid mechanisms, the elastic behaviour of flexible mechanism makes the mathematical formulation of the models, which influence and regulate the real physical behaviour of the system, quite complex.

The approach used here for modelling of the systems with large displacements and small elastic deformation is based on Equivalent Rigid Link System (ERLS) concepts which first was introduced for a planer mechanisms by Giovagnioni in [71], and then expanded to 3D environment by Vidoni in [5], [72] which is briefly explained in this section .

One of the main advantages of the ERLS approach in is that the standard mechanisms definitions and concepts of 3D kinematics could be adopted to formulate and solve the ERLS dynamic model.

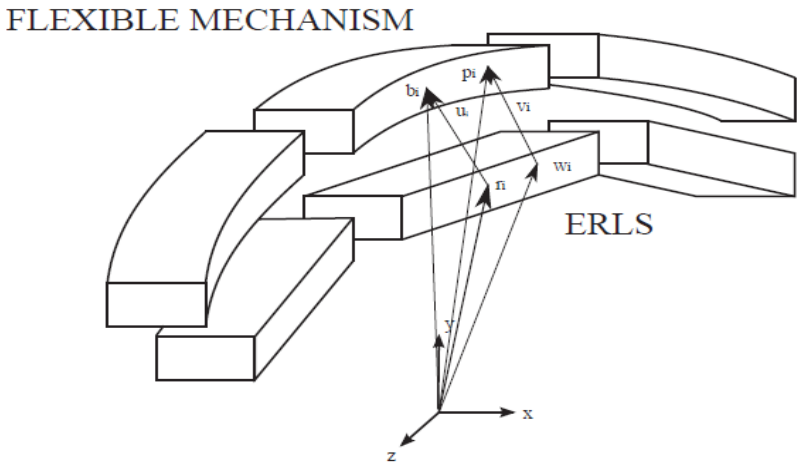

Fig 2.1 Kinematic definition of the ERLS

2.2.1 Kinematics

As shown in Figure 2.1, each flexible link of the mechanism can be divided into finite elements. Being {X, Y, Z} a constant global reference frame, let us consider u_i and r_i as the vector of the nodal elastic displacements of the *i-th* finite element and the vector of nodal position and orientation for the *i-th* element of the ERLS, respectively. Moreover position vector of the generic point of the *i-th* element of the ERLS and its elastic displacement are w_i and v_i respectively. Hence, the absolute nodal position and orientation of the *i-th* finite element b_i with respect to the global reference frame is:

$$b_i = r_i + u_i \tag{2-1}$$

The absolute position p_i of generic point inside the *i*-th finite element is:

$$p_i = w_i + v_i \tag{2-2}$$

For each finite element $\{x_i, y_i, z_i\}$ is the local reference frame that follows the ERLS motion. Given this, it can be defined a block-diagonal global-to-local transformation matrix $T_i(q)$and a

local-to-global transformation matrix $R_i(q)$ can be defined. Therefore it is possible to reform Equation 2-2 as follows:

$$p_i = w_i + R_i(q)N_i(x_i, y_i, z_i)T_i(q)u_i \tag{2-3}$$

Where $N_i(x_i,y_i,z_i)$ is the shape function matrix for the interpolation of the *i-th* finite element defined in local frame, and q is the vector of the generalized coordinates.

It can demonstrated that the expression for the virtual displacement δp_i in the constant reference frame is:

$$\delta p_i = R_i(q)N_i(x_i, y_i, z_i)T_i(q)\delta r_i \delta R_i(q)N_i(x_x, y_x, z_x)T_i(q)u_i + R_i(q)N_i(x_x, y_x, z_x)\delta T_i(q)u_i + R_i(q)N_i(x_x, y_x, z_x)T_i(q)\delta u_i \tag{2-4}$$

Twice differentiating Equation 2-3 leads to the expression of the acceleration of a generic point inside the *i-th* finite element as:

$$\ddot{p}_i = R_i(q)N_i(x_i, y_i, z_i)T_i(q)\ddot{r}_i + R_i(q)N_i(x_i, y_i, z_i)T_i(q)\ddot{u}_i + 2\left(\dot{R}_i(q)N_i(x_i, y_i, z_i)T_i(q) + R_i(q)N_i(x_i, y_i, z_i)\dot{T}_i(q)\right)\dot{u}_i + (\ddot{R}_i(q)N_i(x_i, y_i, z_i)T_i(q) + 2\dot{R}_i(q)N_i(x_i, y_i, z_i)\dot{T}_i(q) + R_i(q)N_i(x_i, y_i, z_i)\ddot{T}_i(q))u_i \tag{2-5}$$

If the kinematic entities of all the finite elements are gathered into one vector, differentiating Equation 2-1 with respect to time leads to:

$$db = du + dr \tag{2-6}$$

The configuration of the ERLS (as well as its velocity and acceleration) basically depends upon on the vector q of the free coordinates. This can be reformulated as:

$$dr = S(q)dq \tag{2-7}$$

S(q) is the matrix of the sensitivity coefficients for all the nodes. Finally, by substituting Equation 2-7 into Equation 2-6 the following equation in matrix form can be obtained:

$$db = \begin{bmatrix} I & S_{in} \\ 0 & S_0 \end{bmatrix} \begin{bmatrix} du_{in} \\ dq \end{bmatrix} \tag{2-8}$$

2.2.2 Dynamics

The dynamic equations of the system can be obtained by applying the principle of virtual works:

$$\delta W^{inertia} + \delta W^{elastic} + \delta W^{external} = 0 \tag{2-9}$$

Which can also be written as:

$$\sum_i \delta u_i^T M_i(\ddot{r}_i + \ddot{u}_i) + 2\sum_i \delta u_i^T (M_{G1i} + M_{G2i)}\, \dot{u}_i + \sum_i \delta u_i^T (M_{C1i} + 2M_{C2i} + M_{C3i)} u_i + \sum_i \delta u_i^T K_i u_i = \sum_i \delta u_i f_{gi} + \delta u^T f \tag{2-10}$$

In which the mass matrix of the *i-th* element is:

$$\int_{vi} T_i^T N_i^T R_i^T R_i N_i T_i\, \rho_i dv = M_i \tag{2-11}$$

The stiffness matrix of the *i-th* element is:

$$\int_{vi} T_i^T\, B_i^T D_i B_i T_i dv = K_i \tag{2-12}$$

The vector of the equivalent nodal loads due to gravity is:

$$\int_{vi} T_i^T N_i^T R_i^T\, \mathrm{g}\, \rho_i dv = f_{gi} \tag{2-13}$$

The Coriolis terms are related to:

$$\int_{vi} T_i^T N_i^T R_i^T \dot{R}_i N_i T_i\, \rho_i dv = M_{G1i} \tag{2-14}$$

$$\int_{vi} T_i^T N_i^T R_i^T R_i N_i \dot{T}_i\, \rho_i dv = M_{G2i} \tag{2-15}$$

The centrifugal stiffness terms are:

$$\int_{vi} T_i^T N_i^T R_i^T \ddot{R}_i\, N_i T_i \rho_i dv = M_{C1i} \tag{2-16}$$

$$\int_{vi} T_i^T N_i^T R_i^T 2\dot{R}_i N_i \dot{T}_i\, \rho_k dv = 2M_{C2i} \tag{2-17}$$

$$\int_{vi} T_i^T N_i^T\, N_i \ddot{T}_i \rho_i dv = M_{C3i} \tag{2-18}$$

Being $\delta\emptyset_i$ the block-diagonal matrix which contains the virtual angular displacement and B_i the strain displacement matrix, the following equations holds:

$$\delta T_i^T = \delta\emptyset_i T_i^T \tag{2-19}$$

Since the virtual nodal elastic displacements δu and virtual displacement of the ERLS δr are independent from each other and taking into account the damping trough Rayleigh model using α and β damping constants, Equation 2-10 can be subdivided in two equations:

$$M(\ddot{r} + \ddot{u}) + 2(M_{G1} + M_{G2})\dot{u} + \alpha M\dot{u} + \beta K\dot{u} + (M_{C1} + 2M_{C2} + M_{C3})u + Ku = f_g + f \quad (2\text{-}20)$$

$$S^T M(\ddot{r} + \ddot{u}) + 2S^T(M_{G1} + M_{G2})\dot{u} + \alpha S^T Mu + S^T(M_{C1} + 2M_{C2} + M_{C3})u = S^T(f_g + f) \quad (2\text{-}21)$$

Dynamic equations, after the substitution of the second order differential equations of the ERLS, can be grouped and rearranged in matrix from after discarding the equations for elastic degrees of freedom that have been zeroed:

$$\begin{bmatrix} M & MS \\ S^T M & S^T MS \end{bmatrix} \begin{bmatrix} \ddot{u} \\ \ddot{q} \end{bmatrix} =$$

$$\begin{bmatrix} -2(M_{G1} + M_{G2}) - \alpha M - \beta K & -\dot{M}S & -(M_{C1} + 2M_{C2} + M_{C3}) - K \\ S^T(-2(M_{G1} + M_{G2}) - \alpha M) & -S^T M\dot{S} & -S^T(M_{C1} + 2M_{C2} + M_{C3}) \end{bmatrix} \begin{bmatrix} \dot{u} \\ \dot{q} \\ u \end{bmatrix} + \begin{bmatrix} M & I \\ S^T M & S^T \end{bmatrix} \begin{bmatrix} g \\ f \end{bmatrix}$$

(2-22)

Then, taking $x = [\dot{u}\ \dot{q}\ u\ q]$ as the augmented state vector, and rearranging the matrices, the system expressing the dynamics of the mechanism can be written also as:

$$\begin{bmatrix} M & MS & 0 & 0 \\ S^T M & S^T MS & 0 & 0 \\ 0 & 0 & I & 0 \\ 0 & 0 & 0 & I \end{bmatrix} \begin{bmatrix} \ddot{u} \\ \ddot{q} \\ \dot{u} \\ \dot{q} \end{bmatrix} =$$

$$\begin{bmatrix} -2M_G - \alpha M - \beta K & -M\dot{S} & -(M_{C1} + 2M_{C2} + M_{C3}) - K & 0 \\ S^T(-2(M_{G1} + M_{G2}) - \alpha M) & -S^T M\dot{S} & -S^T(M_{C1} + 2M_{C2} + M_{C3}) & 0 \\ I & 0 & 0 & 0 \\ 0 & I & 0 & 0 \end{bmatrix} \begin{bmatrix} \dot{u} \\ \dot{q} \\ u \\ q \end{bmatrix} +$$

$$\begin{bmatrix} M & I \\ S^T M & S^T \\ 0 & 0 \\ 0 & 0 \end{bmatrix} \begin{bmatrix} g \\ f \end{bmatrix} \quad (2\text{-}23)$$

The values of acceleration can be computed at each step by solving the Equation 2-22, while the values of velocities and of displacements can be obtained by an appropriate integration scheme (e.g. the Runge-Kutta algorithm) and, hence, the dynamic behaviour of the system can be simulated.

5.5.3 Linearized Model

The dynamic model represented by Equation 2-23 is nonlinear, due to the quadratic relation between the nodal acceleration and the velocities of the free coordinates. Thus it cannot be used to design a linear-model based control. In order to develop a state-space form linearized version of the dynamic system of Equation 2-23 a linearization procedure has been developed. First of all, Equation 2-23 can be written in the following form, by defining a state vector ***x(t)*** and an input vector **v**(t):

$$\boldsymbol{A}(\boldsymbol{x}(t))\dot{\boldsymbol{x}}(t) = \boldsymbol{B}\big(\boldsymbol{x}(t)\big)\boldsymbol{x}(t) + \boldsymbol{C}(\boldsymbol{x}(t))\boldsymbol{v}(t) \tag{2-24}$$

In which matrices ***A***, ***B*** and ***C*** do not depend on ***v(t)***. If $\boldsymbol{x_e}$ is a steady equilibrium point for the system in Equation 2-23, a linearization procedure can be set by applying a Taylor series expansion:

$$\boldsymbol{A}\big(\boldsymbol{x}_e + \Delta\boldsymbol{x}(t)\big)\big(\dot{\boldsymbol{x}}_e + \Delta\dot{\boldsymbol{x}}(t)\big) = \boldsymbol{B}\big(\boldsymbol{x}_e + \Delta\boldsymbol{x}(t)\big)\big(\boldsymbol{x}_e + \Delta\boldsymbol{x}(t)\big) + \boldsymbol{C}\big(\boldsymbol{x}_e + \Delta\boldsymbol{x}(t)\big)\big(\boldsymbol{v}_e + \Delta\boldsymbol{v}(t)\big) \tag{2-25}$$

Since $\boldsymbol{x_e}$(t) is an equilibrium point for the system, the following equation holds:

$$\boldsymbol{B}(\boldsymbol{x}_e)\boldsymbol{x_e} + \boldsymbol{C}_e(\boldsymbol{x}_e)\boldsymbol{v_e} = \boldsymbol{A}(\boldsymbol{x}_e)\dot{\boldsymbol{x}}_e = 0 \tag{2-26}$$

Therefore the system linearized around the equilibrium point can be written as:

$$\boldsymbol{A}(\boldsymbol{x}_e)\Delta\dot{\boldsymbol{x}}(t) = \left[\boldsymbol{B}(\boldsymbol{x}_e) + \left(\left.\frac{\partial \boldsymbol{B}}{\partial \boldsymbol{x}}\right|_{\boldsymbol{x}=\boldsymbol{x}_e} \times \boldsymbol{x}_e\right) + \left(\left.\frac{\partial \boldsymbol{C}}{\partial \boldsymbol{x}}\right|_{\boldsymbol{x}=\boldsymbol{x}_e} \times \boldsymbol{v}_e\right)\right]\Delta\boldsymbol{x}(t) + \boldsymbol{C}(\boldsymbol{x}_e)\Delta\boldsymbol{v}(t) \tag{2-27}$$

The matrices in Equation 2-27 are constant, so we have obtained a linear model in the form:

$$\boldsymbol{A}\Delta\dot{\boldsymbol{x}}(t) = \boldsymbol{B}\Delta\boldsymbol{x}(t) + \boldsymbol{C}\Delta\boldsymbol{v}(t) \tag{2-28}$$

The constant matrices ***A*** and ***B*** can be evaluated as:

$$\boldsymbol{A} = \begin{bmatrix} \boldsymbol{M} & \boldsymbol{MJ} & 0 & 0 \\ \boldsymbol{J}^T\boldsymbol{M} & \boldsymbol{J}^T\boldsymbol{MJ} & 0 & 0 \\ 0 & 0 & \boldsymbol{I} & 0 \\ 0 & 0 & 0 & \boldsymbol{I} \end{bmatrix}_{\boldsymbol{x}=\boldsymbol{x}_e} \tag{2-29}$$

$$\boldsymbol{B} = \begin{bmatrix} -2\boldsymbol{M}_G - \alpha\boldsymbol{M} - \beta\boldsymbol{K} & 0 & -\boldsymbol{K} & \boldsymbol{B}_{14} \\ \boldsymbol{J}^T(-2\boldsymbol{M}_G - \alpha\boldsymbol{M} - \beta\boldsymbol{K}) & 0 & 0 & \boldsymbol{B}_{24} \\ \boldsymbol{I} & 0 & 0 & 0 \\ 0 & \boldsymbol{I} & 0 & 0 \end{bmatrix}_{\boldsymbol{x}=\boldsymbol{x}_e} \tag{2-30}$$

In which:

$$\boldsymbol{B}_{14} = -\frac{\partial \boldsymbol{K}}{\partial \boldsymbol{q}} \times \boldsymbol{u}_e + \frac{\partial \boldsymbol{F}_{\mathrm{g}}}{\partial \boldsymbol{q}} \tag{2-31}$$

$$\boldsymbol{B}_{24} = -\frac{\partial \boldsymbol{J}^T}{\partial \boldsymbol{q}} \times \boldsymbol{F}_g + \boldsymbol{J}^T \times \frac{\partial \boldsymbol{F}_{\mathrm{g}}}{\partial \boldsymbol{q}} \tag{2-32}$$

Matrix $\boldsymbol{C}$ remains unchanged after the linearization process, since it is composed of only zeros and ones. Equation 2-28 can be brought to the most common form of a Linear Time Invariant (LTI) model by using the simple relations $\boldsymbol{F}_{lin} = \boldsymbol{A}^{-1}\boldsymbol{B}$ and $\boldsymbol{G}_{lin} = \boldsymbol{A}^{-1}\boldsymbol{C}$:

$$\begin{cases} \Delta\dot{\boldsymbol{x}}(t) = \boldsymbol{F}_{lin}\Delta\boldsymbol{x}(t) + \boldsymbol{G}_{lin}\boldsymbol{v}(t) \\ \boldsymbol{y}(t) = \boldsymbol{H}_{lin}\boldsymbol{x}(t) + \boldsymbol{D}_{lin}\boldsymbol{v}(\boldsymbol{t}) \end{cases}$$

(2-33)

A comprehensive linearization procedure explanation for a planar flexible mechanism based on ERLS approach is available in [73].

2.3 Reference Mechanism

The mechanism chosen as the basis of the simulations is a flexible L-shape mechanism, made by two steel rods, connected by a rigid aluminium joint (Figure 2.2). The rotational motion of the first link, which is connected to the chassis, can be imposed through a torque-controlled actuator. The whole mechanism can swing in 3D environment and therefore gravity forces affects both the rigid and elastic motion of the mechanism.

Each finite element has 12 degrees of freedom; consequently, whole the mechanism is described with 30 nodal elastic degrees of freedom and one generalized coordinate (angular position q). After assembling 2 links and considering the constraints fixed by the kinematic couplings and neglecting one of the nodal displacements in order to make the system solvable [5]. The resulting flexible link system is described by 24 nodal elastic displacements and one rigid degree of freedom.

The mechanical parameters of the L-shape mechanical components are reported in Table 2.1.

A software program for simulating the dynamics behaviour of a flexible-link has been developed, according to the dynamic model presented in section 2. The structure of the mechanism has been modelled, with four finite elements (Figure 2.3).

Each finite element has 12 degrees of freedom; consequently, whole the mechanism is described with 30 nodal elastic degrees of freedom and one generalized coordinate (angular position q). After assembling 2 links and considering the constraints fixed by the kinematic couplings and neglecting one of the nodal displacements in order to make the system solvable [5]. The resulting flexible link system is described by 24 nodal elastic displacements and one rigid degree of freedom.

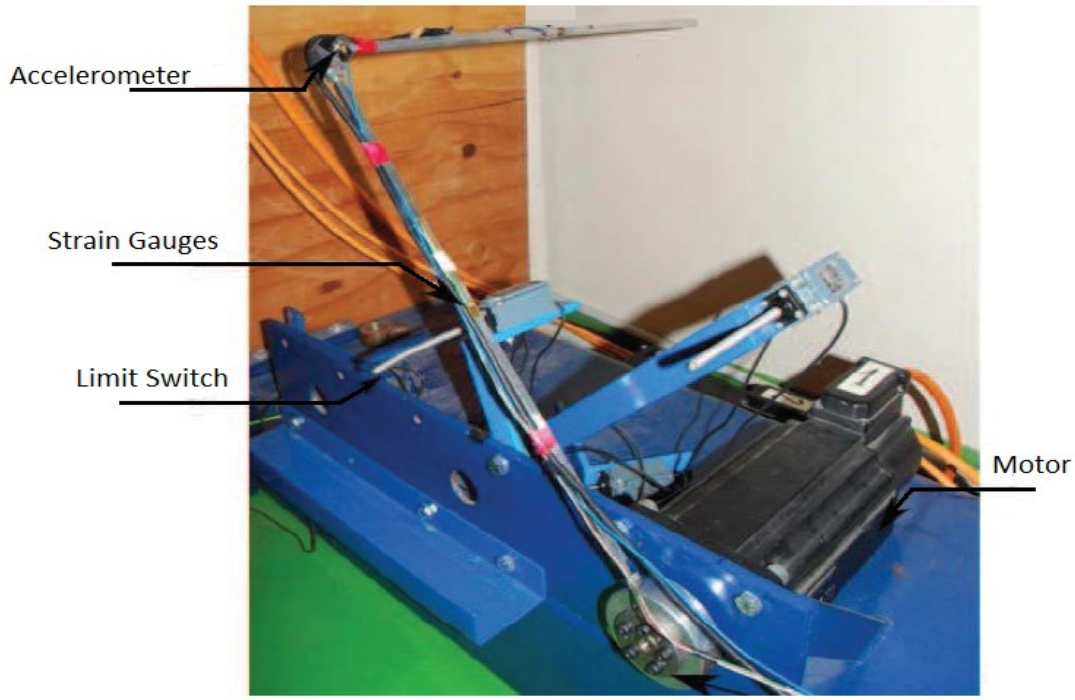

Fig 2.2: The mechanism built in the laboratory for experimental validation of the model

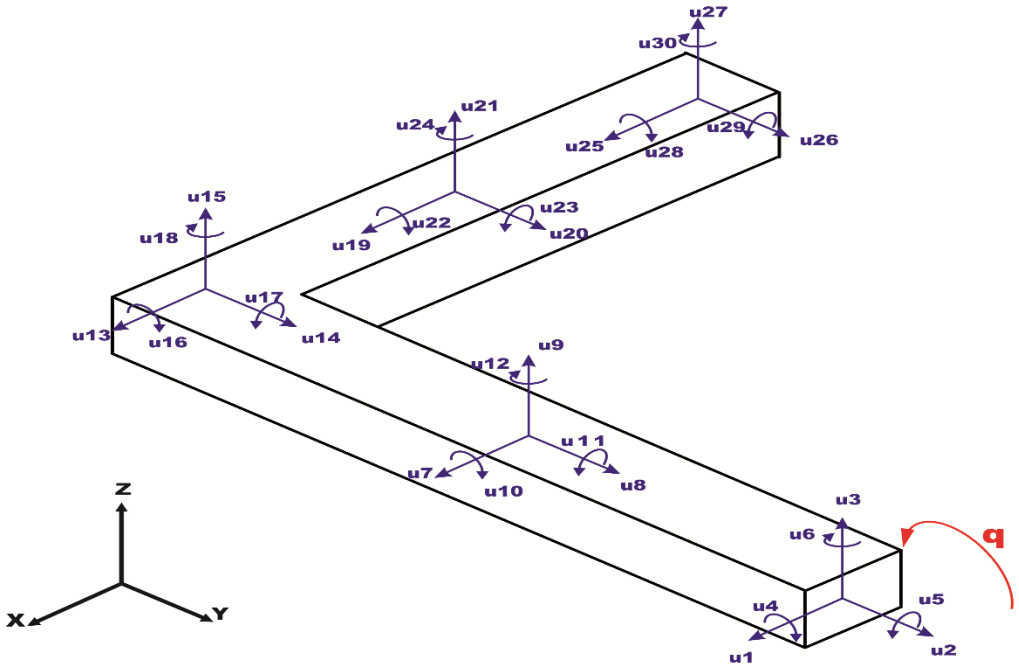

Fig 2.3: Elastic displacement in L-shape mechanism

Table 2.1 - Kinematics and dynamics characteristic of the reference mechanism

	Symbol	Value
Young's modulus	E	$2 \times 10^{11}\ [Pa]$
Flexure inertia moment	J	$11.10^2 \times 10^{-10}\ [m^4]$
Poisson's coefficient	v	0.33
Beam width	a	$30 \times 10^{-3}\ [m]$
Beam thickness	b	$10 \times 10^{-3}\ [m]$
Density	φ	$7850\ [Kg/m^3]$
First link length	L_1	$0.5\ [m]$
Second link length	L_2	$0.5\ [m]$
Rayleigh damping constant	α	$7 \times 10^{-4}\ [s^{-1}]$
	β	$2.13 \times 10^{-7}\ [s]$

2.4 Accuracy of the Linearized Model

In this subsection, a simple comparison test in order to evaluate the extracted accuracy linearized model has been described. The mechanism, introduced in section 2.5, has been fed with 5 *Nm*

torque impulse with 0.05 *sec* delay in the initial configuration of $q_0 = 90°$, i.e. starting from the vertical position; however, it should be mentioned that the test can be implemented to any mechanism configuration with similar results.

From the Figure 2.4 (A) and (B) it can be inferred that linearized model has a very high level of precision as well as the rotation motion of q is considered. As can be seen from the Figure 4, the response of the linear and nonlinear models of q as the generalized coordinate is very close and similar to each other; however, the difference between them increases when moves away from the equilibrium point. Additionally, it can be inferred from Figure 2.4. (B) that the error on q increases slowly as the error after 0.4 s is around 0.06%.

Figure 2.5 (A) shows a comparison of the responses of nonlinear and linearized system impulsive on the subject of nodal displacements u_{11}. According to Figures 2.5 (A), the difference between the linear and nonlinear modelling of u_{11} are negligible while the mechanism moves from the equilibrium configuration as far as u_{11} is concerned. Figures 2.5 (B) shows the modelling error on u_{11}, which is very small at beginning of the motion and grows slowly during the mechanism manoeuvre.

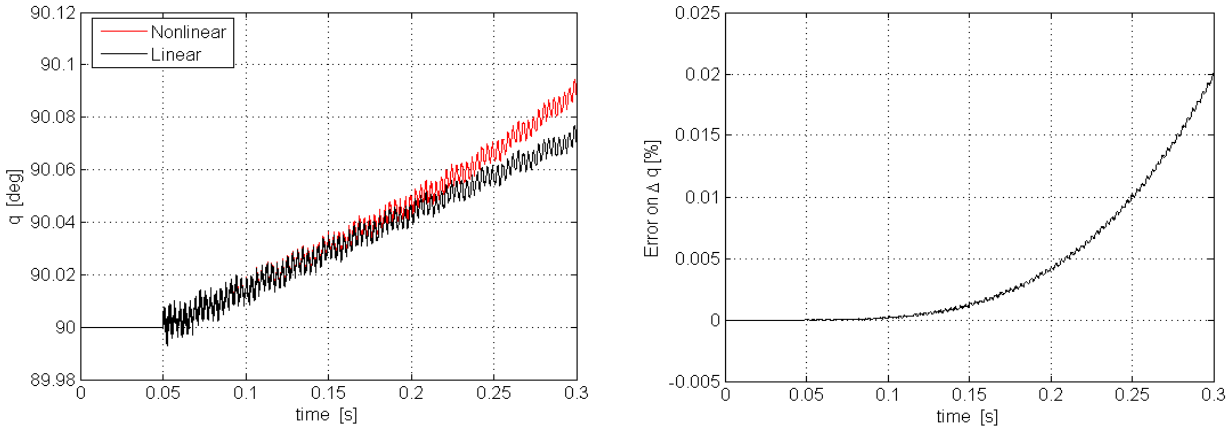

(A) (B)

Fig 2.4: A) Comparison between linear and nonlinear impulsive response: angular position q. B) Comparison between linear and nonlinear impulsive response: percentage error on angular position q

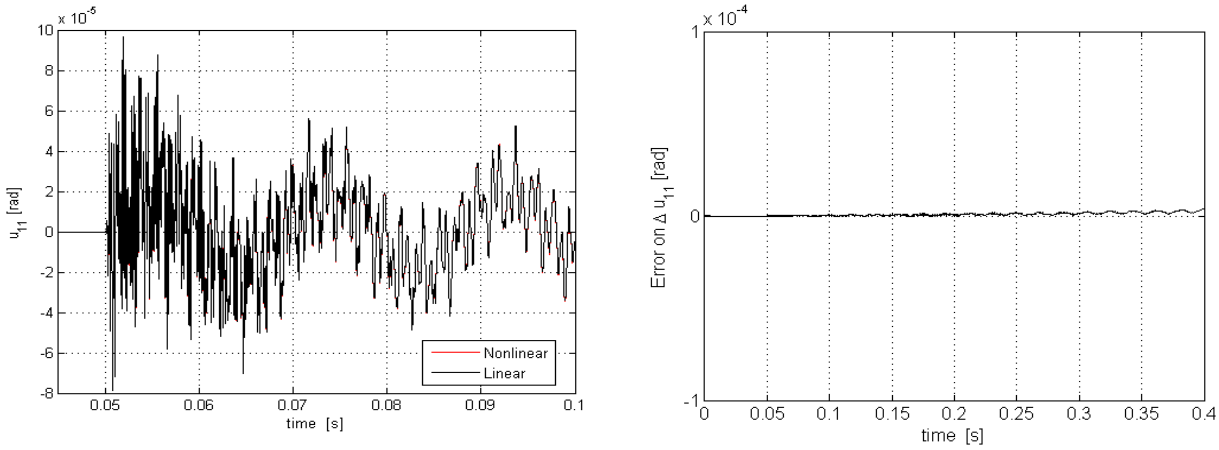

(A) (B)

Fig 2.5: A) Comparison between linear and nonlinear impulsive response: elastic displacement u_{11}. B) Comparison between linear and nonlinear impulsive response: error in radian on elastic displacement u_{11}

2.5 State Observer

Fundamentally, a state observer estimates the state variables by means of measuring a subset of the output and control variables in order to reconstruct the state of a system where the measurement is difficult or even impossible in some specific situations.

A brief explanation of the Kalman observer used in our system, is summarized here. For more details about methodology and designing refer to [74].

Basically an observer design depends upon on two basis, a linear time invariant dynamic model of the system and linear relation between the state variables and the sensed outputs. The dynamic of the overall system is described very briefly by the following system of equations:

$$\Delta\hat{\dot{x}} = F\Delta\hat{x} + G\,\Delta u + L(\Delta y - \Delta\hat{y}) \tag{2-34}$$

$$\hat{y} = H\Delta\hat{x} \tag{2-35}$$

$$\Delta z = -W\Delta\hat{x} \tag{2-36}$$

$$e = \Delta\hat{x} - \Delta x \tag{2-37}$$

Where e and L are the vector of the errors of the state variable estimates ($\hat{x}$) and the time invariant gain matrix of the asymptotic Kalman estimator, respectively.

Additionally W is the time invariant gain vector of linear regulator and F and H matrices are used to assess the system observability as well. The control vector is shown by u while y and $\hat{y}$ present the real output signals and estimated ones respectively. G is a matrix which is related to the linearized model of the equilibrium configuration. However, it should be noticed that these equations only hold in the neighbourhood of an equilibrium configuration.

In order to evaluate our system observer, a similar test described in the previous subsection with the same input and configuration has been implemented. In this test knowledge about nodal displacement u_{19} and generalized coordinate q are available by the measurement in the purpose of estimating all states of the system.

From the Figure 2.6 (A) and (B), it can be concluded that the Kalman observer has a good accuracy for estimating the generalized coordinate q as a one system state. Regarding the Figure 2.6 (A), the impulsive response of nonlinear and observer are very similar; although, more far from the equilibrium point, more differences among the responses. Particularly, Figure 2.6 (B) shows the error on q that is, after 0.4 *sec* the error between nonlinear and estimator is still so small and converge to zero.

Figure 2.7 (A) illustrates the comparison between the impulsive respond of actual measurement of displacement u_{19} and estimated u_{19} by Kalman observer. As it can be seen from Figure 2.7 (B) the difference is not so significant during the transient. Nevertheless they increase as the mechanism moves from the equilibrium configuration. In particular the difference on u_{19} between the nonlinear system and the observer are so small as long as the motion from the original position is kept.

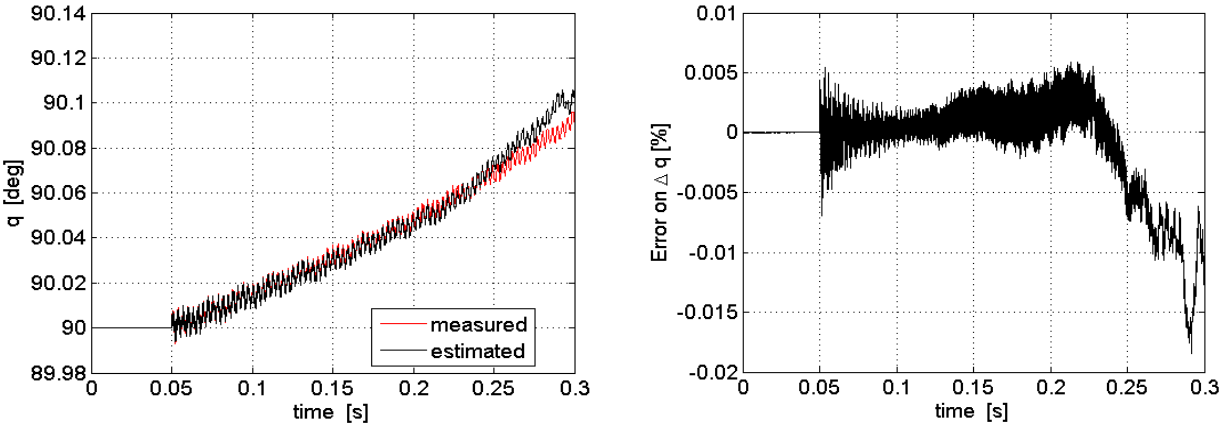

(A) (B)

Fig 2.6: A) Comparison between measured and estimated angular position q. B) Percentage error on estimation of angular position q

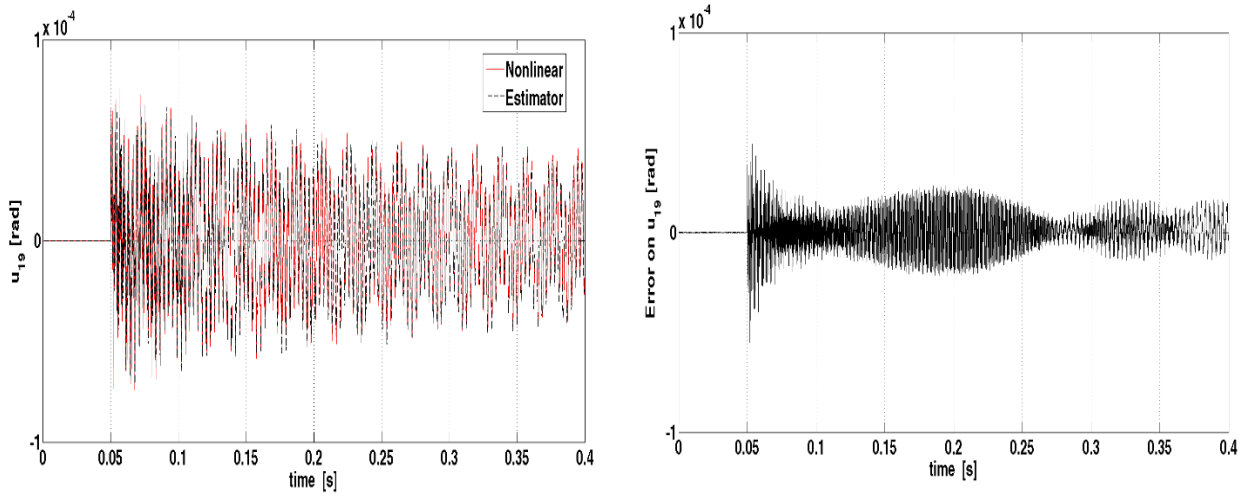

(A) (B)

Fig 2.7: A) Comparison between response of impulsive response of nonlinear and estimated u_{19}. B) error in radian on estimation of elastic displacement u_{19}

CHAPTER 3

Linear Quadratic Optimal Control

3.1 Introduction

Optimal control emerged as a distinct filed of investigation in the 1950s. Beyond the traditional analytical and computational technique, referring in a unique mode of optimization problem arising in listing and the control of engineering devices and equipment [75].

The theory of optimal control is concerned with operating a dynamic system at minimum cost. The case where the system dynamics are described by a set of linear differential equations and the cost is described by a quadratic function is called the LQ problem. One of the main results in the theory is that the solution is provided by the linear-quadratic regulator (LQR), a feedback controller whose equations are given below. The LQR is an important part of the solution to the LQG (Linear-Quadratic-Gaussian) problem. Like the LQR problem itself, the LQG problem is one of the most fundamental problems in control theory [76].

5.6 Synthesis of the Optimal Control

In this section a brief explanation of the optimal linear quadratic regulator (LQR) is given [77]. The synthesis has been done for the spatial flexible mechanism explained in Section 2.5. The linearized dynamic model of the system, obtained in Section 2.3, leads to the following state-space for the system under investigation:

$$\begin{aligned} \dot{x}(t) &= Fx(t) + G\tau(t) \\ y(t) &= Hx(t) \end{aligned} \tag{3-1}$$

In order to perform the simulations tests, the output vector $\boldsymbol{y}$ was defined to be the full state vector (i.e. H was taken as the identify matrix).

We can use optimal control theory to design a feedback law $u = \alpha(x)$ that stabilizes a given equilibrium point. Generally speaking, we do this by continuously re-solving the optimal control problem from the current state $x(t)$ and applying the resulting input $u(t)$. Of course, this approach is impractical unless we can solve explicitly for the optimal control.

The controller synthesis has been carried out by designing an optimal LQR for the system represented in the sate-space form of Equation 3-1. The goal is to determine the control vector $\tau(t)$, which allows minimizing the performance index *J*, defined as:

$$J = \int_0^\infty [y^T(t)Qy(t) + \tau^T(t)L\tau(t)]dt = \int_0^\infty [x^T(t)H^TQHx(t) + \tau^T(t)L\tau(t)]dt \quad (3\text{-}2)$$

Where $Q_x \geq 0,\ Q_u > 0, P_1 \geq 0$ are symmetric, positive (semi-) definite matrices. Note the factor of $\frac{1}{2}$ is usually left out, but we included it here to simplify the derivation.

To find the optimal control, the maximum principle has been applied. Hence, the Hamiltonian H can be written as:

$$H = \frac{1}{2}x^TQ_xx + \frac{1}{2}u^TQ_uu + \lambda^T(Ax + Bu) \quad (3\text{-}3)$$

By applying maximum principle Theorem, the necessary condition can be obtained:

$$\begin{aligned} \dot{x} &= (\frac{\partial H}{\partial \lambda})^T = Ax + Bu, x(0) = x_0 \\ -\dot{\lambda} &= \left(\frac{\partial H}{\partial x}\right)^T = Q_x + A^T\lambda, \lambda(T) = P_1 = x(T) \\ 0 &= \frac{\partial H}{\partial u} = Q_u + \lambda^TB \end{aligned} \quad (3\text{-}4)$$

The optimal controller can be obtained from the last condition.

$$u = -Q_u^{-1}B^T\lambda \quad (3\text{-}5)$$

The above equation can be substituted into the dynamic equation (3-5). In order to solve the latter equation for the optimal control, two point boundary value problems using the initial condition $x(0)$ and the final condition $\lambda(T)$ should be solved. Unfortunately, solving such problems in general is very difficult.

Given the linear nature of the dynamics, for finding a solution by setting $\lambda(t) = P(t)x(t)$ where $P(t) \in \mathbb{R}^{n\times n}$. By substituting this into the necessary condition, following equation can be obtained:

$$\dot{\lambda} = \dot{P}x + P\dot{x} = \dot{P}x + P(Ax - BQ_u^{-1}B^TP)x \Longrightarrow -\dot{P}x - PAx + PBQ_u^{-1}BPx = Q_x + A^TPx$$

By finding $P(t)$, the above equation is satisfied.

$$-\dot{P} = PA + A^TP - PBQ_u^{-1}B^TP + Q_x,\ P(T) = P_1 \quad (3\text{-}6)$$

Equation 3-6 represents a matrix differential equation that defines the elements of $P(t)$ from a final value $P(T)$. Solving it is conceptually no different than solving the initial value problem for vector-valued ordinary differential equations, except that we must solve for the individual elements of the matrix $P(t)$ backwards in time. Equation 3-6 is called the Riccati ODE.

An important property of the solution to the optimal control problem when written in this form is that $P(t)$ that can be solved without knowing either $x(t)$ or $u(t)$. This leads to the two point boundary value problems which should be separated into first solving a final-value problem and then solving a time-varying initial value problem. More specifically, given $P(t)$ satisfying Equation 3-6, the optimal input can be applied $u(t) = -Q_u^{-1}B^T P(t)x$ and then solving the original dynamics of the system forward in time from the initial condition $x(0) = x_0$. Note that this is a (time-varying) feedback control that describes how to move from any state to the origin. An important variation of this problem is the case when $T = \infty$ and eliminate the terminal cost (set $P_1 = 0$). This brings up the cost function

$$J = \int_0^\infty (x^T Q_x x + u^T Q_u u)dt \tag{3-7}$$

Since there is no the terminal cost, there is any constraint on the final value of λ or, equivalently $P(t)$. Thus, it is possible seeking to find a constant P satisfying Equation 3-6. In other words, we seek to find P such that

$$PA + A^T P - PBQ_u^{-1}B^T P + Q_x = 0 \tag{3-8}$$

This equation is representation of the algebraic Riccati equation. Given a solution, the input is chosen as $u = -Q_u^{-1}B^T Px$. This represents a constant gain $K = Q_u^{-1}B^T P$ where P the solution of the algebraic Riccati equation.

The implications of this result are interesting and important. First, Noticing that if $Q_x > 0$ and the control law corresponds to a finite minimum of the cost, then obtaining $\lim_{t\mapsto\infty} \mathrm{x(t)} = 0$, otherwise the cost will be unbounded. This means that the optimal control for moving from any state x to the origin can be obtained by applying a feedback $u = -Kx$ for K chosen as described as above and letting the system evolve in closed loop. Furthermore, the gain matrix K can be expressed in the terms of the solution to a (matrix) quadratic Equation 3-8.

In our system for spatial L-shape flexible mechanism, in Equation 3-7 the first term of inside the integral minimizes the absolute values of the elastic displacements (which represent the amplitude of vibrations) and velocities at the nodes, as well as displacements and velocities of the free coordinates. The second term minimizes the absolute values of the system input, i.e. the motor torques. Matrices Q_u and Q_x contain the weight attributed to the system output (vibration

amplitude) and to the control input (motor torques), respectively. Minimization of the performance index ***J*** is achieved if the system input is taken to be the result of a linear feedback from the output.

Figure 3.1 shows a schematic representation of the synthesized control system. It should be mentioned that the maximum value of torque that can be provided by the available motors is 20 Nm and also the technique described above is based on a linearization and is only valid in a vicinity of the equilibrium point.

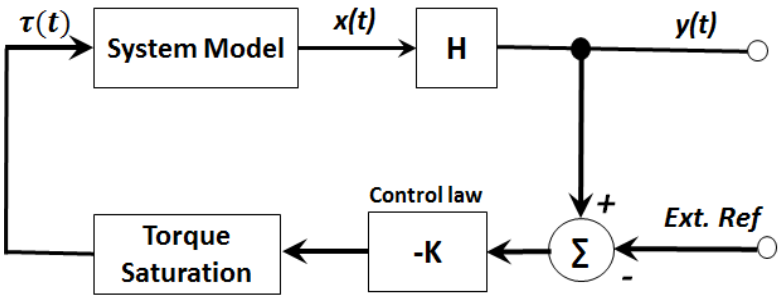

Fig 3.1: The control system

5.7 Results

In this section the results of the application of the designed LQR controller in Section 3.1 to the flexible L-shape mechanism, described in Section 2.5, has been presented. The system for obtaining the defined position and vibration reduction has been tested in order to check its operation. The initial position of the L-shape mechanisms is taken as $q = 90^o$. A step reference input with amplitude $\Delta q = 4°$ with 0.05 sec delay was given to the mechanisms actuator which is an electrical motor. Four displacement directions on the four nodes of mechanisms has been considered. The displacements are u_7,u_{17},u_{24} and u_{25} including both axial and angular displacement are shown in Figure 2.3.

Our aim is to reach the defined position for generalized coordinate and reduce the amplitude of vibrations. To this end, we consider the optimal control described in the previous section. The size of matrices Q_u and Q_x is [50×50] and [1×1], respectively. Synthesizing the optimal controller is just a matter of choosing the values of the diagonal elements of matrices Q_u and Q_x.

A sound feature of this type of controller is that we can consider only the displacements whose vibrations we want to reduce, and set the values of the corresponding diagonal elements, leaving to zero all the others. Thus, if displacement in u_7 is considered, the corresponding element is q_{26} (axial X displacement). The other diagonal element of matrix Q_x can then be set to zero, with the exception of the last element (q_{50}), which is the weight of the free coordinate.

$$Q_x = \begin{bmatrix} 0 & & & & & & & & & \\ & \ddots & & & & & & & & \\ & & q_{26} & & & & & & & \\ & & & 0 & & & & & & \\ & & & & \ddots & & & & & \\ & & & & & q_{36} & & & & \\ & & & & & & 0 & & & \\ & & & & & & & \ddots & & \\ & & & & & & & & q_{43} & \\ & & & & & & & & & q_{44} \\ & & & & & & & & & & 0 \\ & & & & & & & & & & & \ddots \\ & & & & & & & & & & & & q_{50} \end{bmatrix}, Q_u = [l_1] \quad (3\text{-}9)$$

The nonzero elements of the Q and L matrices have been given the following values:

$q_{26} = q_{36} = q_{43} = q_{44} = 10^8, q_{50} = 10^4$

$l_1 = 1$ (3-10)

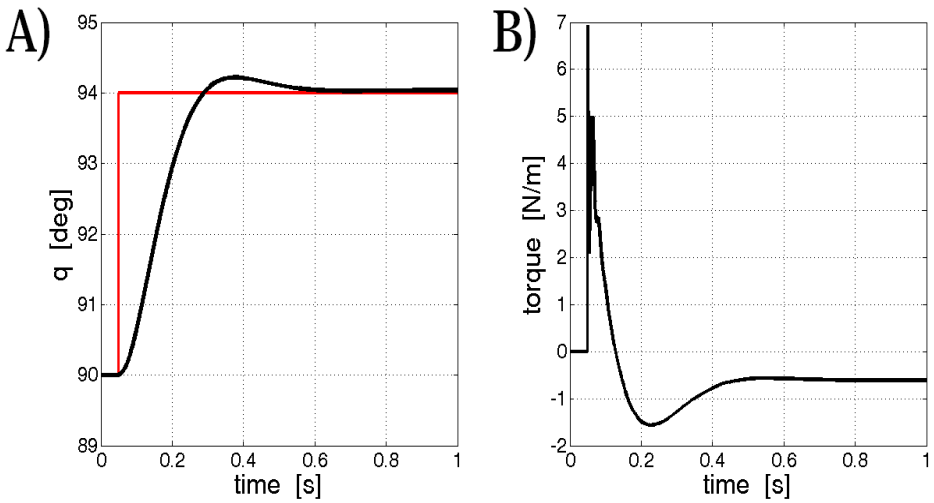

Fig 3.2: A) step response of free coordinate. B) The applied torque by motor

Figure 3.2 (A) shows the step response of the free coordinate and Figure 3.2 (B) demonstrates the torque produced by the actuator which could not provide larger than 20 *Nm*. Consequently, the plots in Figure 3.3 and Figure 3.4 illustrate a considerable reduction of the amplitude of vibrations: actually, vibrations are suppressed after 0.05 *sec* approximately.

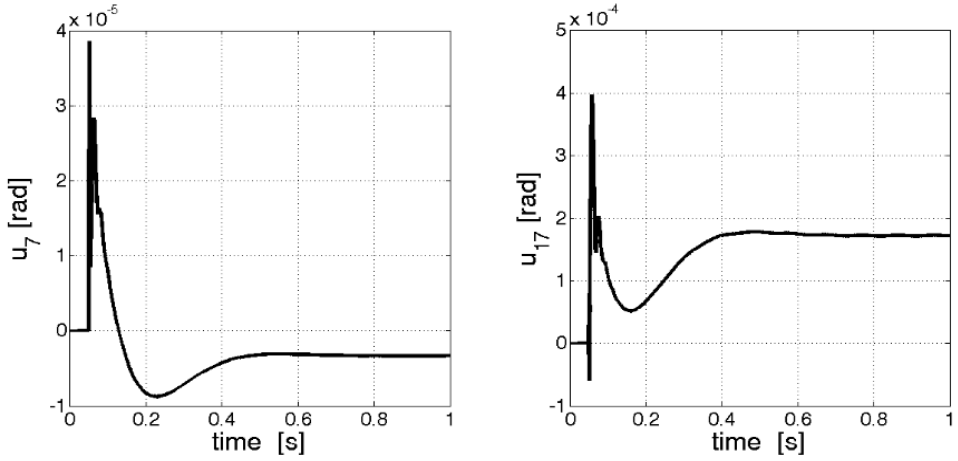

Fig 3.3: Vibration reduction achieved through optimal control for u_7 and u_{17}

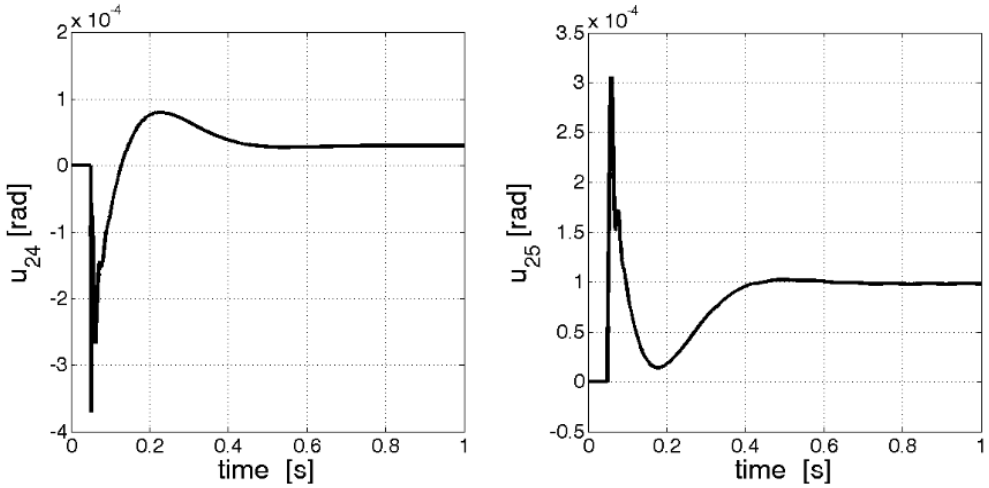

Fig 3.4: Fig. 9 Vibration reduction achieved through optimal control for u_{24} and u_{25}

5.8 Conclusion

In this chapter an optimal linear quadratic regulator for the linear model described in Section 2.3 has been designed and tested. Linear quadratic (LQ) optimal control is one of the optimal control techniques, which takes into account the states of the dynamical system and control input to

make the optimal control decisions. The nonlinear system states are fed to LQ which is designed using a linear state-space model.

A model design procedure has been applied to build a Linear quadratic (LQ) optimal control position and vibration control. The results are satisfactory and illustrate that the synthesized Linear quadratic (LQ) optimal control approve a remarkable and fast response of free coordinate and also the reduction of the amplitude of the mechanism vibrations. The applied torque by the motor is always kept below the maximum limit.

CHAPTER 4

Model Predictive Control

4.1 Introduction

Model predictive controller (MPC) is traced back to the 1970s. It started to emerge in the industry in 1980s as IDCOM [78] and DMC [79]. The initial IDCOM and MPC algorithms represented the first generation of MPC approach. In general, MPC is the type of controllers in which there is a direct use of an explicit identifiable model. It is also described as a class of computer control schemes that uses a process model for two principal tasks:

- Definite prediction of future plant behavior
- Computation of appropriate corrective control action needed to drive the predicted output as close as possible to the reference target value.

Control design techniques based on MPC concept have found wide acceptance in industrial applications and have been studied by academia. It is currently the most widely utilized of all advanced control methodologies in industrial applications. The main reason for such popularity is the ability of MPC design to reach high performance control systems which are capable of operating without expert intervention for long periods of time. In this section a short introduction to constrained MPC is given. For further reading on constrained MPC see [80].

4.2 General Concept of MPC

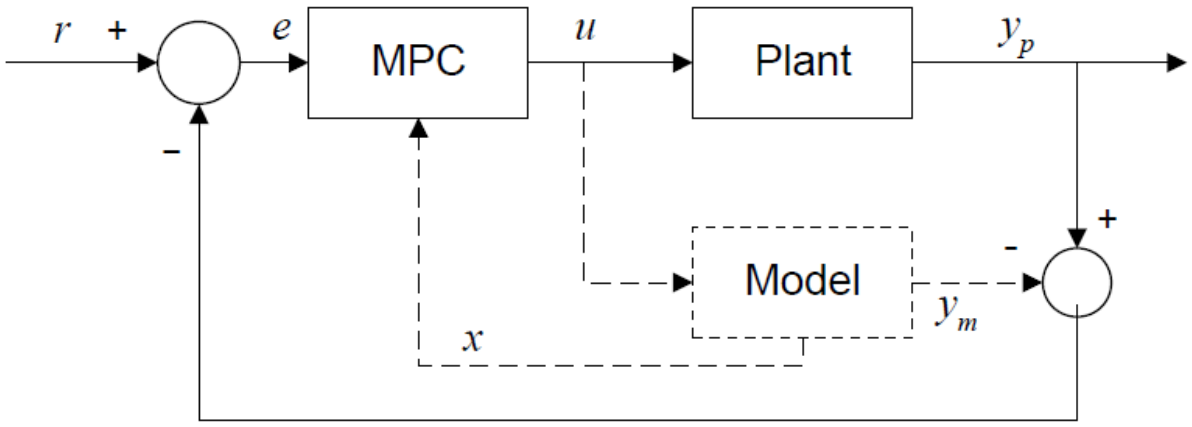

Fig 4.1: Block Diagram of MPC Implementation

Block diagram for the MPC implementation is depicted in Figure 4.1. As shown in the figure, a process model is used in parallel to the plant. MPC uses a dynamic model of the process in the purpose of predicting the controlled variable. The predicted controlled variable is fed back to the controller where it is used in an on-line optimization procedure, which minimizes a proper cost function to define the manipulated variable. The controller output is applied in real time and then the procedure is repeated every sampling time with actual process data. The difference between the plant measurement, y_p and the model output y_m is also fed to the controller in order to eliminate steady state offset. Usually the cost function depends on the quadratic error between the future reference variable and the future controlled variable within limited time horizon.

4.3 Prediction and Control Horizons

Prediction horizon H_P is the number of samples over which a prediction of the plant outputs is evaluated at each iteration of the controller, while control horizon H_C is the number of samples over which the control variables can change their value.

As it can be seen in Figure 4.2, the MPC controller performs a prediction from current time step k to the future time step $k + H_P$. In the same figure it is shown that the control action can change only over the time interval $[k, k + H_C]$. The control action is chosen in order to minimize a given cost function. The first value of the optimal control sequence is actually fed to the plant, and the whole calculation is be repeated at subsequent control intervals. Prediction horizon is moving forward for every iteration in time and the MPC controller predicts the plant output again.

4.4 Model Prediction and Cost Function

A discrete time state-space model is often used to provide predictive capability in MPC controller:

$$x_{k+1} = Ax_k + Bw_k \tag{4-1}$$

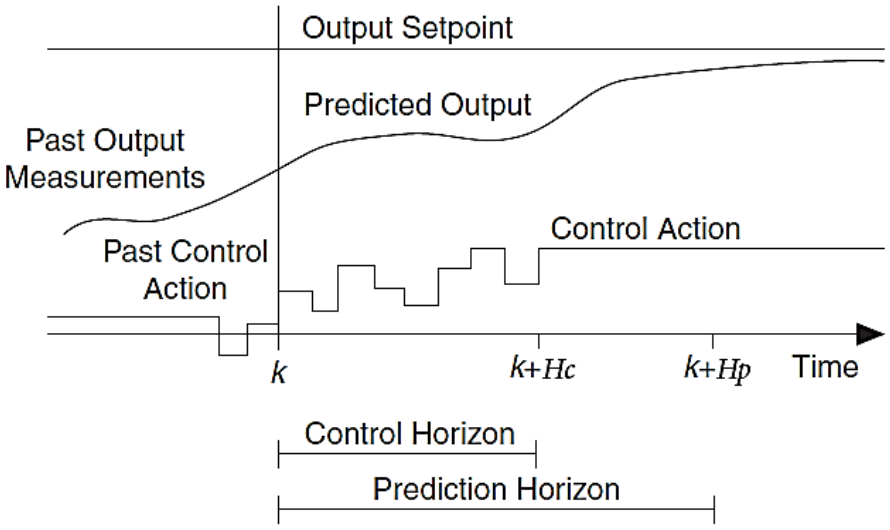

Fig 4.2: A discrete MPC controller scheme

$$y_k = Cx_k + Dw_k \tag{4-2}$$

The MPC controller computes a sequence of the predicted a new control input vector in order to minimize a cost function. Often used cost function in MPC is the linear quadratic function:

$$J = \sum_{k=0}^{H_P} (\hat{y} - r)^T Q (\hat{y} - r) + \sum_{k=0}^{H_c} \Delta w^T R_1 \Delta w + \sum_{k=0}^{H_C} w^T R_2 w \tag{4-3}$$

in which $\hat{y}$, r, Δw, w are the predicted plant outputs, the reference signal for outputs, the change rate of control action and the control action, respectively. Q, $R_1$and R_2 are the weighting matrices used to tune the control performance. Q is used to penalize the tracking error, while R_1 and R_2 are used to penalize the change rate and the absolute value of control action, respectively. In general, Equation 4.3 is used in MIMO systems (Multiple Input and Multiple Outputs) and also could be expanded to MISO systems (Multiple Input and Single Output) such as our case, a system with 50 inputs (states) and one output (torque).

Constrained MPC controller has ability to take into account constraints of physical systems in its future control performance calculations. The formulation used in this paper allows to define constraints as follows:

$$y_{min} \leq y \leq y_{max} \tag{4-4}$$

And inputs constrains can be defined as:

$$\Delta w_{min} \leq \Delta w \leq \Delta w_{max} \tag{4-5}$$

$$w_{min} \leq w \leq w_{max} \tag{4-6}$$

4.5 Result of Model Predictive Control with Constraint

In this section the results of several numerical tests are provided and discussed to show the capabilities of the MPC controller for position and vibration control of flexible mechanisms. The tuning of the MPC controller depends on weight on u_{19} weight on q, *s*ampling time (T_S), prediction horizon (H_P) and control horizon (H_C).

In practical applications, the values of T_S, H_P and H_C should be selected on the basis of the available computational resources. The computational cost of solving the optimization problem of each iteration of the controller depends on both H_P and H_C.

Generally speaking, longer H_C results in aggressive control action while longer H_P causes more damped response and more precise reference tracking [61].

The whole behaviour of the controller relies on a large set of variables. Constraints on actuation torque are chosen to comply with the physical limitations of the actuator. Other parameters can be tuned quite freely. In this case, constraints can be imposed on elastic displacement (u), angular position (q) and input torque (τ) as:

$$u_{k_{min}} \leq u_k \leq u_{k_{max}} \ , k = 1 \ldots 24 \tag{4-7}$$

$$q_{min} \leq q \leq q_{max} \tag{4-8}$$

$$\tau_{min} \leq \tau \ \leq \tau_{max} \tag{4-9}$$

It should be mentioned that in our system just the constraint on torque, which is $-8 \leq \tau \leq 8$ Nm, is active.

In the following the effects of choosing different values for tuning parameters of MPC controlled are discussed by means of numerical tests.

4.5.1 Effects of f_c on the Closed-loop System

Figure 4.3 (A) and (B) demonstrate the response of angular position q and elastic displacement u_{12} with different sampling frequency. In all the tests reported in this work, the mechanisms

performs a 30 degree of rotation in counter-clockwise direction starting from the horizontal position.

It can be seen from Figure 4.3 (A) that the performance of the angular position response for both values of sampling frequency 100 Hz and 1k Hz are very similar; however, it should be mentioned that the values of H_P and H_C are chosen 20 and 5 for $f_c = 100\ Hz$ and 200 and 50 for $f_C = 1k\ Hz$, respectively. The vibration amplitude for the system with $f_C = 100\ Hz$ is bigger than the system with $f_C = 1k\ Hz$ during the transient as it is depicted in Figure 4.3 (B) for elastic displacement u_{12}. The more effective vibration damping achieved by the 1k Hz control can be explained by taking into consideration the faster control has a sufficient bandwidth to take into account all the significant vibration modes of the flexible mechanism.

From the Figure 4.4 it can be inferred that applied torque by the control system is within the range defined by the constraint.

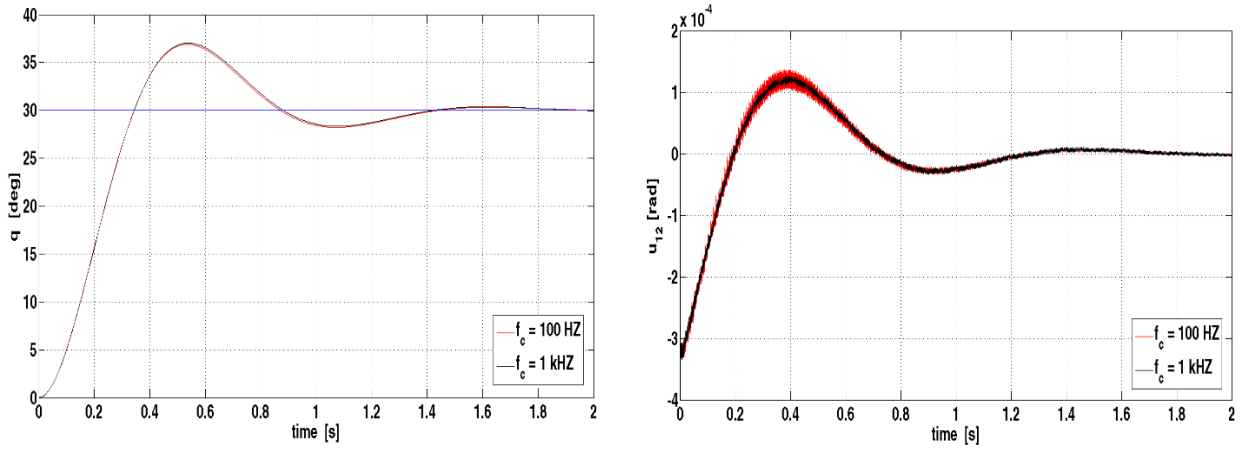

(A) (B)

Fig 4.3: A) Response of the Angular position q at with different sampling frequency, 1 kHz and 100 kHz. B) Effect analysis of different sampling frequency (f_c) on the elastic displacement u_{12}

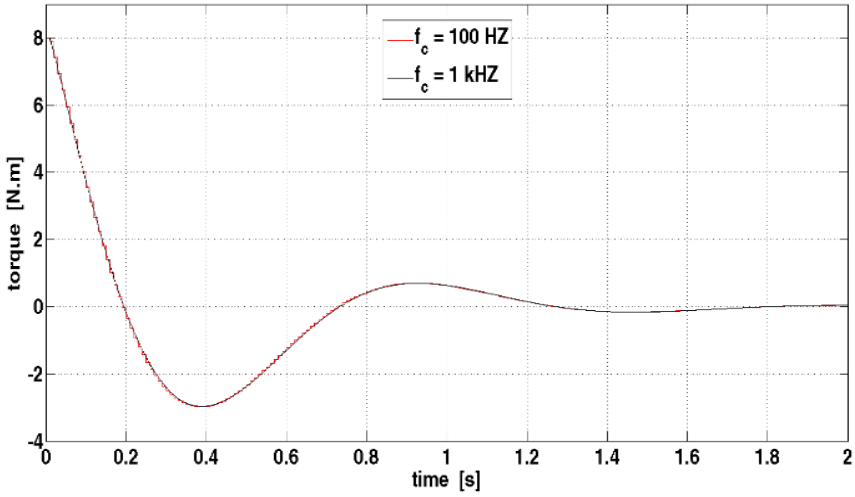

Fig 4.4: Applied torque to the mechanism

4.5.2 Effects of H_C and H_P on the Closed-loop System

In Figure 4.5 (A) and (B) the effects of choosing different control horizon has been investigated. It can be inferred that tuning the H_C parameter has a limited effect on the response of the closed loop system. Consequently, H_C can be increased up to H_P but the performance of the controller will not be improved significantly. In most cases H_C should be kept quite small, since a longer control horizon increases the computational effort required to solve the minimization problem defined by Equations 4-1 to 4-3.

Regarding Figure 4.6 (A) and (B), changing the value of the prediction horizon (H_P) has a significant effect on the performance of the controller. As it can be inferred from Figure 4.6 (A), selecting bigger value for H_P causes more damped response for angular position $q;$ conversely, smaller value for H_P result in more aggressive response. A similar consideration can be achieved by analysing the Figure 4.6 (B), which reports the time evolution of elastic displacement u_{12}. Again, higher values of the prediction horizon leads to a higher damping of vibrations.

Therefore we can conclude that the prediction horizon should be set as high as the computational resources allows it. Since the performance of the closed-loop system are less sensitive to the choice of the control horizon, H_C can be set to a low value to reduce the computational effort required to solve the optimization problem.

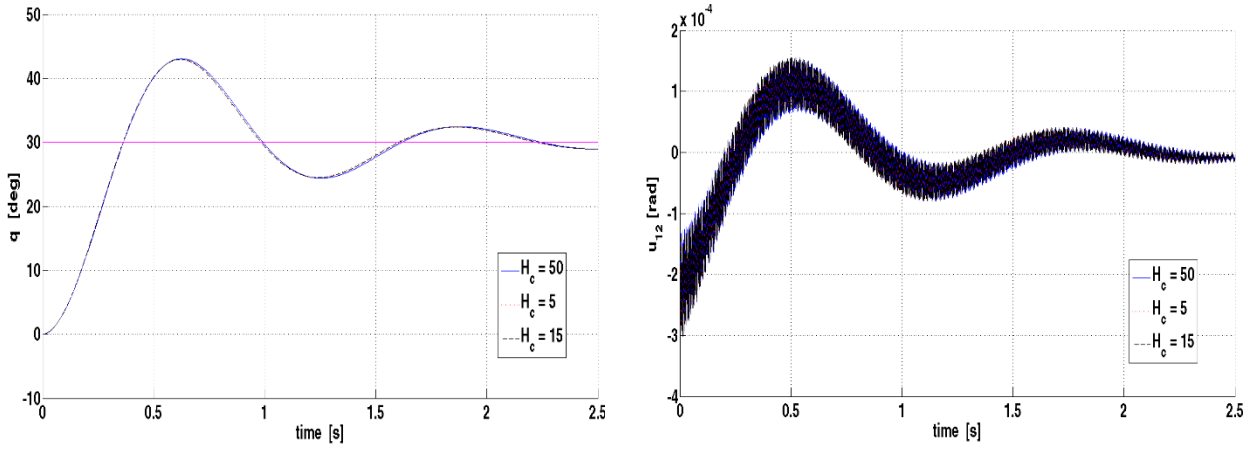

(A) (B)

Fig 4.5: A) Effect analysis of different control horizon (H_c) on angular position q. B) Effect analysis of different control horizon (H_c) on elastic displacement u_{12}

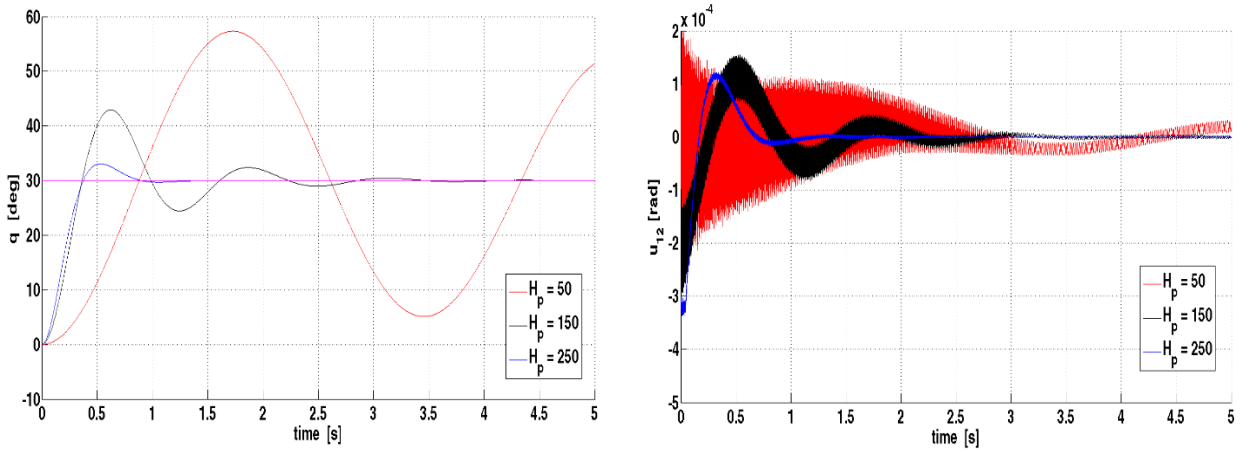

(A) (B)

Fig 4.6: A) Effect analysis of different control horizon (H_c) on elastic displacement u_{12}. B) Effect analysis of different control horizon (H_p) on angular position q

4.6 Robustness

In this section the results of two tests which are implemented in order to evaluate robustness of the proposed control scheme are discussed.

Several simulations have been performed with applying the same control system on the nonlinear model with different parameters. The tests have been done with uncertainties of different sign $(i.e. +20\%, -20\%)$ on the mechanism links lengths $(L = L_1 + L_2)$ and on the Young's elastic modulus E. These tests that have been developed in order to evaluate the robustness properties of the proposed control scheme, using an approach already reported in other works such as [70], [81].

In Figure 4.7 (A) the effects of changing the mechanism length ($L=L_1+L_2$) of the mechanism have been shown. According to the Figure 4.7 (B), the tolerance in the mechanism length does not bring the closed loop to instability. If the actual length of the links is 20% larger than the nominal value, the response of the system will be more damped. On the other hand, by decreasing by 20% the mechanism length, the overshoot of angular position q is increased with respect to the nominal case.

In Figure 4.7 (A) the effects of changing the mechanism length $(L = L_1 + L_2)$ of the mechanism have been shown. According to the Figure 4.7 (A), the tolerance in the mechanism length does not bring the closed loop to instability. If the actual length of the links is 20% larger than the nominal value, the response of the system will be more damped. On the other hand, by decreasing by 20% the mechanism length, the overshoot of angular position q is increased with respect to the nominal case.

Thus it can be inferred that the developed controlled is quite robust to this kind of uncertainty, as far as angular position tracking is concerned. It can be seen in Figure 4.7 (B) that also vibration damping is influenced by mismatches in mechanism length. If mechanism length is under-estimated, a more effective vibration damping can be achieved, since the overall response of the closed-loop system is slower.

According to Figure 4.8 (A) and (B), changing the value of elastic modulus E of a $+30\%$ does not alter significantly the performance of the control scheme, thus the designed MPC controller is also robust respect to changes in the vibration models of the plant.

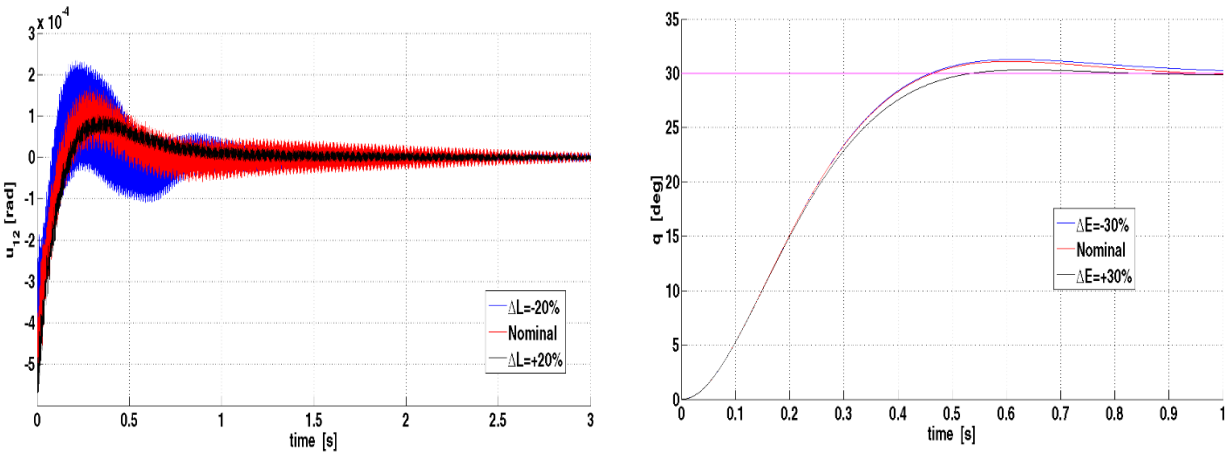

(A) (B)

Fig 4.7: A) Robustness analysis of the change in the mechanisms links lengths ($L=L_1+L_2$) on angular position *q. B)* Robustness analysis of the change in the mechanisms links lengths ($L=L_1+L_2$) on elastic displacement u_{12}

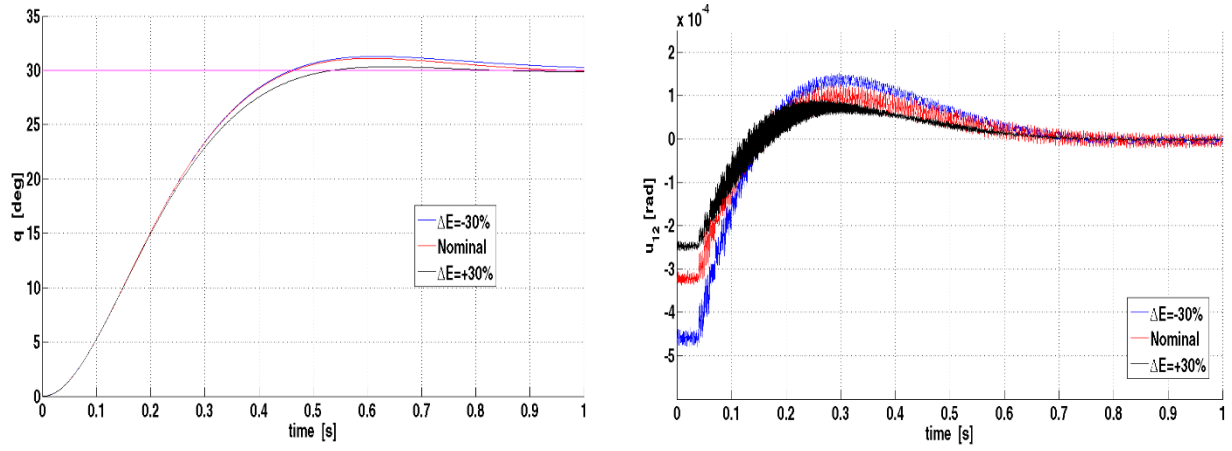

(A) (B)

Fig 4.8: A) Robustness analysis of the change of elastic modulus *E* on angular position *q.* B) : Robustness analysis of the change of elastic modulus *E* on elastic displacement u_{12}

4.7 MPC Controller vs. PID Controller

In this section a comparison between results of MPC and PID controller has been made and discussed. While PID controller are applied in single loop controllers, MPC controller are used for overall system. PID controllers support only a single input put system but MPC are applicable in multi input and multi output systems (MIMO system).

As is shown at Figure 4.9 (A) PID controller follow the target reference with high speed and low error but with remarkable overshoot ($\approx 35\%$). The tuning of the PID control has been chosen to provide for a similar rise time. Moreover, it can be inferred from the Figure 4.9 (B) that the amplitude of elastic displacement u_{12} is significantly larger if a simple PID controller is used.

It can be therefore inferred that in this case MPC control outperforms PID, which is currently the most widely used control technology in industrial applications.

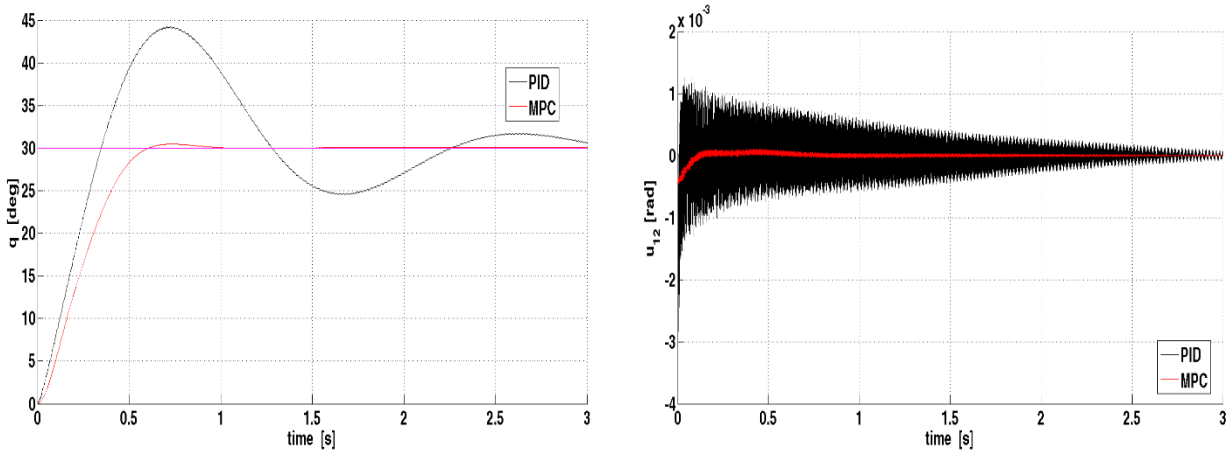

(A) (B)

Fig 4.9: A) Response of the closed loop system with PID and MPC controller on angular position *q*. B) Response of the closed loop system with PID and MPC controller on elastic displacement u_{12}

4.8 Conclusion

In this chapter, a model predictive control with constrains for a 3D L-shape mechanism has been designed and tested. The proposed control scheme allows to minimize a performance index which takes into consideration both the amplitude of vibrations and the angular position of the mechanism. Meanwhile two tests on different perturbed plants has been implemented in order to

analyse the robustness performance of the proposed control scheme. Finally a comparison between performance of the standard PID controller and MPC controller performance has been done and the results show that MPC controller not only is very effective for both reference position tracking and vibration suppression but also represent a high level of robustness to uncertainties on the plant.

CHAPTER 5

Robust Control

5.1 Introduction

Flexible link manipulators possess many advantages over the traditional bulky manipulators. The most important benefits include high payload-to arm weight ratio, fast motion, safer operation, improved mobility, cheapness, larger workspace and better energy efficiency, etc. Although, the reduction of weight leads to the increase of the link elasticity that significantly makes the control of the manipulator a difficult task. The difficulty in control is due to the fact that the link model is a distributed parameter plant. In this case, several elastic modes are needed to reach adequately high accuracy. Furthermore, the plant has several uncertain parameters (payload mass, hub and structural damping factors, etc.) that effect remarkably the performance of the system [82].

The control of uncertain systems is often accomplished using either robust control or an adaptive control approach. In the adaptive technique, one designs a controller that attempts to "learn" the uncertain parameters of the system and, if properly designed, will consequently be a "best" controller for the plant. In the robust approach, the controller has a constant structure that yields "acceptable" performance for a class of plants which contain some uncertainties. Generally speaking, the adaptive approach is applicable to a wide range of uncertainties, but robust controller is simpler to perform and no time is required to "tune" the controller for a particular plant.

5.2 Sensitivity of the Linearized Model

In order to evaluate the sensitivity of the linearized model for synthesizing of robust controllers, comparison test in the frequency domain is explained in this section through the simulation environment. According to Equation 2-28, the linear model in state space formulation includes 50 states and one input which is the torque applied by the motor; in other words, the flexible L-shape mechanism has been modelled with four finite elements, one rigid and 24 elastic degrees of freedom. Consequently, the system can recognized as a SIMO (single input, multi output) system. By considering $\pm 20\%$ uncertainty in the elasticity (E) and mass density (m) of the system, frequency response of the linearized model in open loop system has been investigated. Two transfer functions have been employed in this test, one from the input torque (τ) to the elastic displacement u_{25} (44^{th} state) as output and the other from input torque (τ) to output angular position q (50^{th} state) as output.

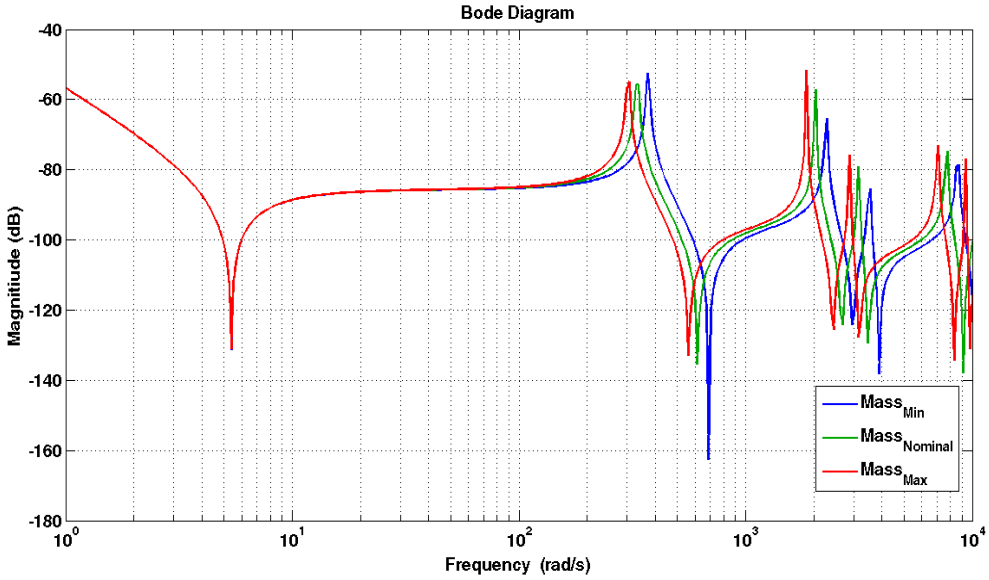

Fig 5.1: Frequency response of the linear model from input torque (τ) to output angular position (q) with $\pm 20\%$ uncertainty in mass density (m)

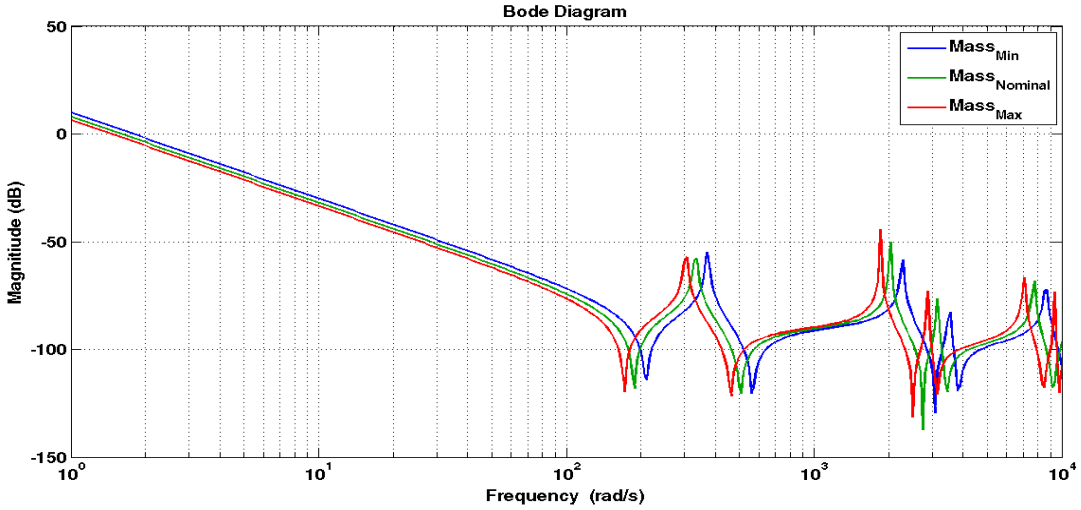

Fig 5.2: Frequency response of the linear model from input torque (τ) to output u_{25}(elastic displacement) with $\pm 20\%$ uncertainty in mass density (m).

Figure 5.1 and Figure 5.2 illustrate the frequency response of the linear models from input torque (τ) to output angular position (q) and input torque (τ) to output u_{25} (displacement) respectively, with $\pm 20\%$ uncertainty in the mass density. Regarding these figures, both systems have several resonance frequencies between the frequencies of 200 rad/sec and 10 rad/sec.

As can be seen from the Figure 5.1 and Figure 5.2, decreasing in the mass density results in higher aptitude in mechanism vibrations as well as operating in higher frequencies.

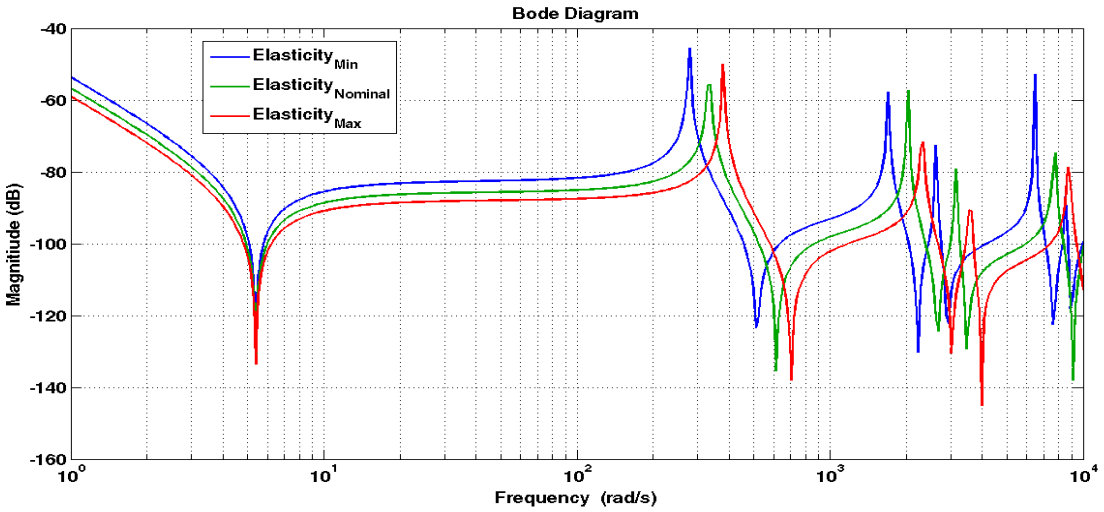

Fig 5.3: Frequency response of the linear model from input torque (τ) to output angular position (q) with $\pm 20\%$ uncertainty in elasticity (E).

Figure 5.3 and Figure 5.4 shows frequency response of the linear models with input torque (τ) to angular position (q) and input torque (τ) to output u_{25} (elastic displacement) with $\pm 20\%$ uncertainty in the elasticity respectively. As it can be seen from both diagrams, the sensitivity of both linear models increase by increment of the frequency however the sensitivity of the first linear model (from torque to angular position) is very small at low frequencies. Moreover, the amplitude of resonance frequencies decline by increasing of the frequency for the both models.

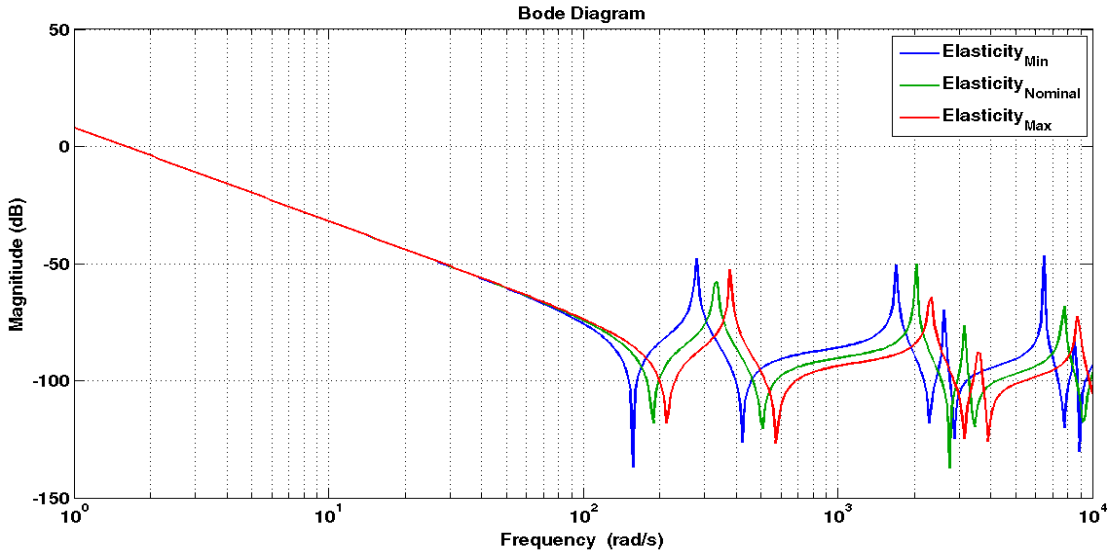

Fig 5.4: Frequency response of the linear model from input torque (τ) to output u_{25} (elastic displacement) with $\pm 20\%$ uncertainty in elasticity (E).

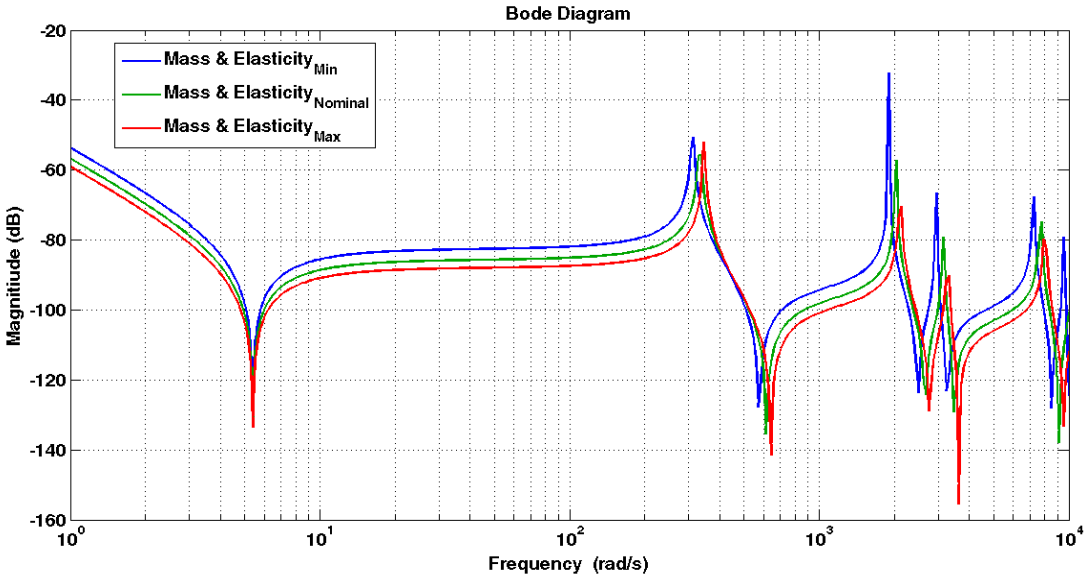

Fig 5.5: Frequency response of the linear model from input torque (τ) to angular position (q) with $\pm 20\%$ uncertainty in elasticity (E) and mass density (m).

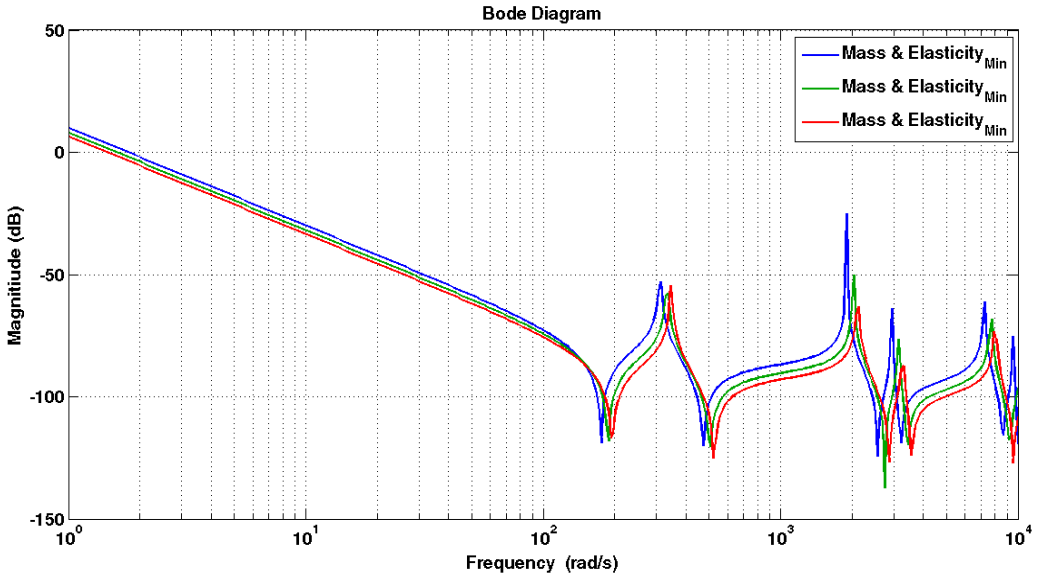

Fig 5.6: Frequency response of the linear model from input torque (τ) to output u_{25} (elastic displacement) with $\pm 20\%$ uncertainty in elasticity (E) and mass density (m).

The frequency response of the linear model from torque to angular position q and to elastic displacement of u_{25} as the system outputs with $\pm 20\%$ uncertainty in the elasticity (E) and mass density (m) are shown in Figure 5.5 and Figure 5.6 respectively. From both figures, it can be concluded that the sensitivity of these linear systems respect to variations in the elasticity (E) and mass density (m) is extended to the whole frequency range.

5.3 Linear Model Reduction

In order to apply modern control techniques such as H_∞ and LTR, linear controllers whose order are at least equal or higher to order of the models are used. Although the application of high-order controllers with the existence of advance microprocessors and microcontrollers is not a difficult task, the use of low-order controllers are still desirable for control designers due to practical issues.

The linear model extracted from Equation 2-33 has been reduced with the use of Hankel-Norm theory [83] which is briefly restated in this section. In control theory, the eigenvalues express the

stability of the system while the Hankel singular values demonstrate the energy of the system states. The Hankel singular values can be defined as follows:

$$\sigma_H = \sqrt{\lambda_i(PQ)} \tag{5-1}$$

Where P and Q are the controllability and observability Gramian matrix that satisfy:

$$AP + PA^T + BB^T = 0 \tag{5-2}$$

$$A^T Q + QA + C^T C = 0 \tag{5-3}$$

And (A, B, C, D) are state space matrices of the system. The Hankel singular values of the plant, computed by $Matlab^{TM}$, are shown in Figure 5.7.

Based on Figure.14, a model with order of 24 for estimating and obtaining an accurate reduced model is chosen since the extracted system has the most energy in the first 24 states and the states from 25 to 50 have been removed from calculations.

The algorithm based on Hankel singular values for reducing order of linear model can be described as follows:

If the quadratic stable transfer function $G(s)$ has the following Hankel singular values:

$$\sigma_1 \geq \sigma_2 \geq \cdots \geq \sigma_k \geq \sigma_{k+1} = \sigma_{k+2} = \cdots = \sigma_{k+1} > \sigma_{k+1+1} \geq \cdots \sigma_n > 0 \tag{5-4}$$

The k^{th} order of optimal Hankel-Norm of the transfer function of the plant can be shown as $G_a^k(s)$. If (A, B, C, D) are the matrices of state space equation form of $G(s)$ and are arranged based on Hankel singular values so the Gramian matrix of the system is:

$$\sum = diag(\sigma_1, \sigma_2, \dots, \sigma_k, \sigma_{k+l+1}, \dots, \sigma_{k+1}) = diag(\sum_1, \sigma_{k+l} I) \tag{5-5}$$

If we partition (A, B, C, D) with accordance of $\sum$, the following equation can be obtained:

$$A = \begin{bmatrix} A_{11} & A_{12} \\ A_{21} & A_{22} \end{bmatrix}, B = \begin{bmatrix} B_1 \\ B_2 \end{bmatrix} \text{ and } C = [C_1 \quad C_2] \tag{5-6}$$

And $(\hat{A}, \hat{B}, \hat{C}, \hat{D})$ can be defined as:

$$\hat{A} = \Gamma^{-1}(\sigma_{k+1}^2 A_{11}^T + \sum_1 A_{11} \sum_1 - \sigma_{k+1} C_1^T U B_1^T) \tag{5-7}$$

$$\hat{B} = \Gamma^{-1}(\sum_1 B_1 + \sigma_{k+1} C_1^T U) \tag{5-8}$$

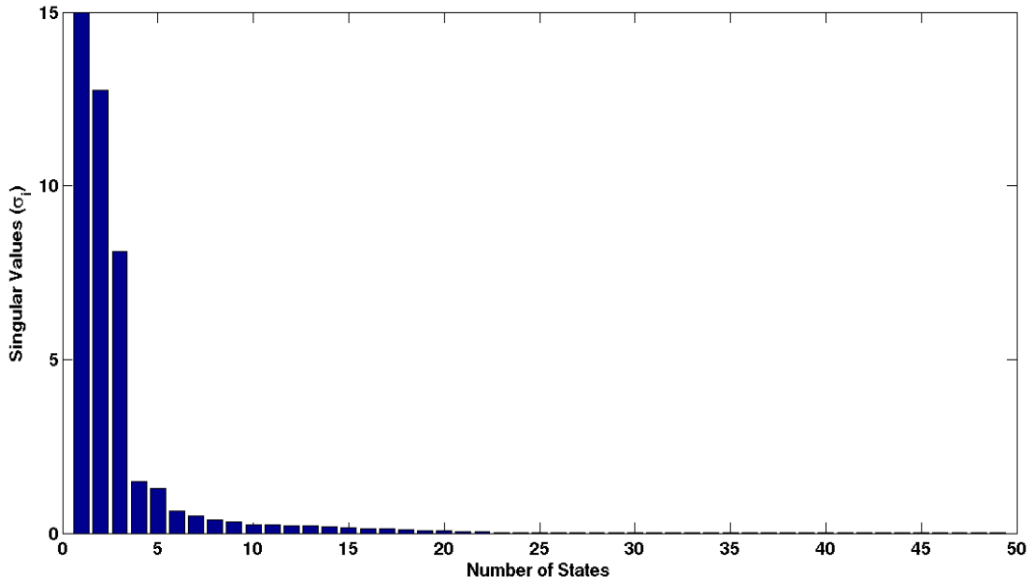

Fig 5.7: Hankel singular values of the linear model

$$\hat{C} = C_1 \sum_1 + \sigma_{k+1} U B_1^T \tag{5-9}$$

$$\widehat{D} = D - \sigma_{k+1} U \tag{5-10}$$

Where U is a singular matrix that satisfies the following equation:

$$B_2 = -C_2^T U \tag{5-11}$$

And

$$\Gamma = \sum_1^2 - \sigma_{k+1}^2 I \tag{5-12}$$

Where matrix $\hat{A}$ has k eigenvalues in the left side of complex plane and the rest of them are reminded in the right side; therefore:

$$G_a^k(s) + F(s) = \begin{bmatrix} \hat{A} & \vdots & \hat{B} \\ \cdots & \vdots & \cdots \\ \hat{C} & \vdots & \widehat{D} \end{bmatrix} \tag{5-13}$$

In which $G_a^k(s)$ is an estimation of k^{th} order of stable Hankel norm and $F(s)$ is transfer function of instability with the poles in right hand side of complex plan with order of $n - k - 1$. Hankel norm of the error between G and optimum estimation G_a^k is equal to $k + 1$ Hankel singular value of G:

$$\|G - G_a^k(s)\|_\infty = \sigma_{k+1}(G) \tag{5-14}$$

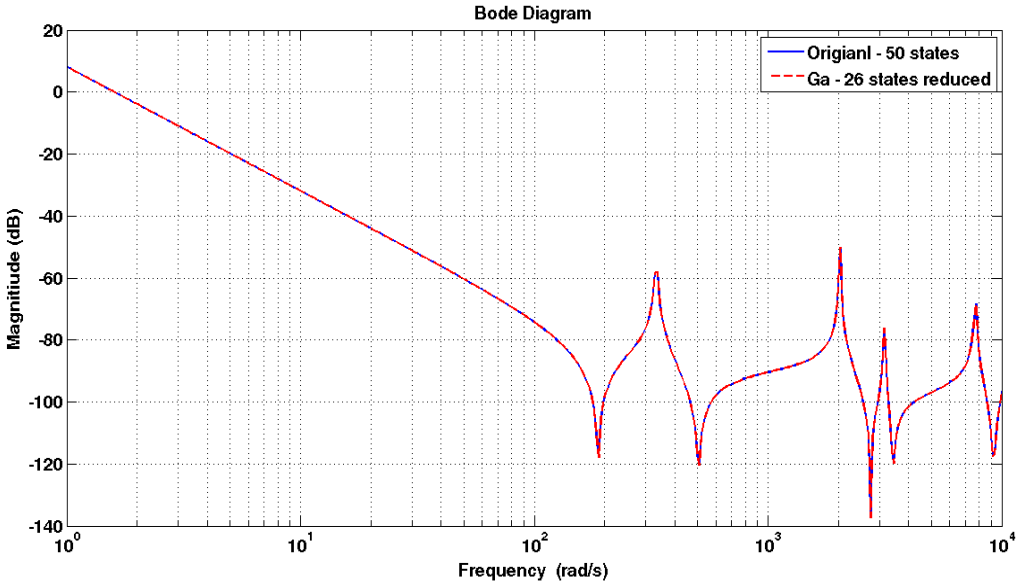

Fig 5.8: Bode diagram of the original model and reduced model from input torque (τ) to output angular position (q) with use of Hankel theory

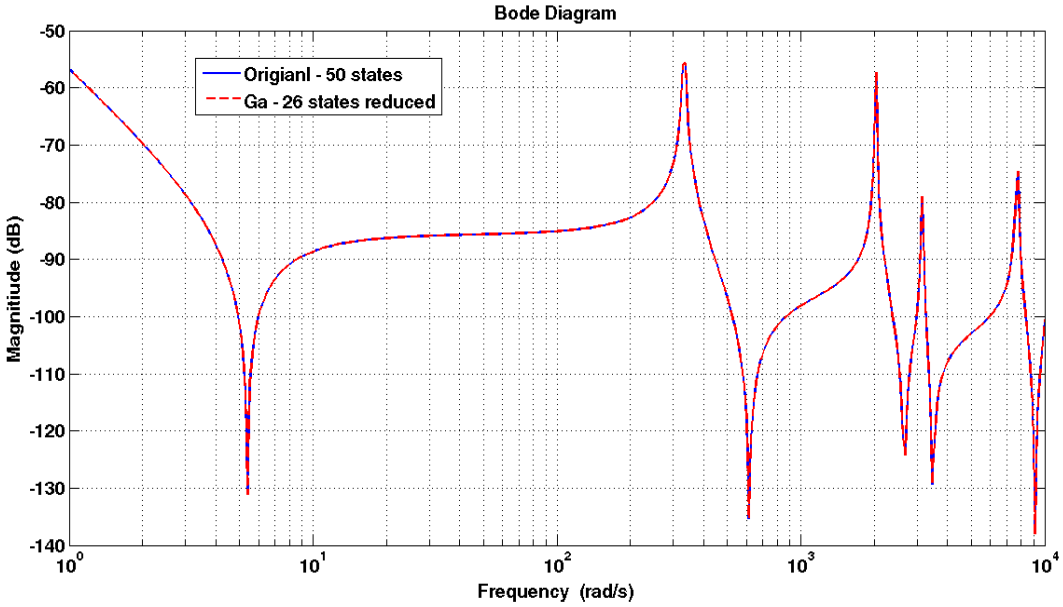

Fig 5.9: Bode diagram of the original model and reduced model from input torque (τ) to output u_{25} (elastic displacement) with use of Hankel theory

The frequency response of the model of the reduced linear system with input torque (τ) to output angular position (q) and u_{25} (elastic displacement) are shown Figure 5.8 and Figure 5.9 respectively.

According to Figure 5.8 and Figure 5.9 the diagram of frequency response of original linear models and state reduced models match each other very closely. Consequently, the reduced model can be a proper choice for the synthesis of robust control systems.

5.4 Synthesis of Robust Controller

A controller that has ability to assurance the performance of the system controlling respect to changes in plant dynamic within predefined variations is named robust controller. In this section, a brief description of H_∞ loop shaping and μ-synthesis is presented.

5.4.1 H_∞ Loop Shaping

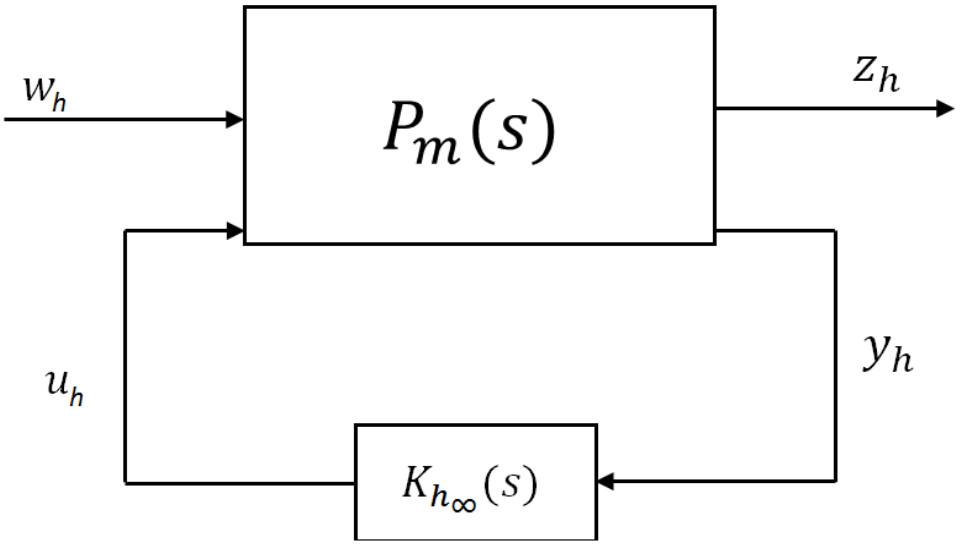

Fig 5.10: The standard H_∞ configuration

The basic idea of the design method is to construct the system $P_m(s)$ in the form of:

$$\begin{pmatrix} z_h \\ y_h \end{pmatrix} = \begin{pmatrix} P_{m_{11}}(s) & P_{m_{12}}(s) \\ P_{m_{21}}(s) & P_{m_{22}}(s) \end{pmatrix} \begin{pmatrix} w_h \\ u_h \end{pmatrix} = P_m(s) \begin{pmatrix} w_h \\ u_h \end{pmatrix} \quad (5\text{-}15)$$

By appending the open loop system $y_h = G_h(s)u_h$ with the weights $W_u(s)$,$W_S(s)$ and $W_T(s)$, the system $z_h = F_l(P_m, K_{h_\infty})w_h$ shown in Figure 5.10, can be expressed as:

$$F_l(P_m, K_{h_\infty}) = \begin{pmatrix} W_u(s)G_{wu}(s) \\ -W_T(s)T_{M_s}(s) \\ W_S(s)M_s(s) \end{pmatrix}, \tag{5-16}$$

Where $M_s(s) = (I + G_h(s)K_{h_\infty})^{-1}$ is the sensitivity function, $T_{M_s}(s) = I - M_s(s)$ is the complementary sensitivity function and $G_{wu}(s) = -K_{h_\infty}(I + G_h(s)K_{h_\infty})^{-1}$ is the transfer function from w_h to u_h.

Minimizing the H_∞-norm of the system $F_l(P_m, K_{h_\infty})$ brings up the H_∞-controller; In other words, $\|F_l(P_m, K_{h_\infty})\|_\infty < \gamma$. By using Equation (27), the following equations can be obtained:

$$\left|W_u(iw_f)G_{wu}(iw_f)\right| < \gamma \quad ,\forall w_f \tag{5-17}$$

$$\left|W_T(iw_f)T_{M_s}(s)(iw_f)\right| < \gamma, \forall w_f \tag{5-18}$$

$$\left|W_S(iw_f)M_s(iw_f)\right| < \gamma \quad ,\forall w_f \tag{5-19}$$

The transfer function $G_{wu}(s)$, M_s (s) and T_{M_s} (s) can now be employed for assuring the requirements by choosing the weights $W_u(s)$, $W_s(s)$ and $W_T(s)$ at each frequency ω_f. The goal is to achieve value of γ close to 1 because of achieving the robust stability. More details about designing approach are available in [84].

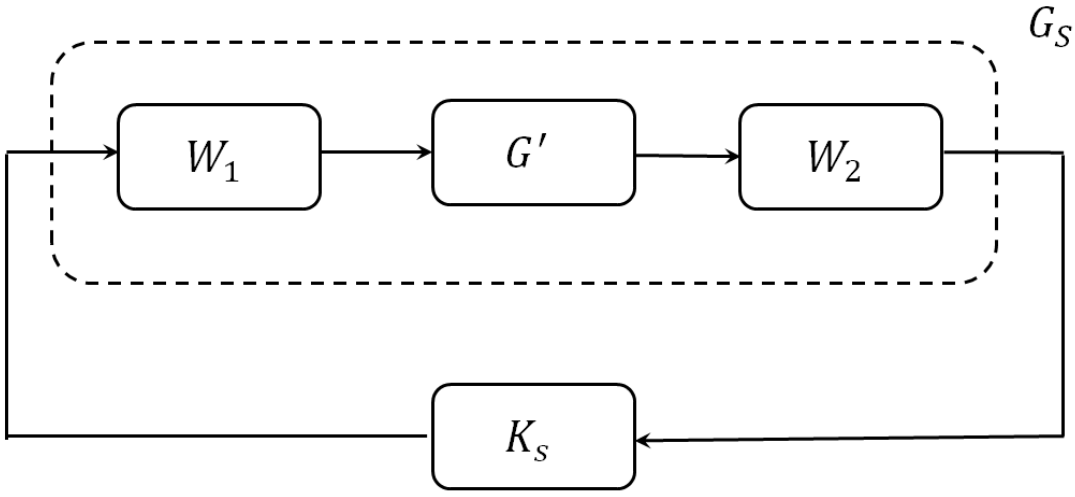

Fig 5.11: System description for loop shaping

Consequently, the system $G'(s)$ is pre-and post-multiplied with weights $W_1(s)$ and $W_2(s)$in standard H_∞ loop shaping [85]. As it can be seen from Figure 5.11, shaped system $G_s(s) = W_2(s)G'(s)\,W_1(s)$ has the desired properties. $K_s(s)$ can be acquired using the method described in [86] applied on the system $G'(s)$. Finally, the controller K_{h_∞} can be written as:

$$K_{h_\infty} = W_1(s)K_s(s)W_2(s) \tag{5-20}$$

System in Figure 5.10 for loop shaping can be reconstructed for a standard H_∞ problem with accordance of Figure 5.11, refer to [87] for more details.

5.4.2 μ-synthesis

A basic framework for robustness analysis of linear system is shown in Figure 5.12. Any linear interaction of control inputs u_c, measured output y_c, disturbance d', controlled outputs (error signals) e', perturbations $w_c = \Delta z_c$ and a controller K_c can be explained through this frame work.

The robust control problem can then be modelled to design and synthesize a controller K_c in the case that the perturbed closed loop system is stable and the error signal e' is hold "small" in the presence of disturbance d' and perturbations w_c.

The general framework analysis and synthesis can be subdivided into two special cases as depicted in Figure 5.12 such that scaling and weights are involved into the transfer function N_c in order to consider the normalization of d', e' and Δ to norm of 1. The transfer function F_u from d' to e' for purpose of robust analysis may be partitioned as linear fractional transformation as follows:

$$e' = F_u(M_c, \Delta)d' = \left[M_{c_{22}} + M_{c_{21}}\Delta(I - M_{c_{11}}\Delta)^{-1}M_{c_{12}}\right]d' \tag{5-21}$$

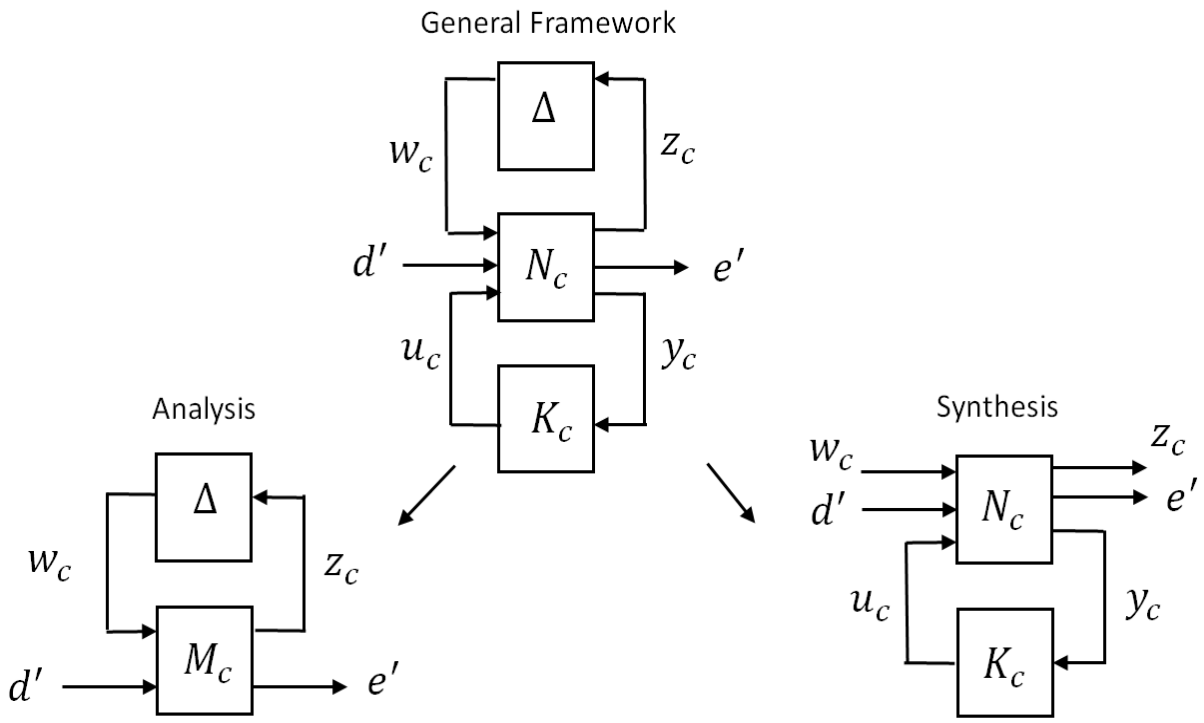

Fig 5.12: The basic framework with emphasis on analysis and synthesis [88]

Here Δ is a member of the bounded subset:

$$\mathbf{B}_s\mathbf{\Delta} = \{\Delta \in \mathbf{\Delta} | \bar{\sigma}(\Delta) < 1\} \tag{5-22}$$

Where $\bar{\sigma}$ specifies the largest singular value and $\mathbf{\Delta}$ is expressed by:

$$\mathbf{\Delta} = \{\mathrm{diag}\left(\delta_1^{\mathrm{r}}\mathrm{I}_{\mathrm{r}1}, \dots, \delta_{\mathrm{m_r}}^{\mathrm{r}}\mathrm{I}_{\mathrm{r_{m_r}}}, \delta_1^{\mathrm{c}}\mathrm{I}_{\mathrm{r_{m_r+1}}}, \dots, \delta_{\mathrm{m_c}}^{\mathrm{c}}\mathrm{I}_{\mathrm{r_{m_r+m_c}}}, \Delta_1, \dots, \Delta_{\mathrm{n}}\right) | \delta_{\mathrm{i}}^{\mathrm{r}} \in \mathfrak{R}, \delta_{\mathrm{i}}^{\mathrm{c}} \in \mathfrak{J}, \Delta_j \in \mathfrak{J}^{r_{m_r+m_c+j} \times r_{m_r+m_c+j}}\} \tag{5-23}$$

Defining also the corresponding complex perturbation set $\mathbf{\Delta}_c$ as:

$$\mathbf{\Delta}_{\mathrm{c}} = \{\mathrm{diag}(\delta_1^{\mathrm{c}}\mathrm{I}_{\mathrm{r}_1}, \dots, \delta_{\mathrm{m_r+m_c}}^{\mathrm{c}}\mathrm{I}_{\mathrm{r_{m_r+m_c}}}, \Delta_1, \dots, \Delta_{\mathrm{n}} | \delta_{\mathrm{i}}^{\mathrm{c}} \in \mathfrak{J}, \Delta_{\mathrm{j}} \in \mathfrak{J}^{r_{m_r+m_c+j} \times r_{m_r+m_c+j}}\} \tag{5-24}$$

The definition of the positive real-valued function μ is as follows:

$$\mu_\Delta(M_c) \triangleq \frac{1}{\min\{\bar{\sigma}(\Delta): \Delta \epsilon \mathbf{\Delta}, \det(\mathrm{I} - \mathrm{M}_c\Delta) = 0\}} \tag{5-25}$$

Unless no $\Delta \epsilon \mathbf{\Delta}$ forms $I - M_c\Delta$ singular, in which case $\mu_\Delta(M_c) = 0$.

Regarding multiple local maxima because of the implementation of the optimized problem, Equation 5-25 is not a proper choice for computing μ. Though upper and lower bounds for μ might be calculated for both complex and mixed perturbation sets effectively. Several algorithms

have been presented in the literature for computing these bounds [89], [90]. Evaluating robust stability and robust performance now may be done by following two theorems:

Theorem 5.3.2.1: The controlled system is stable for all $\Delta \in \mathbf{B}_{\boldsymbol{s}}\boldsymbol{\Delta}$ iff:

$$\left\|\mu_{\boldsymbol{\Delta}}(M_{c_{11}})\right\|_{\infty} \leq 1 \tag{5-26}$$

Where:

$$\left\|\mu_{\boldsymbol{\Delta}}(M_{c_{11}})\right\|_{\infty} \triangleq \sup_{w_f} \mu\left(M_{c_{11}}(jw_f)\right) \tag{5-27}$$

Theorem 5.3.2.2: Taking into consideration a H_∞ performance specification given on the transfer function from d' to e' which is a type of weighted sensitivity function in the form of:

$$\|F_u(M_c, \Delta)\|_{\infty} = \sup_{w} \bar{\sigma}\left(F_u(M_c, \Delta)\right) < 1 \tag{5-28}$$

Hence $F_u(M_c, \Delta)$ is stable and $\|F_u(M_c, \Delta)\|_{\infty} < 1 \; \forall \Delta \in \mathbf{B}_{\boldsymbol{s}}\boldsymbol{\Delta}$ iff

$$\|\mu_{\tilde{\Delta}}(M_c)\|_{\infty} \leq 1 \tag{5-29}$$

Where the perturbation set is appended via a full complex performance block:

$$\tilde{\boldsymbol{\Delta}} = \{\mathrm{diag}(\Delta, \Delta_p) | \Delta \in \boldsymbol{\Delta}, \Delta_{\boldsymbol{p}} \in \mathfrak{F}^{\boldsymbol{k}\times\boldsymbol{k}}, \bar{\sigma}\left(\Delta_p\right) < 1\} \tag{5-30}$$

Theorem 5.3.2.2 is the real payoff for performance measurement with reference to the ∞-norm and the uncertainty in the bounding model similarly. There is the possibility of evaluating both the robust stability and the robust performance in a neoconservative manner by using μ. Indeed, if the uncertainty is modelled precisely by Δ, i.e. if all plants in the norm-bounded set can actually take place in practice, the μ condition satisfies the necessity and sufficiency of the robust performance [88] .

5.5 Results

The reduced linearized model, obtained in section. 5.2, can be used to design H_∞ loop shaping and μ-synthesis controller. The performance of mentioned robust controllers on the mechanism considering $\pm 20\%$ uncertainty in the elasticity (E) and mass density (m) of the system has been investigated in this section. $Matlab^{TM}$ Software has been used in this work in order to synthesize the controllers.

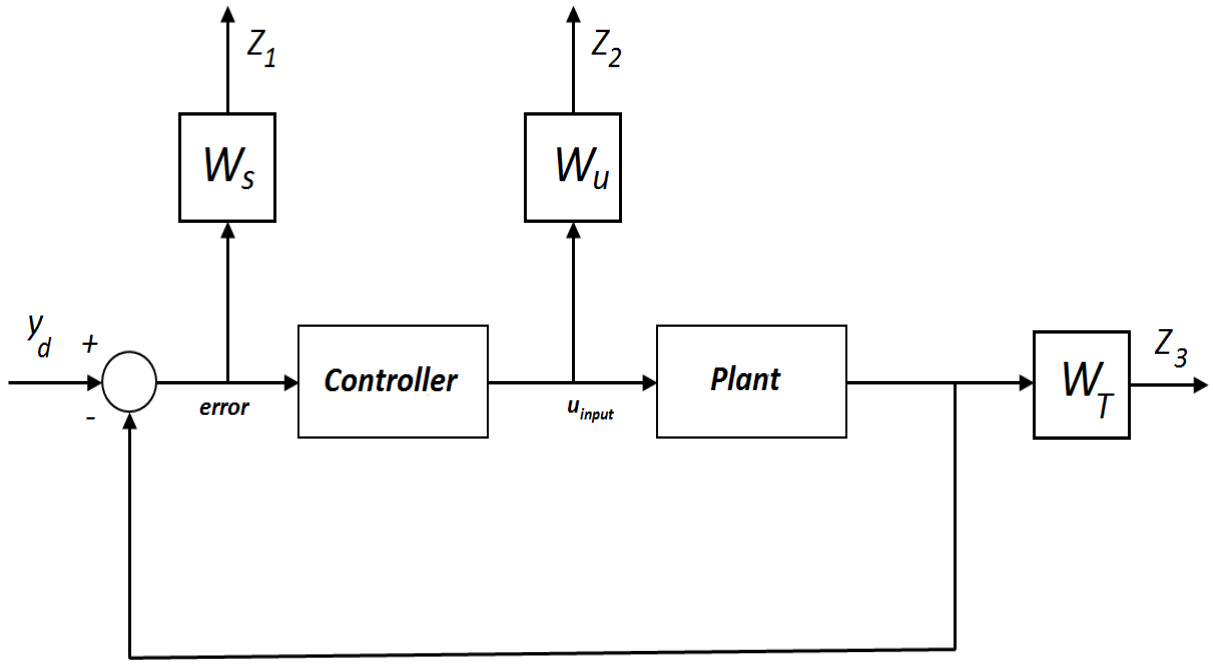

Fig 5.13: Common block diagram of the setting weight functions for a robust controller

5.5.1 Design of H_∞ Loop Shaping Controller

In this section, synthesis of H_∞ loop shaping controller for applying on a spatial flexible L-shape mechanism has been discussed. The goal is to achieve a controller that guarantee not only robust stability but also proper performance, it is worth to mention that weighting function $W_s(s)$ and $W_T(s)$ represent sensitivity and complimentary sensitivity function respectively and determine the behavior of the system. Furthermore, $W_u(s)$ is the control effort weighting function and is related to the amplitude of input signal to plant. These weighting functions are chosen as follows:

$$W_s(s) = \begin{bmatrix} 0.025\frac{(s+5)}{(s+0.05)} & 0 \\ 0 & 0.025\frac{(s+5)}{(s+0.05)} \end{bmatrix} \quad (5\text{-}31)$$

$$W_T(s) = \begin{bmatrix} 2\frac{(s+1)}{(s+100)} & 0 \\ 0 & 2\frac{(s+1)}{(s+100)} \end{bmatrix} \quad (5\text{-}32)$$

$$W_u(s) = \begin{bmatrix} 10^{-3}\frac{(s+0.1)}{(s+1)} \\ 10^{-3}\frac{(s+0.1)}{(s+1)} \end{bmatrix} \quad (5\text{-}33)$$

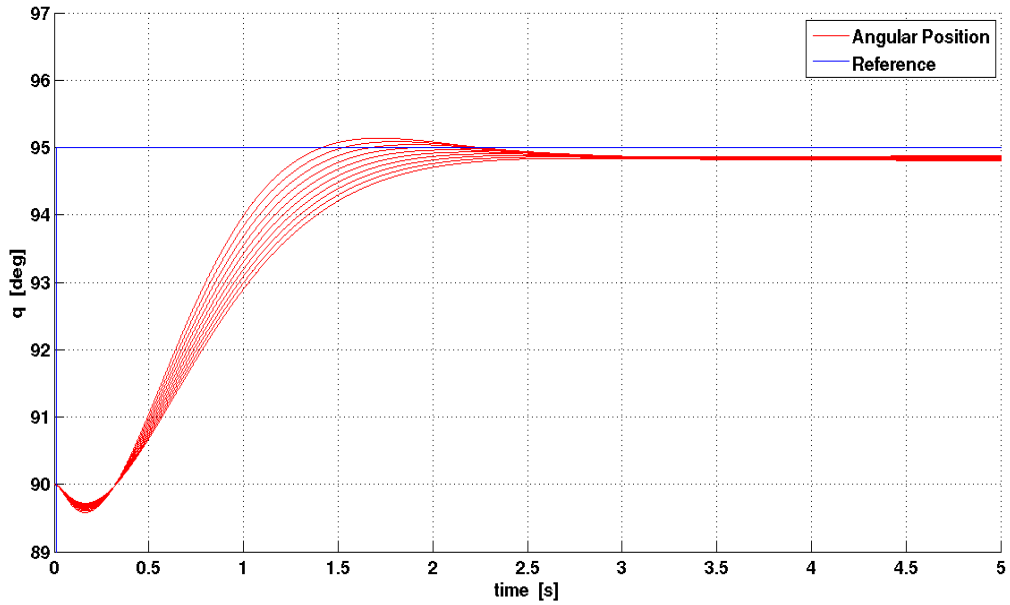

Fig 5.14: Step response of the angular position q considering $\pm 20\%$ uncertainty in elasticity (E) and mass density (m) with use of H_∞ loop shaping controller

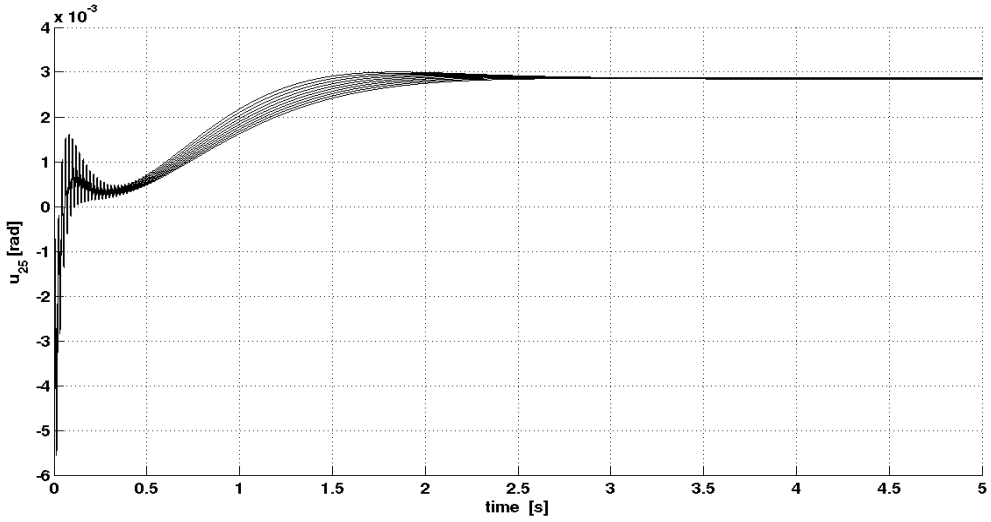

Fig 5.15: Step response of the elastic displacement u_{25} considering uncertainty and disturbance with use of H_∞ loop shaping controller

Figure 5.14 shows the step response of the closed loop system in terms of angular position with $\pm 20\%$ uncertainty on the elasticity (E) and mass density (m). It can be clearly seen that the angular position is tracked with high accuracy and high speed.

Figure 5.15 shows the response to the same test in terms of elastic displacement u_{25}. As it can be seen, elastic vibration are very effectively damped. However, u_{25} cannot reach zero value, due to the effects of the gravity.

5.5.1.2 Response of H_∞ Loop shaping to Disturbance

In this section the response of synthesized H_∞ loop shaping controller to disturbance in the closed loop system have been discussed. One pulse signal with amplitude of 30 $m\,rad$, pulse width of 5 sec and 15 sec time delay has been added to the measurement of the angular position q during mechanism maneuverer. Figure 5.16 and Figure.24 demonstrate the effect of the disturbance to plant output on the angular position q and on the elastic displacement u_{25} respectively. It can be inferred from Figure.23 and Figure.24 that the controller has clearly attenuated the effect of the disturbance while retaining not only precise tracking performance but also proper vibration damping.

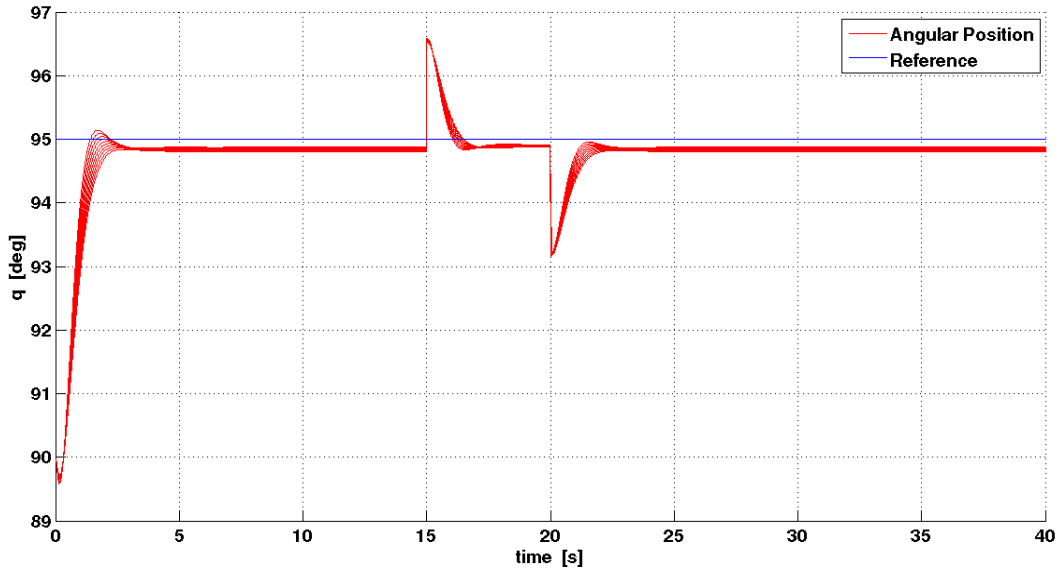

Fig 5.16: Step response of the angular position q considering uncertainty and disturbance with H_∞ loop shaping controller in closed loop system

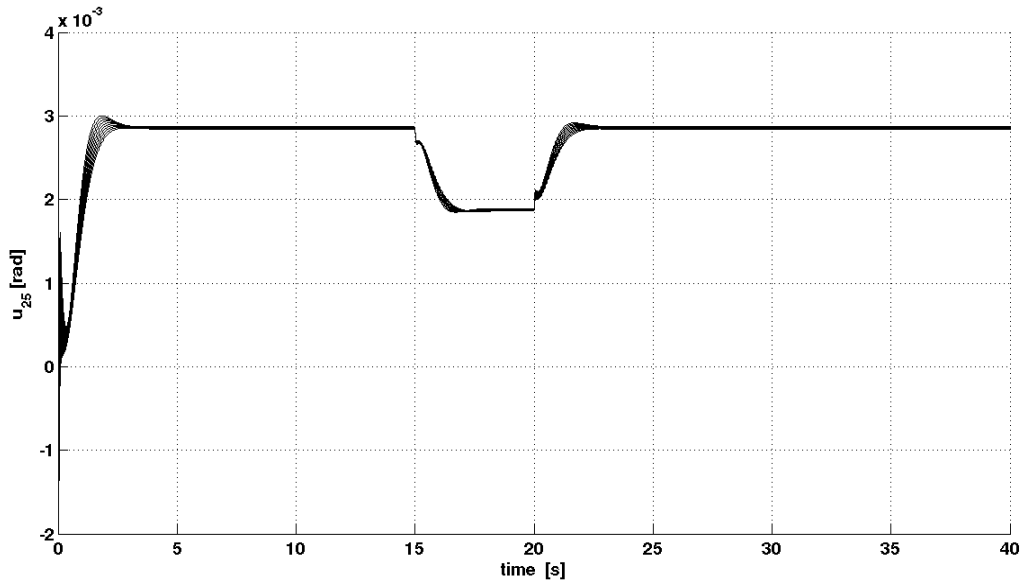

Fig 5.17: Step response of the elastic displacement u_{25} considering uncertainty and disturbance with H_∞ loop shaping controller in closed loop system

5.5.2 Design of the μ-Synthesis Controller

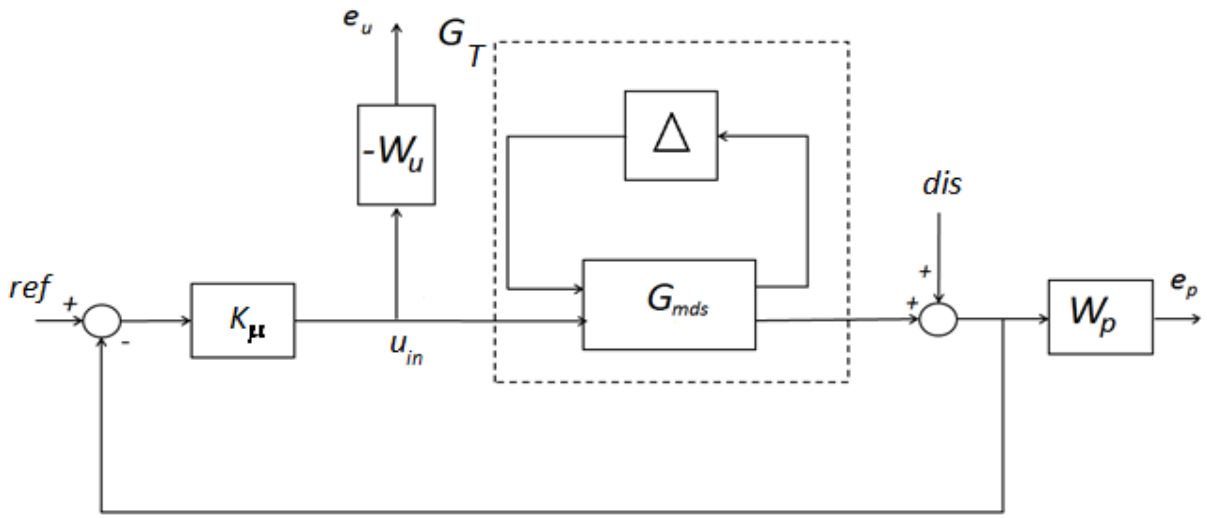

Fig 5.18: Structure of closed-loop system for μ-Synthesis controller

The block diagram of the closed-loop system used in the μ-Synthesis is depicted in Figure 5.18. According to the explanation reported in Section 2.3 and Section 2.4, the linear plant model of the flexible L-shape mechanism has 50 states, 2 outputs and one inputs (SIMO). Uncertainties (in the form of parameter variations) are considered on elasticity (E) and mass density (m) with $\pm 20\%$ variation for all the links of the mechanism.

Being $P_{tf}(s)$ the transfer function matrix of the input and two outputs of the open loop system and considering block structure of the uncertainty matrix Δ_p is specified as:

$$\Delta_p := \left\{ \begin{bmatrix} \Delta & 0 \\ 0 & \Delta_F \end{bmatrix} \right\} : \Delta \in \Re^{7\times 7}, \Delta_F \in \Im^{2\times 3} \tag{5-34}$$

The first block Δ of the matrix Δ_p is diagonal and corresponds to the parametric uncertainties in the flexible mechanism. Another diagonal block, Δ_F is a fictitious uncertainty block, which is used to introduce the performance requirements in the μ-Synthesis design framework. Stabilizing controller $K_\mu(s)$ is a necessary condition to assure robust performance. Based on that, at each frequency ω_f over the relevant frequency range, the following equation of the structured singular value must holds:

$$\mu_{\Delta p}\left[F_L\left(P_{tf}, K_\mu\right)\left(j\omega_f\right)\right] < 1 \tag{5-35}$$

The robust performance of the closed-loop system can be guaranteed with above condition [91] .

In our system the perturbation parameter and weighting functions are chosen as follows:

$$\Delta = \frac{1}{s} \tag{5-36}$$

$$W_u = \begin{bmatrix} 0.4\times 10^{-3}\,\frac{100s+0.05}{s+10} \\ 0.4\times 10^{-3}\,\frac{100s+0.05}{s+10} \end{bmatrix} \tag{5-37}$$

$$W_p = \begin{bmatrix} 0.15\,\frac{s^2+1.8s+5}{(s+0.001)(0.01s+1.2)(s+1)} & 0 \\ 0 & 0.15\,\frac{s^2+1.8s+5}{(s+0.001)(0.01s+1.2)(s+1)} \end{bmatrix} \tag{5-38}$$

Results of the μ-Synthesis on the spatial flexible mechanism have been demonstrated in following figures. Figure 5.19 and Figure 5.20 show the step response of angular position q and

elastic displacement u_{25} with $\pm 20\%$ uncertainty in the elasticity (E) and mass density (m) values respectively.

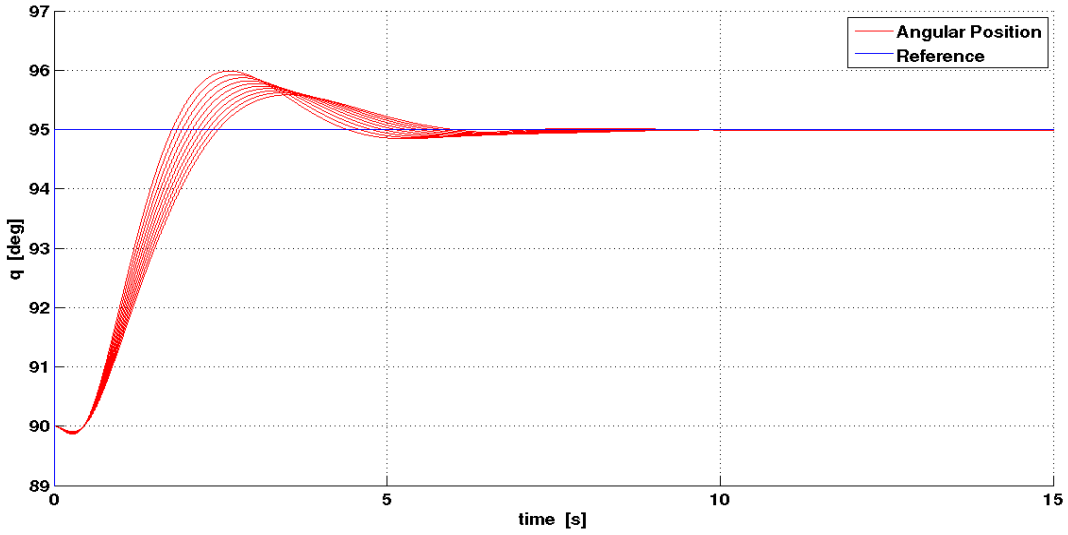

Fig 5.19: Step response of the angular position q considering $\pm 20\%$ uncertainty in elasticity (E) and mass density (m) with μ-Synthesis controller

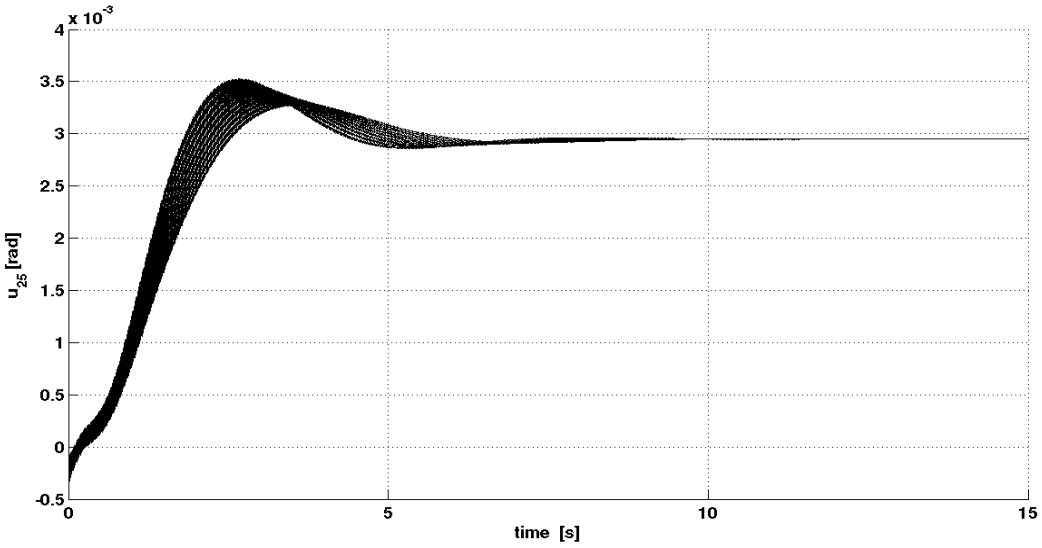

Fig 5.20: Step response of the elastic displacement u_{25} considering $\pm 20\%$ uncertainty in elasticity (E) and mass density (m) with μ-Synthesis controller

According to Figure 5.19, angular position of the mechanism starts from the vertical position (90 degree) and moves to reference position (95 degrees). As it can be seen, the flexible mechanism has a desired maneuverer with overshoot near to 30 % and approximate settling time of 8 sec. From Figure 5.20, it can be seen that the amplitude of the vibration is small during the mechanism motion and the existence of steady state error is due to the gravity force.

5.5.2.1 Response of the μ-Synthesis to Disturbance

In order to evaluate the disturbance rejection μ-Synthesis controller, a test similar to the one developed in section 5.4.1.2 has been done in this section. The amplitude, pulse width and time delay of the disturbance signals are equal to previous ones. The results are depicted in Figure 5.21 and Figure 5.22 for both angular position q and elastic displacement u_{25} .

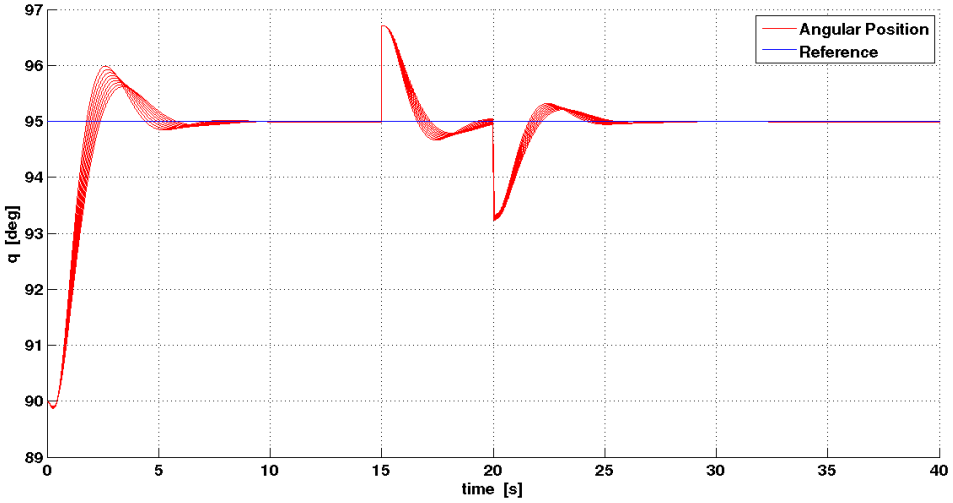

Fig 5.21: Step response of the angular position q considering disturbance signal and $\pm 20\%$ uncertainty in elasticity (E) and mass density (m) with μ-Synthesis controller

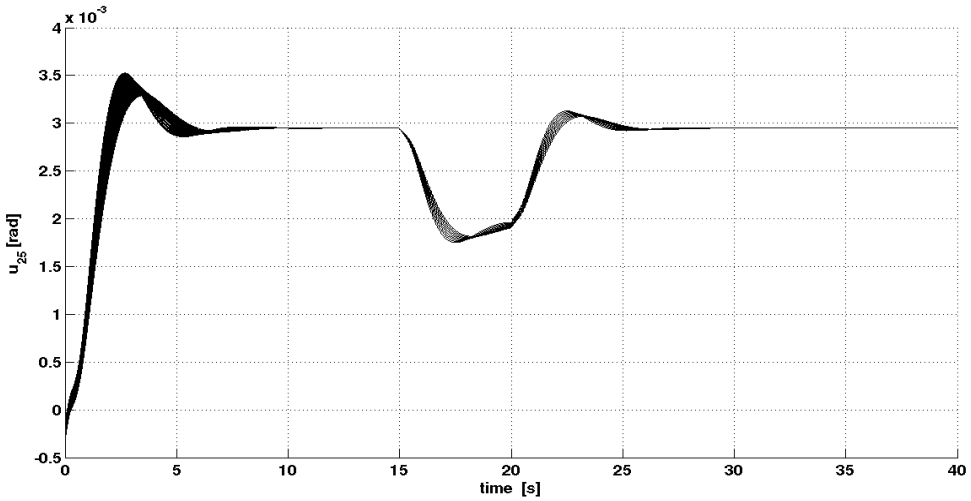

Fig 5.22: Step response of the elastic displacement u_{25} considering disturbance signal and $\pm 20\%$ uncertainty in elasticity (E) and mass density (m) with μ-Synthesis controller

As it can be seen from the above figures, the μ-Synthesis controller has attenuates the disturbance effect properly for both angular position and elastic displacement and the steady state error of disturbance signal is close to zero.

5.6 Comparison between Controllers

This section reports a comparative analysis of the robust performance of the synthesized controllers for the spatial flexible mechanism through the μ-analysis and the frequency response.

5.6.1 Comparison through μ-analysis

The result of the μ-analysis on the two controllers is shown in Figure 5.23. As it can be inferred from Figure 5.23, the μ-Synthesis controller guarantees robust performance of the system in wider frequency range since the gain of the μ-Synthesis controller is less than one for all range of frequencies except 2-10 rad/sec; however, the H_∞ loop shaping controller has better robust performance at low frequencies.

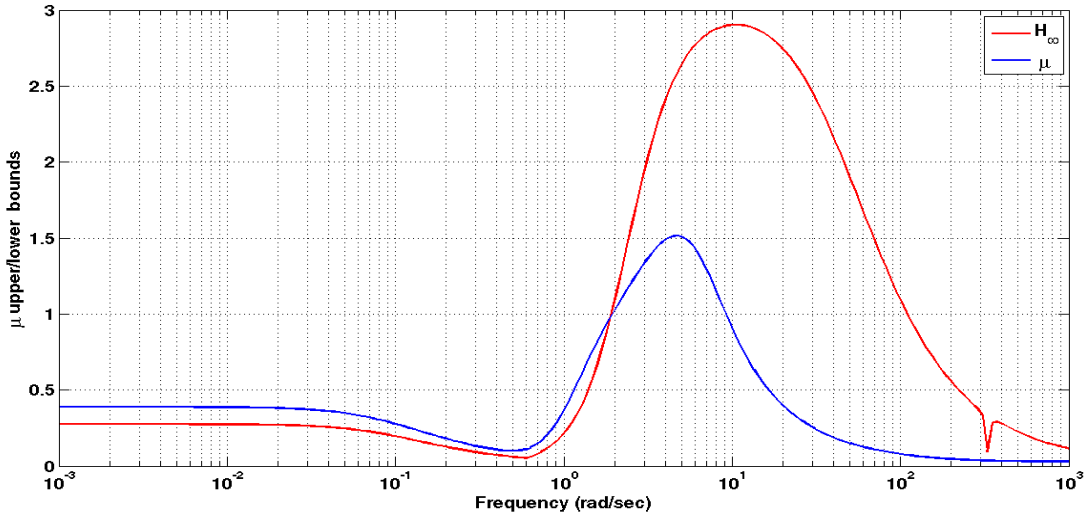

Fig 5.23: Robust performance of the synthesized controllers through μ-analysis

5.6.2 Comparison through Frequency Response

In order to make a comparison among the controllers, their frequency response have been evaluated here. It should be mentioned that controller for the linear plant from torque (input) to angular position (output) has been taken into account. Regarding Figure 5.24, the controller gain for H_∞ loop shaping is higher than the gain of the μ-Synthesis controller for frequencies, which results in higher controller effort and more precise tracking.

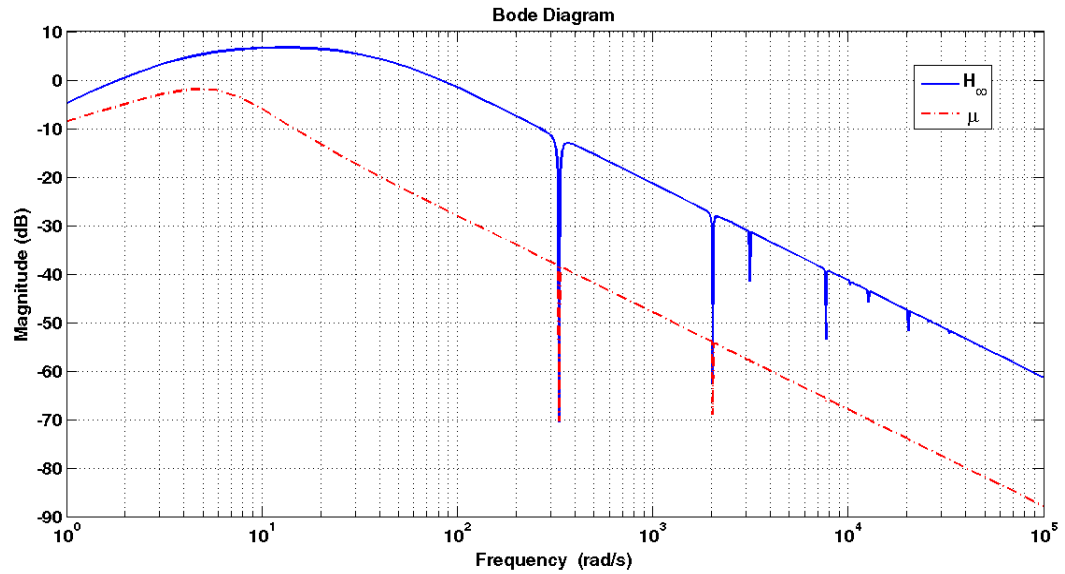

Fig 5.24: Robust performance of the synthesized controllers through frequency response

5.7 Conclusion

In this chapter the synthesis of two robust controllers for a spatial L-shape flexible mechanism, which has been modelled with high accuracy FEM-based approach, has been investigated and presented. The model has been implemented $MATLAB^{TM}$ simulation environment for the purpose of testing robust controllers, namely H_∞ loop shaping and μ-synthesis, for both position control and vibration damping in a spatial flexible L-shape mechanism under gravity. In order to implement the robust controller, a linearization procedure and model reduction of linearized model for state-space model of the dynamic system has been developed. These linearized and reduced models demonstrate highly precision approximation of mechanism dynamic behaviour. The H_∞ loop shaping and μ-Synthesis robust controllers have been employed for controlling both the position and the vibrations of the flexible mechanism. The optimal performance of each controller considering $\pm 20\%$ uncertainty in the elasticity (E) and mass density (m) and perturbed plant for μ-Synthesis have been tested. Finally, the performance of these controllers have been compared to each other through μ-analysis and frequency analysis. The μ-Synthesis has proved to have a good level of robustness to uncertainties and can compensate the first two resonant frequencies; moreover, the H_∞ loop shaping requires a higher control effort but also provides faster position tracking and has ability dampen the first six resonance frequencies.

CHAPTER 6

Hybrid Position/Force Control

6.1 Introduction

For some specific tasks by robot manipulators, such as moving payloads or painting objects, position controllers provides enough performance because these types of tasks only need the manipulator to follow a desired trajectory. Although, during grinding or an assembly task, the robot manipulator comes in contact with the environment; consequently, interaction forces appear between the robot manipulator and the environment. Therefore, these interaction forces, as well as the end effector position, should be controlled.

To motivate the need of the combination of force and position control, consider the problem of controlling a manipulator to write a sentence on a blackboard. To shape the letters in the sentence, the end-effector position or, equivalently, the position of the chalk should be controlled. Regarding to the experience of writing on a blackboard, the force with which one presses on the blackboard must also be controlled. That is, pressing too lightly can cause letters that are not easily readable, while pressing too hard can result in broken chalk. This example shows that many robotic applications will need that a desired positional trajectory and a desired force trajectory must be defined. In this chapter, the hybrid position/force control for the spatial L-shape flexible mechanism in order to control the manipulator end-effector position based on the applied eternal force.

The main concept of hybrid position/force control is based on subjecting the end effector of the manipulator to external constraints which are experienced in the form of interaction forces when the manipulator interacts with the environment. Accordingly, interaction forces should be accommodated rather than resisted which occur in disturbance compensator [92] so the control approach should handle tracking error properly to improve the contact.

6.2 External Force Estimation

In order to develop a hybrid position/force control for the L-shape mechanism, an external force measurement or estimation is required. Often force/torque sensors mounted at the robot wrist are used for this task [93]. Some approaches for force estimation by means of the signals obtained from strain measurements have been presented [94] as well.

In this section, an approach to the external force estimation based on the comparison between the motion of the flexible mechanism and its rigid counterpart is presented. Figure 6.1 shows a schematic view of the proposed approach. As it can be seen from Figure 6.1, while the external force and torque produced by the electrical motor are applied to the flexible mechanism, only the torque produced by the electrical motor is applied to the rigid mechanism; furthermore, joint accelerations of both of the mechanisms are measured and compared to each other. It should be mentioned that the main assumption in this work is considering the external force applies to the tip of the mechanism along the tangential direction of the first link motion.

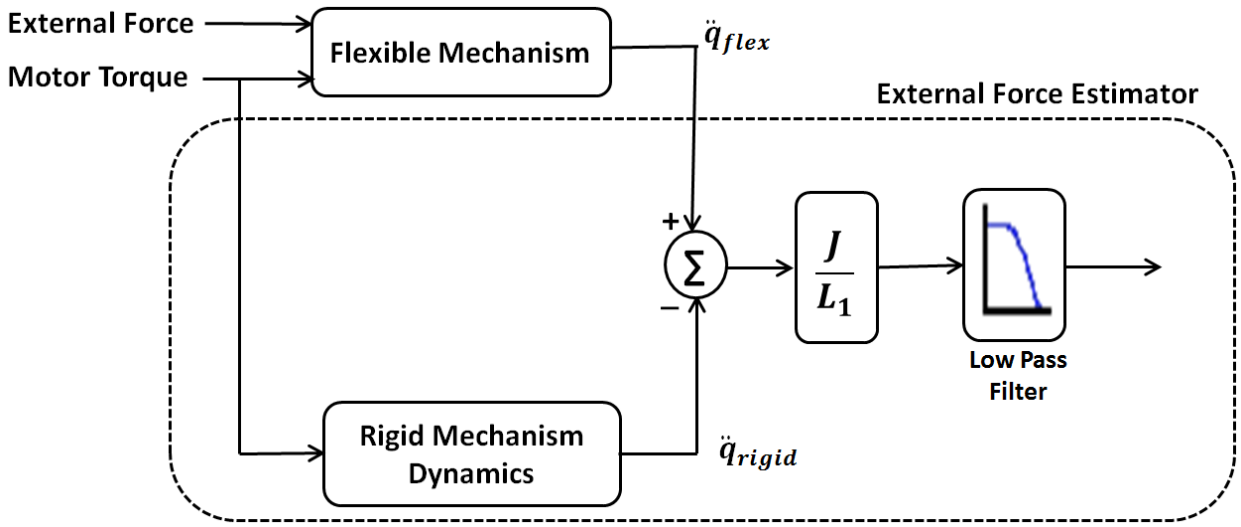

Fig 6.1: Schematic view of the external force estimation approach

By assuming that the external force is applied on the tip of the mechanism along the tangential direction of the first link motion, the dynamic model states in Equation 6-1, can be rewritten as:

$$\boldsymbol{M}_{ERLS}(q,\dot{q})\begin{bmatrix}\ddot{\boldsymbol{u}}\\ \ddot{q}_{flex}\end{bmatrix} = \boldsymbol{A}(\boldsymbol{u},\dot{\boldsymbol{u}},q,\dot{q})\begin{bmatrix}\dot{\boldsymbol{u}}\\ \dot{q}\\ \boldsymbol{u}\end{bmatrix} + \boldsymbol{B}(q,\dot{q})\begin{bmatrix}\boldsymbol{g}\\ \boldsymbol{f}\end{bmatrix} \tag{6-1}$$

So that:

$$\begin{bmatrix}\ddot{\boldsymbol{u}}\\ \ddot{q}_{flex}\end{bmatrix} = \boldsymbol{M}_{ERLS}^{-1}(q,\dot{q})\boldsymbol{A}(\boldsymbol{u},\dot{\boldsymbol{u}},q,\dot{q})\begin{bmatrix}\dot{\boldsymbol{u}}\\ \dot{q}\\ \boldsymbol{u}\end{bmatrix} + \boldsymbol{M}_{ERLS}^{-1}(q,\dot{q})\boldsymbol{B}(q,\dot{q})\begin{bmatrix}\boldsymbol{g}\\ \boldsymbol{f}\end{bmatrix} \tag{6-2}$$

Equation 6-2 is the explicit from of the flexible mechanism dynamic model, which can be used

to evaluate the joint acceleration ($\ddot{\boldsymbol{q}}_{flex}$). The vector of external forces ($\boldsymbol{f}$) in Equation 6-1 includes both the torque (τ_m) provided by the actuator and the external force (f_{ext}) applied on the tip of the mechanism.

The dynamics of the rigid counterpart of the flexible mechanism is represented by following expression:

$$J\ddot{q}_{rigid} = \tau_m \tag{6-3}$$

In the equation above, $\ddot{q}_{rigid}$ accounts for the joint acceleration of the rigid link-mechanism. According to Equation 6-2, joint acceleration $\ddot{q}_{flex}$ can be expressed as:

$$\ddot{q}_{flex} = \boldsymbol{f}(q, \dot{q}, \boldsymbol{u}, \dot{\boldsymbol{u}}, \tau_m, f_{ext}) \tag{6-4}$$

By neglecting the effects of flexibility in Equation 6-4, $\ddot{q}_{flex}$ can be written as:

$$\ddot{q}_{flex} \simeq \frac{1}{J}\tau_m + \frac{1}{J}L_1 f_{ext} \tag{6-5}$$

where L_1 is the length of the first link and J represents the moment of inertia of the mechanism.

Finally, an estimation of the external force $\hat{f}_{ext}$ acting on the tip of the mechanism along the tangential direction can be achieved by comparing $\ddot{q}_{flex}$ and $\ddot{q}_{rigid}$ as follows:

$$\hat{f}_{ext} = \left(\ddot{q}_{flex} - \ddot{q}_{rigid}\right).\frac{J}{L_1} \tag{6-6}$$

When neglected, link flexibility can lead to large estimation errors [95]. Figure 6.2 illustrates the comparison between the actual and the estimated force applied on the tip of the mechanism along the tangential. It can be clearly seen that a pronounced error is introduced by the neglected flexibility of the estimation model. Therefore, a second order low pass filter with cut-off frequency of 20 rad/s has been used to improve the accuracy of the external force estimation.

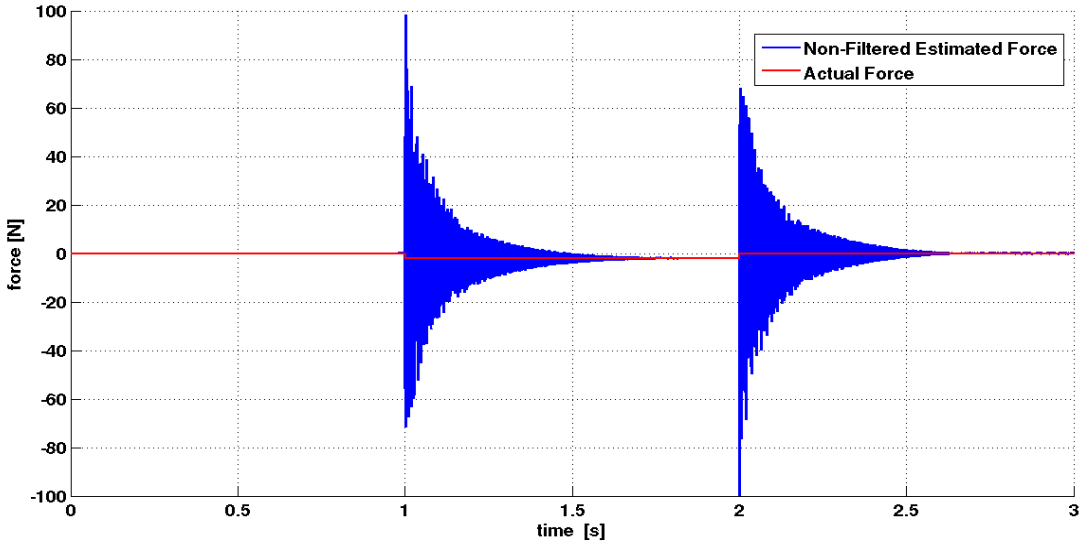

Fig 6.2: Comparison between non-filtered estimated and actual external force applied on the tip of mechanism

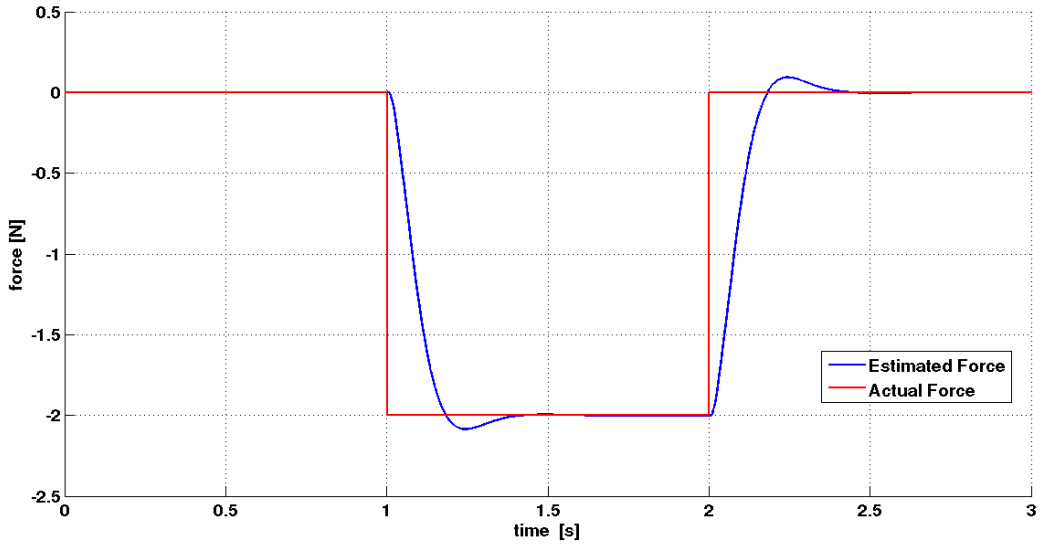

Fig 6.3: Comparison between estimated and actual external force applied on the tip of mechanism

Figure 6.3 shows a comparison of the estimated and actual force applied on the tip of mechanism when using a low pass filter. The lagging difference between two curves is due to the low-pass filtering action included in the force estimator.

6.3 Hybrid Position/Force Control

In this section a short description of the hybrid position/force control for the L-shape flexible mechanism is given. Hybrid position/force control combines position and force data into the control loop, for moving the mechanism in a nondeterministic environment. The main advantages of hybrid control is that the position and force data are analyzed independently to benefit of well-known control approach for each one [96].

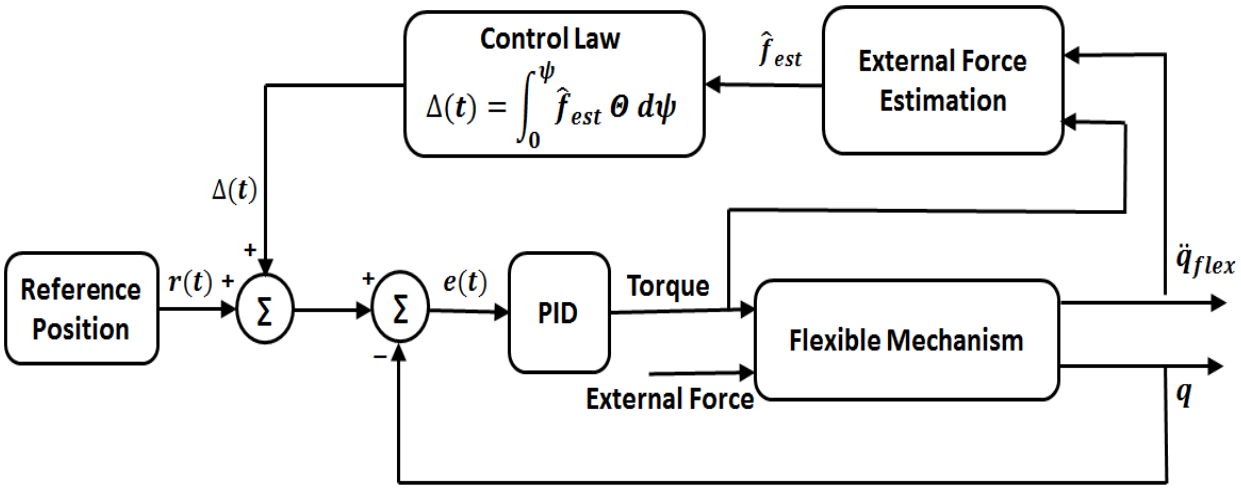

Fig 6.4: Hybrid position/force control scheme for spatial L-shape flexible mechanism

The block diagram of hybrid position/force control approach used in this work is shown in Figure 6.4; accordingly, the main idea is to separate the position control from force control and to combine the achieved data. While the angular position of the mechanism (q) is gathered from an encoder and compared to the reference position signal in order to measure the position error, the joint acceleration of the mechanism $(\ddot{q}_{flex})$ is used for estimating the external force applied to the tip of the mechanism according to the technique explained in Section 6.1. The estimated external force is used in the following control law:

$$\Delta(t) = \int_0^{\Psi} \hat{f}_{ext}\, \Theta\, d\psi \tag{6-7}$$

where f_{ext} is the estimation of the external is applied force to the tip of the mechanism, Θ is a positive constant with value of $5\ \frac{deg}{N.t}$. In fact, $\Delta(t)$ is used to change the reference position based

on the direction and the magnitude of the external force applied to the tip of the flexible mechanism. The value of Θ can be chosen arbitrarily based on the desired performance.

If $\Delta(t)$ is equal to zero, the control loop in Figure 6.4 acts as tracking joint position control based on PID controller. Other types of position controller can be used as well [97]. If $\Delta(t)$ is either positive or negative, the joint reference position is altered in order to regulate to zero the contact force.

For example, by applying a $1\,N$ force for $2\,sec$ to the tip of the mechanism along the tangential direction of the first link motion, the mechanism should be moved by $10\,deg$ from its initial configuration in the same direction of the force.

6.4 Results

In this section, the results of the application of the hybrid position/force control approach to the L-shape flexible mechanism in 3D environment are presented. Hence, a force signal with pulse width of $1\,sec$ and amplitude of $-2\,N$, shown in Figure 6.3, is applied to the tip of the mechanism; meanwhile, the initial angular position reference is set to $90\,deg$.

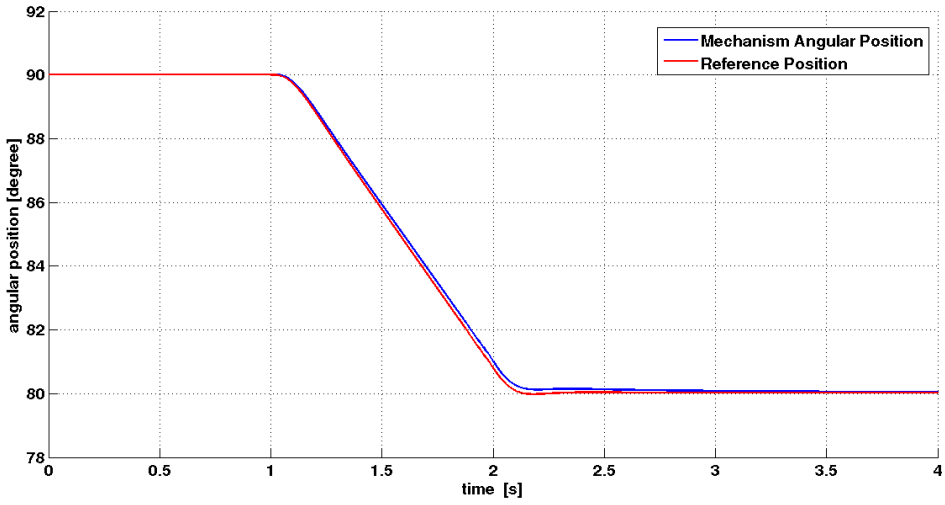

Fig 6.5: The response of the flexible mechanism to applied external force in terms of angular position

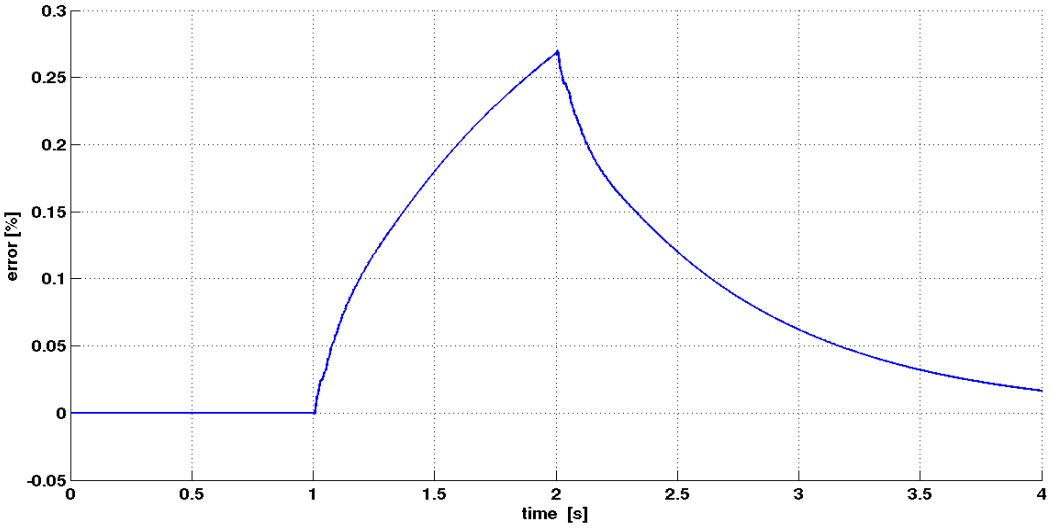

Fig 6.6: Percentage error on difference between mechanism angular position and reference position

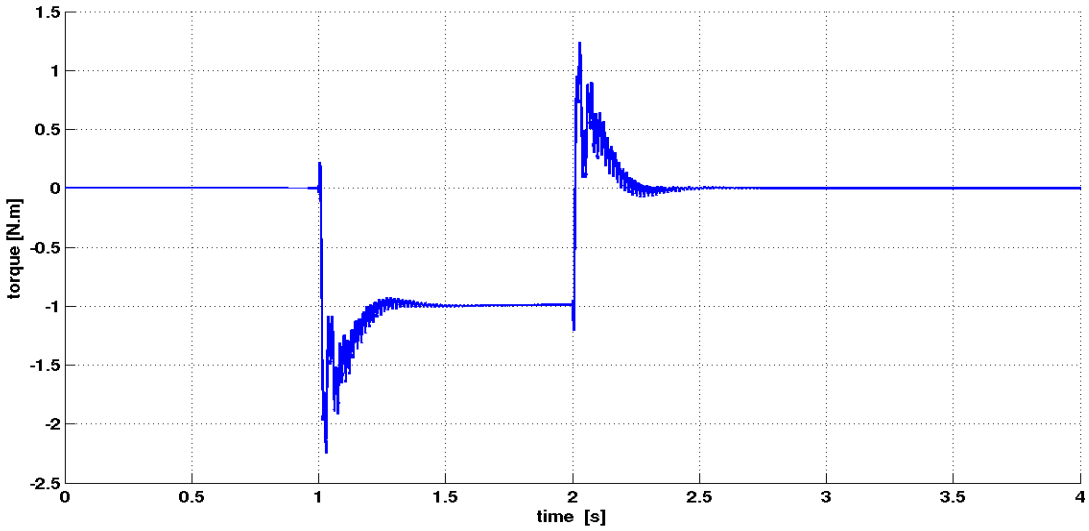

Fig 6.7: Torque profile

As it can be seen from Figure 6.5, the mechanism starts to move in the same direction of the external force as soon as the latter is applied. The angular displacement of the mechanism is equal to 10 deg; in other words, the mechanism moves from its initial configuration (90 deg) to the configuration of 80 deg such displacement is determined by the control law in Equation 6-7. As it can be seen from Figure 6.6, the control-loop has a fast response with a highly accurate

tracking behavior. From Figure 6.6, it can be inferred that the position controller has a good accuracy in terms of trajectory tracking and the error between the actual joint position and the reference position is very small.

Furthermore, according to from Figure 6.7, the overall torque produced by electric motor always within the $\pm 2.5\ N$ range.

6.5 Conclusion

In this chapter, in order to implement the hybrid position/force control, an external force estimation approach has been presented. The estimation technique is based on the comparison between the actual joint acceleration and the joint acceleration computed through a simplified rigid model.

The control scheme is composed by two loops: one performs the angular position tracking, while the other is responsible for the indirect regulation of the interaction forces between the tip of the mechanism and the environment. Hence the reference position, fed to the position controller, can be changed according to a control law which depends on the direction and the amplitude of the external force. The controller demonstrates good trajectory tracking performance and an accurate external force regulation.

CHAPTER 7

Linear Quadratic Optimal Control of Cable-Driven Parallel Robots

7.1 Cable Robots

Cable-driven parallel robots are a special type of parallel robots with adjustable actuated cables, and an end-effector. These robots can be made lighter, stiffer, safer, and more economical than traditional serial manipulators since their structure consists of lightweight and high load-bearing cables. Very large workspace and high acceleration due to less mass and inertia are some advantages of such robots. however inaccuracy and necessity of cables to be kept in tension can be considered as disadvantages [98]. Therefore, modeling, workspace analysis, and design of cable robots are different from parallel manipulators. Cable driven robots have been used in many applications such SkyCam [99], rehabilitation [100], and high speed manipulation [101].

In the dynamic modelling of cable driven robots, it should be considered that a quite dynamic model for cable driven robots is very complicated task. Additionally, because the extracted model shall be used in controller design, moreover make simplifications are required. Hence, in practice attitude, it is proposed to only include the dominant effects in the dynamic analysis. For this reason in many robotic applications, cable mass is ignored and cable is considered as a rigid element [103], [104]. Regarding to these assumptions the dynamics of cable driven robot is reduced and summarized to the end-effector dynamics.

Cables are usually flexible and show elongation under tension. This flexibility may lead to position and orientation errors. Moreover, the system may encounter unavoidable vibrations which may cause uncontrollability of the robot. Cable induced vibration may be a major concern for applications which require high bandwidth or high stiffness [104]

The aim of this chapter is to design a linear quadratic optimal controller for a planar cable-driven parallel robot. The statics modelling of the system is presented and the dynamics equations are obtained in terms of state space equation form. From the control point of view, an optimal controller is designed and applied by defining a performance index which accounts for the position and velocity of the end-effector as well as applied torques by electric motors during the trajectory tracking.

7.2 Dynamics of the System

The Feriba-3 is a 3-DOF planar robot with 4 cables and a circular end-effector. Each cable is fixed to the lateral side of the end-effector which is able to wind around it. The other end of the cable is wound around a pulley, which is directly connected to a motor shaft. A sheet of glass is fixed on the base and a flux of compressed air is blown towards the glass through a series of little holes drilled in the lower side of the end-effector to eliminate end-effector friction. The radius of the pulleys are same as end-effector, which makes easier solution for the kinematics of the robot. The kinematics and stability of the system has been discussed in [105]. Figure 7.1 illustrates the robot built in the laboratory.

The static equilibrium of a $n-DOF$ cable driven robot, manipulated by m cables, can be expressed by the following linear equation system:

$$ST = F \tag{7-1}$$

where $S \in \mathbb{R}^{n\times m}$ is the structure matrix of the robot which is related to the geometrical configuration of the system, $T \in \mathbb{R}^{\mathrm{m}}$ is cable tension vector, and $F \in \mathbb{R}^{n}$ is the wrench acting on the end-effector. In force-closure workspace, vector T can be calculated as sum of a particular (T_p) and kernel solution (T_k).

$$T = T_p + T_k = T_p + N\lambda(T_{min}) \tag{7-2}$$

where $N \in \mathbb{R}^{m\times(m-n)}$ is a basis of structure matrix kernel; $\lambda \in \mathbb{R}^{m-n}$ is the weights of the linear combination of columns of N yielding T_k. By changing T_{min} based on system constraints, a proper vector of T can be calculated.

In the case of four cable-driven robot with 3 degrees of freedom, the following results can be obtained:

$$\mathrm{S} = \begin{bmatrix} \cos\eta_1 & \cos\eta_2 & \cos\eta_3 & \cos\eta_4 \\ \sin\eta_1 & \sin\eta_2 & \sin\eta_3 & \sin\eta_4 \\ r & -r & r & -r \end{bmatrix} \tag{7-3}$$

$$T = \begin{bmatrix} T_1 \\ T_2 \\ T_3 \\ T_4 \end{bmatrix} \tag{7-4}$$

$$F = \begin{bmatrix} F_x \\ F_y \\ M \end{bmatrix} \tag{7-5}$$

where r is the end-effector and pulleys radius. The directional and rotational frictions are ignored due to very low quantities. In order to apply linear quadratic optimal control, the standard mathematical form of the system in terms of state space formulation is developed which is a set of 6 coupled first-order ordinary differential equations.

$$\begin{bmatrix}\dot{q}_1\\ \dot{q}_2\\ \dot{q}_3\\ \dot{q}_4\\ \dot{q}_5\\ \dot{q}_6\end{bmatrix} = \begin{bmatrix}0&0&0&1&0&0\\ 0&0&0&0&1&0\\ 0&0&0&0&0&1\\ 0&0&0&0&0&0\\ 0&0&0&0&0&0\\ 0&0&0&0&0&0\end{bmatrix}\begin{bmatrix}q_1\\ q_2\\ q_3\\ q_4\\ q_5\\ q_6\end{bmatrix} + \begin{bmatrix}0&0&0&0&0&0\\ 0&0&0&0&0&0\\ 0&0&0&0&0&0\\ 0&0&0&\frac{1}{m}&0&0\\ 0&0&0&0&\frac{1}{m}&0\\ 0&0&0&0&0&\frac{1}{I}\end{bmatrix}\begin{bmatrix}0\\ 0\\ 0\\ F_x\\ F_y\\ M\end{bmatrix} \tag{7-6}$$

Fig 7.1: Feriba-3 overall view (a), and manipulability analysis [105] (b)

where m, and I are the end-effector mass, and moment of inertia respectively. $q_1, .., q_6$ are states variables of the system. In our system the values of r, m and I are equal to $3 \times 10^{-2}\ m$, $0.1\ Kg$ and $4.5 \times 10^{-5}\ Kg.m^2$ respectively.

7.3 Synthesis of the Optimal Controller

In this section a very brief explanation of the optimal linear quadratic regulator (LQR) is given (see [106] for more details). The dynamic model of the system, obtained from Equation 7-6, brings on the following state-space form for the system under study:

$$\begin{cases}\dot{q}(t) = Aq(t) + BT(t)\\ \quad y(t) = Cq(t)\end{cases} \tag{7-7}$$

The input vector $T(t) = [T_1 T_2 T_3 T_4]^T$ contains the torques produced by four electrical motor shafts. The system state vector q can be specified as:

$$q^T = [p_x p_y\ \theta\ v_x v_y\ \omega] \tag{7-8}$$

Where p_x , p_y , v_x and v_y are linear positions and velocities of the end effector in x and y directions, θ and ω are the angular position and angular velocity of the end effector respectively; hence, the actual size of the system state variable is six. Due to reason of the brevity, the dependence from the time has been removed. The output vector y is considered to be a full state vector due to implementation of the experimental tests. In other words, the matrix C is took into account as an identity matrix.

The controller design is based on optimal linear quadratic regulator (LQR) for the modelled system stands on the state-space form presented by Equation 7-6. The aim is to determine $T(t)$ as the control function in order to minimize the performance index J , which is the integral of a quadratic function of the system output variables $y(t)$ and control function $f(t)$. The performance index is described as follows:

$$J = \int_0^\infty [y^T(t)Qy(t) + T^T(t)LT(t)]dt = \int_0^\infty [q^T(t)C^T Qq(t) + T^T(t)LT(t)]dt \tag{7-9}$$

Q and L are weighting matrices related to the system output and to the control input respectively. The index takes both the tracking error of the end effector and the control effort. The first term inside the integral in Equation 7-10, minimizes the entire values related to the end effector linear and angular positions. The second term reduces the absolute values related to the system inputs which are forces calculated via CTC and applied by electrical motors.

Performance index J is minimized, if the system input is taken to be the result of a linear feedback from the output [58].

$$T(t) = -Ky(t) = -KCq(t) \tag{7-10}$$

where the optimal value of K is obtained by:

$$K = L^{-1}B^T P \tag{7-11}$$

And P is achieved by solving Riccarti's equation:

$$-A^T P - PA + PBL^{-1}B^T P - C^T QC = 0 \tag{7-12}$$

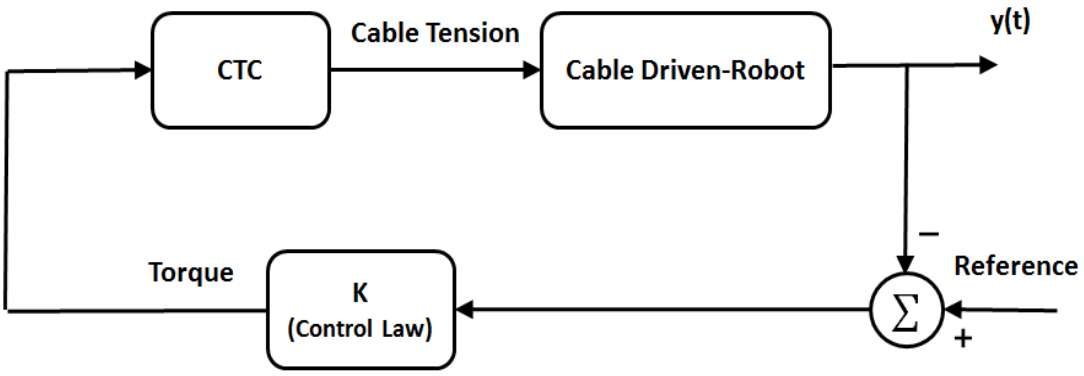

Fig 7.2 The block diagram of the control system

By including the optimal controller, the equations of the system are written as:

$$\begin{cases} \dot{q}(t) = (A - BKC)q(t) \\ y(t) = Cq(t) \end{cases} \tag{7-13}$$

Figure 7.2, shows the block diagram of the designed controller system. The required wrench quantity is calculated based on inverse dynamic equations of the system and controller with respect to reference. The estimated wrench is inserted to CTC (Cable Tension Calculation) block. Regarding to the required wrench on the end-effector, CTC calculates proper cable tensions based on Equation 7-1 and 7-2 to be applied by the actuators (electrical motors). Both linear and angular position and velocity of the end-effector is obtained with respect to data from motors encoders through forward kinematics in a closed loop system.

7.4 Experimental Results

In this section, the results of experimental tests are provided and discussed to show the capabilities of the proposed LQR controller for position and velocity control of Feriba-3 cable robot. The tuning of the LQR controller depends on displacement and velocity along X and Y direction, and also the angular rotation of the end-effector. Our aim is to track the reference trajectory with the least error in displacement and velocity. To this end, we considered the optimal control described in the previous section with following weighting matrices:

$$Q = \begin{bmatrix} q_x & 0 & \cdots & 0 \\ 0 & q_y & & \\ & & q_\theta & \vdots \\ \vdots & & q_{v_x} & \\ & & & q_{v_y} \quad 0 \\ 0 & \cdots & 0 & q_{v_\theta} \end{bmatrix} \tag{7-14}$$

$$L = \begin{bmatrix} l_1 & 0 & 0 \\ 0 & l_2 & 0 \\ 0 & 0 & l_3 \end{bmatrix} \tag{7-15}$$

The size of diagonal matrices Q and L are [6×6] and [3 × 3], respectively. To synthesize the optimal controller, values of the diagonal elements of the matrices Q and L should be selected properly. Parameters q_x , q_y, q_θ correspond to linear and angular positions, while q_{v_x} , q_{v_y}, q_{v_θ} are related to linear and angular velocities.

Two different reference trajectories were designed to test the proposed optimal control algorithm. The first one is a combination of linear and circular trajectory in $x-y$ plane and also a rotation. The end-effector starts from the center of the plane where $(x, y) = (0,0)$, then a motion in x-direction based on an 3^{rd} order time-function polynomial occurs which locates the end-effector in the surroundings of a circle where $(x, y) = (r, 0)$. In the next step, a 360 degree counter clockwise circular motion in $x-y$ plane happens, and the end-effector returns to the former position of $(x, y) = (r, 0)$. Last step of the motion dedicates to another $x-$direction motion based on a 3^{rd} order time-function polynomial to move the end-effector back to the $(x, y) = (0,0)$. In all periods of $x-y$ motion, rotation of end-effector occurs based on a time sinusoidal reference.

The second reference trajectory includes four linear motions in $x-y$ plane, and a sinusoidal function of time as the rotational motion. The $x-y$ linear motions in x and y directions are planned considering a trapezoidal velocity profile. The end-effector starts from the center of the plane and after the designed trajectories returns to the initial position.

For the combination of linear and circular reference trajectory in $x-y$ plane and a sinusoidal rotation, the nonzero elements of the Q and L matrices were selected the following values:

$$q_x\,, q_y = 2.5 \times 10^6 \quad , q_\theta = 1.8 \times 10^3, q_{v_x}\,, q_{v_y} = 1.6 \times 10^3\,, q_{v_\theta} = 3 \tag{7-16}$$

$l_1 = l_2 = l_3 = 1$

On this basic, the matrix of the optimal value of the controller is:

$$K = \begin{bmatrix} 1581.84 & 0 & 0 & 43.77 & 0 & 0 \\ 0 & 1581.4 & 0 & 0 & 43.77 & 0 \\ 0 & 0 & 42.43 & 0 & 0 & 2.07 \end{bmatrix} \quad (7\text{-}17)$$

And for the combination of trapezoidal velocity profiles, the nonzero elements of the Q and L matrices were given as follows:

$$q_x , q_y = 1.6 \times 10^6 \ , q_\theta = 3.9 \times 10^3 , q_{v_x} , q_{v_y} = 1 \times 10^3 \ , \ q_{v_\theta} = 5 \quad (7\text{-}18)$$

$l_1 = l_2 = l_3 = 1$

Therefore, the optimal value of the controller can be written achieved as:

$$K = \begin{bmatrix} 1264.91 & 0 & 0 & 35.40 & 0 & 0 \\ 0 & 1264.91 & 0 & 0 & 35.40 & 0 \\ 0 & 0 & 62.45 & 0 & 0 & 2.62 \end{bmatrix} \quad (7\text{-}19)$$

Figures 7.3 (a-c) show the reference trajectory and also the response of the both closed loop employed LQR controller and the open loop system for just circular part of trajectory in terms of end-effector linear and angular motion. It is clear that the open-loop control system tracks the reference with high errors. According to Figures 7.3 (d-e), the LQR controller made the system tracks the reference efficiently with very low error.

Figures 7.4 (a-c) depict the reference trajectory and the results of the response of the both LQR controller and open loop system for the trapezoidal reference trajectory in terms of end-effector linear and angular motion. Like the former experiment, open loop application presents unsatisfactory results, however employing LQR controller results in outstanding conclusions. The errors of trajectory tracking are very small which is depicted in Figures 7.4 (d-f) as well.

In Figures 7.5 and 7.6, the cable tensions in four cables through circular and trapezoidal trajectories have been shown respectively. The minimum tension in cables was set to $0.5\ N$. The motors have torque of maximum $3.5\ N$. According to these figures, the overall torque applied to control the cable-driven parallel robot for each motor does not exceeds the range of 1.8 N which is much lower than desired limit (3.5 N) for both circular and trapezoidal trajectory.

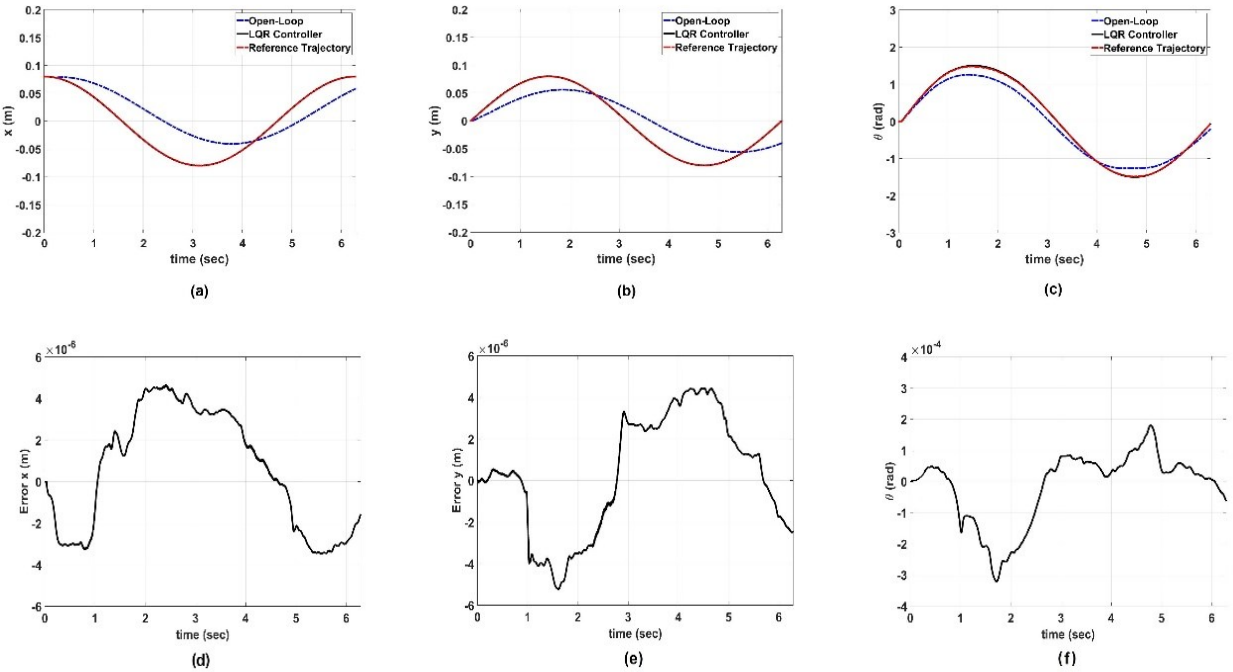

Fig 7.3:Comparison of open loop and LQR methods for position of circular reference trajectory (x-y plane) tracking for x-axis (a), y-axis (b), and sinusoidal rotation $\boldsymbol{\theta}$ (c). Reference tracking error on LQR controller in terms of x-axis (d), y-axis (e) and sinusoidal rotation $\boldsymbol{\theta}$ (f).

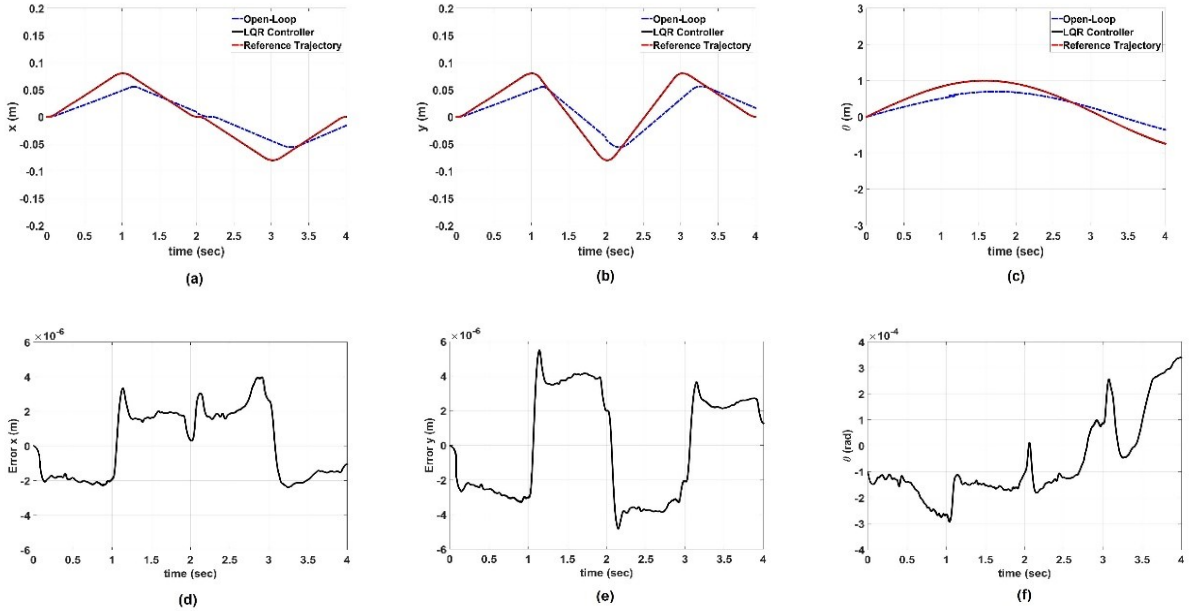

Fig 7.4: Comparison of open loop and LQR methods for trapezoidal reference trajectory for x-axis (a), y-axis (b), and sinusoidal rotation $\boldsymbol{\theta}$ (c). Reference tracking error on LQR controller in terms of x-axis (d), y-axis (e) and sinusoidal rotation $\boldsymbol{\theta}$ (f).

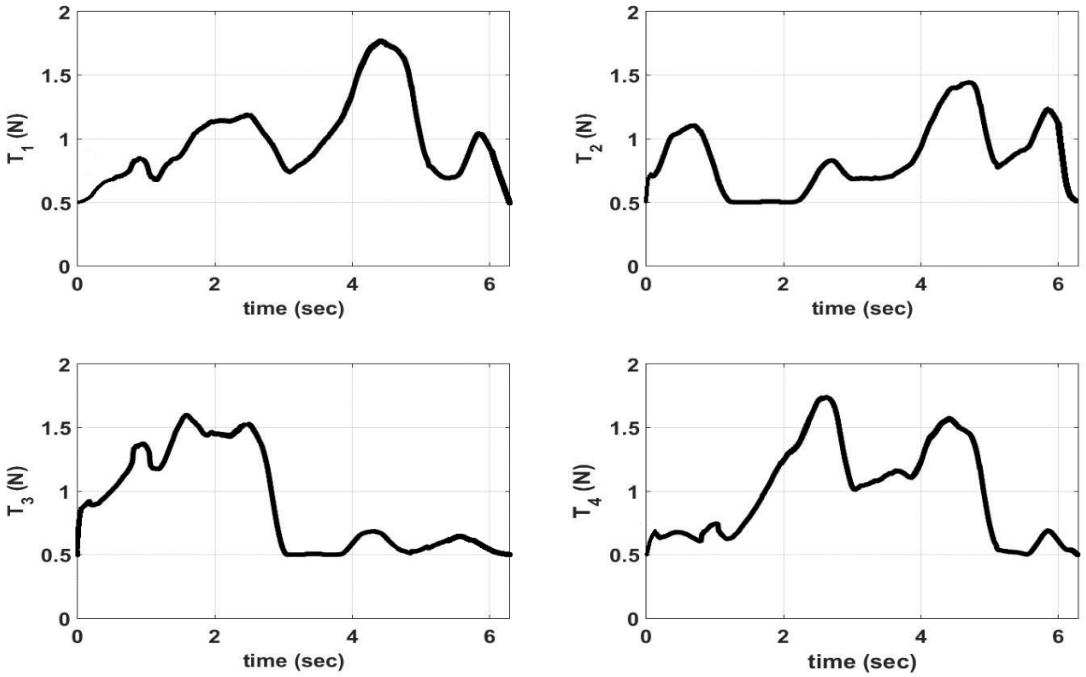

Fig 7.5: Cable tension in four cables for circular reference trajectory (x-y plane) and sinusoidal rotation

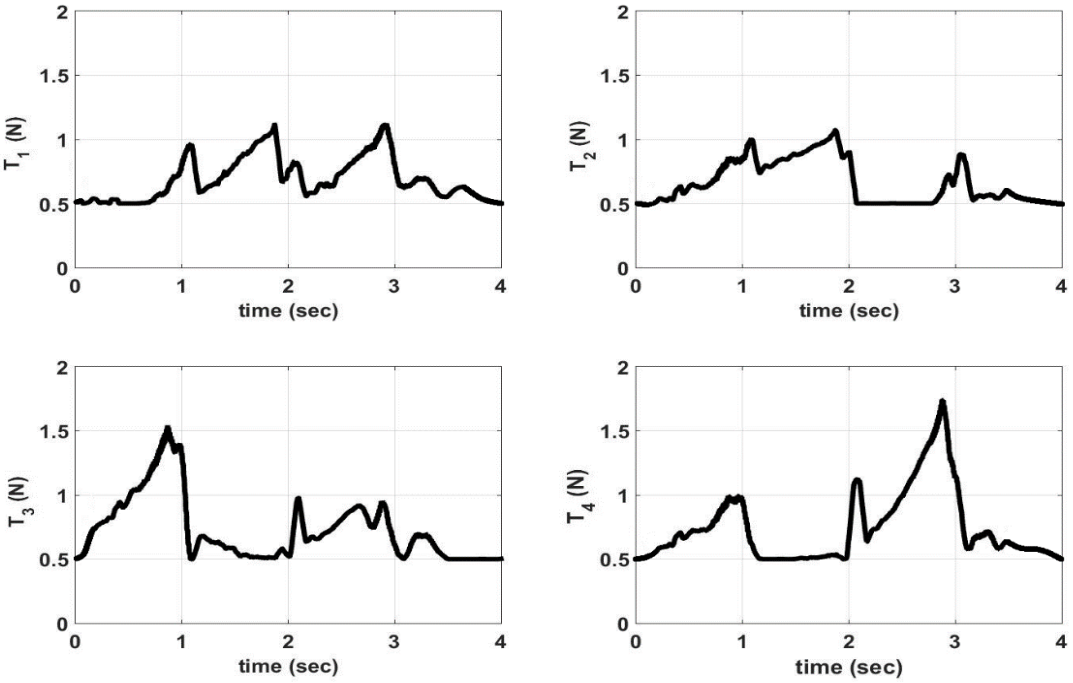

Fig 7.6: Cable tension in four cables for trapezoidal trajectory and sinusoidal rotation

7.5 Conclusion

In this chapter, an optimal linear quadratic regulator (LQR) for both position and velocity control of a Parallel cable-driven robot has been designed and experimentally tested. The dynamic behaviour of the Parallel cable-driven robot has been modelled and in order to implement the control system, the state equations of the dynamic system have been written.

The application of proposed control leads to minimizing a performance index which takes into consideration both the “tracking error” of the system output variables and the control effort. Riccati’s equations is solved in order to obtain the optimal value of the cable tensions. Appropriate weights have been associated with the most significant elements of the output vector, which are linear and angular positions and velocities of the end-effector.

The optimal controller has been tested both on circular position and trapezoidal velocity trajectories for both linear and angular position. The performance of this control system have been compared to the ones that can be achieved with open loop controller. The results are quite satisfactory and the synthesized LQR proved to be effective both for linear and angular reference position tracking by the desired time. Furthermore, the torques applied on cables are always kept well-below the design limit.

CHAPTER 8

Conclusion

This thesis focuses on modeling and control of flexible mechatronic systems. A spatial flexible L-shape mechanism and a cable driven parallel robot are the systems which are investigated in this thesis.The problem of dynamic modeling and simulation of the flexible mechanism has been approached using a highly accurate nonlinear dynamic model based on finite element model (FEM) and equivalent rigid link system (ERLS). The Feriba-3 which is 3-DOF planar cable robot is chosen for the purpose of dynamic modeling of the cable robot.

The application of an optimal controller, a model predictive controller (MPC), the robust controllers (H_∞ loop shaping and μ-Synthesis), a hybrid position/force control sequentially in order to control the position and reduce the vibrations of the flexible L-shape mechanism and to regulate the external force applied to the mechanism as well has been discussed and described. Moreover, the synthesis of a linear quadratic optimal controller for both position and velocity control of a parallel cable-driven robot has been designed and experimentally tested.

Linear quadratic (LQ) optimal control and model predictive control (MPC) are recognized as the optimal controllers which can guarantee the closed-loop stability. While the linear quadratic (LQ) optimal control optimize a true performance index of the closed-loop control system, MPC controllers explicitly takes into account constraints on the parameters in the system, which is an important feature in many industrial processes. Although the archived result from the both controllers are satisfactory and illustrate fast and accurate response of free coordinate and also the reduction of the amplitude of the mechanism vibrations, the MPC can provide stability and robust stability during the robot motion as the additional pros with respect to LQ. The applied torque by the motor(s) is always kept below the maximum limit with use of the both controllers.

Robust control deals with uncertainty in its method to controller design. Controllers designed using robust control methods tend to be able to overcome with differences between the true system and the nominal model used for design. Both robust controllers were robust with respect to a range of uncertain parameters and will guarantee the blondeness of the position-tracking error in present of the disturbance. The question of which robust control method to choose for the flexible mechanism is difficult to answer analytically, but the following guideline is suggested. While the μ-Synthesis controller guarantees robust performance of the system in wider frequency range, employing H_∞ loop shaping for complaint mechanisms results in higher controller effort and more precise tracking.

The purpose of the hybrid position/force control is for some complex application of robot manipulators. It is often necessary to not only control the position of the manipulator but also regulate the force exerted by the end effector on an object. While it has been generally recognized that force control may cause unstable behaviour during contact with environment, the stability of hybrid position/force control can be pre-investigated in order to avoid instability in control parts with different situations.

The summary of application of different controllers to flexible mechatronic systems is reported in Table 8.1.

Table 8.1 – Summary of different controllers' application to flexible mechatronic systems

CONTROLLER	MAIN PURPOSE	MAIN ADVANTAGE
LQR	Position control and vibration reduction	Good performance in position control and vibration reduction
MPC	Position control and vibration reduction	Good performance in position control and vibration reduction Stability and robust stability during motion
μ-synthesis	Dealing with uncertainty in the system	Guarantees robust performance of the system in the wider frequency range
H_∞ loop shaping	Dealing with uncertainty in the system	Precise trajectory tracking
Hybrid Position/Force control	Regulating the external force	System stability can be pre-investigated

Future development of this work could include:

- Designing and development of a real-time dynamic simulator for a complex 3D multi-body flexible mechanisms with taking into account some parametric mismatches, nonlinearities, noise, gravity force effect, etc. to simulation model.

- Applying some feedback control strategies on the bench-mark mechanism in order to position control, vibration reduction along the flexible links and regulation of external forces applied on the links during the mechanism manoeuvre and validating the results from real-time simulator through experimental tests.

BIBLIOGRAPHY

[1] C.-H. Lee, M.-Y. Yang, C.-W. Oh, T.-W. Gim, and J.-Y. Ha, "An integrated prediction model including the cutting process for virtual product development of machine tools," *Int. J. Mach. Tools Manuf.*, vol. 90, pp. 29–43, 2015.

[2] M. Cortese, M. Cempini, P. R. de Almeida Ribeiro, S. R. Soekadar, M. Carrozza, and N. Vitiello, "A mechatronic system for robot-mediated hand telerehabilitation," 2014.

[3] G. Schitter, "Advanced Mechatronics for Precision Engineering and Mechatronic Imaging Systems," in *Mathematical Modelling*, 2015, vol. 8, no. 1, pp. 942–943.

[4] T. Brezina, J. Vetiska, Z. Hadas, and L. Brezina, "Simulation Modelling and Control of Mechatronic Systems with Flexible Parts," in *Mechatronics SE - 69*, R. Jabloński and T. Březina, Eds. Springer Berlin Heidelberg, 2012, pp. 569–578.

[5] R. Vidoni, A. Gasparetto, and M. Giovagnoni, "Design and implementation of an ERLS-based 3-D dynamic formulation for flexible-link robots," *Robot. Comput. Integr. Manuf.*, vol. 29, no. 2, pp. 273–282, Apr. 2013.

[6] O. Tokhi and A. K. M. Azad, *Flexible Robot Manipulators: Modelling, Simulation and Control*. Institution of Engineering and Technology, 2008.

[7] J. Paik, "Soft Robotics: Transferring Theory to Application,' Soft Components for Soft Robots,'" Springer, 2015.

[8] S. K. Dwivedy and P. Eberhard, "Dynamic analysis of flexible manipulators, a literature review," *Mech. Mach. Theory*, vol. 41, no. 7, pp. 749–777, Jul. 2006.

[9] A. De Luca, "Flexible Robots," 2014.

[10] O. A. Bauchau, *Flexible Multibody Dynamics*. Springer, 2010.

[11] F. Xu, J. Hu, X. Wang, and G. Jiang, "Helix Cable-Detecting Robot for Cable-Stayed Bridge: Design and Analysis," *Int. J. Robot. Autom.*, vol. 29, no. 4, 2014.

[12] Y. Su, Y. Qiu, and P. Liu, "The continuity and real-time performance of the cable tension determining for a suspend cable-driven parallel camera robot," *Adv. Robot.*, no. ahead-of-print, pp. 1–10, 2015.

[13] H. C. Liaw and B. Shirinzadeh, "Robust adaptive constrained motion tracking control of piezo-actuated flexure-based mechanisms for micro/nano manipulation," *Ind. Electron. IEEE Trans.*, vol. 58, no. 4, pp. 1406–1415, 2011.

[14] N. J. Cowan, K. Goldberg, G. S. Chirikjian, G. Fichtinger, R. Alterovitz, K. B. Reed, V. Kallem, W. Park, S. Misra, and A. M. Okamura, "Robotic needle steering: Design, modeling, planning, and image guidance," in *Surgical Robotics*, Springer, 2011, pp. 557–582.

[15] I. Barkana and J. Z. Ben-Asher, "Simple adaptive control applications to large flexible structures," *J. Guid. Control. Dyn.*, vol. 34, no. 6, pp. 1929–1932, 2011.

[16] J. G. De Jalon and E. Bayo, *Kinematic and dynamic simulation of multibody systems: the real-time challenge*. Springer Science & Business Media, 2012.

[17] M. Benosman, F. Boyer, G. Le Vey, and D. Primault, "Flexible links manipulators: from modelling to control," *J. Intell. Robot. Syst.*, vol. 34, no. 4, pp. 381–414, 2002.

[18] T. M. Wasfy and A. K. Noor, "Computational strategies for flexible multibody systems,"

Appl. Mech. Rev., vol. 56, no. 6, pp. 553–613, Nov. 2003.

[19] L. Meirovitch, "Analytical methods in vibration," *New York, NY. Mcmillan Co.*, vol. 19, 1967.

[20] J.-S. Chen and C.-H. Menq, "Experiments on the payload-adaptation of a flexible one-link manipulation with unknown payload," *Robotics and Automation, 1990. Proceedings., 1990 IEEE International Conference on*. pp. 1614–1619 vol.3, 1990.

[21] K. Cho, N. Hori, and J. Angeles, "On the controllability and observability of flexible beams under rigid-body motion," in *Industrial Electronics, Control and Instrumentation, 1991. Proceedings. IECON'91., 1991 International Conference on*, 1991, pp. 455–460.

[22] M. Saad, J.-C. Piedboeuf, O. Akhrif, and L. Saydy, "Modal analysis of assumed-mode models of a flexible slewing beam," *Int. J. Model. Identif. Control*, vol. 1, no. 4, pp. 325–337, 2006.

[23] G. Naganathan and A. H. Soni, "Nonlinear Modeling of Kinematic and Flexibility Effects in Manipulator Design," *J. Mech. Des.*, vol. 110, no. 3, pp. 243–254, Sep. 1988.

[24] S. Nagarajan and D. A. Turcic, "Lagrangian Formulation of the Equations of Motion for Elastic Mechanisms With Mutual Dependence Between Rigid Body and Elastic Motions: Part I—Element Level Equations," *J. Dyn. Syst. Meas. Control*, vol. 112, no. 2, pp. 203–214, Jun. 1990.

[25] P. Kalra and A. M. Sharan, "Accurate modelling of flexible manipulators using finite element analysis," *Mech. Mach. Theory*, vol. 26, no. 3, pp. 299–313, 1991.

[26] S. S. Ge, T. H. Lee, and G. Zhu, "A nonlinear feedback controller for a single-link flexible manipulator based on a finite element model.," *J. F. Robot.*, vol. 14, no. 3, pp. 165–178, 1997.

[27] J. M. Martins, Z. Mohamed, M. O. Tokhi, J. Sa da Costa, and M. A. Botto, "Approaches for dynamic modelling of flexible manipulator systems," *Control Theory and Applications, IEE Proceedings* -, vol. 150, no. 4. pp. 401–411, 2003.

[28] A. A. Shabana, *Dynamics of multibody systems*. Cambridge university press, 2013.

[29] M. Moallem, "Control and Design of Flexible-Link Manipulators." Concordia University, 1996.

[30] M. W. Spong, "Underactuated mechanical systems," in *Control problems in robotics and automation*, Springer, 1998, pp. 135–150.

[31] B. Siciliano, L. Sciavicco, L. Villani, and G. Oriolo, *Modellistica, Pianificazione E Controllo*. THE MCGRAW-HILL, 2008.

[32] B. Siciliano and O. Khatib, *Springer handbook of robotics*. Springer Science & Business Media, 2008.

[33] M. Benosman and G. Le Vey, "Control of flexible manipulators: A survey," *Robotica*, vol. 22, no. 05, pp. 533–545, 2004.

[34] A. De Luca, L. Lanari, and G. Ulivi, "End-effector trajectory tracking in flexible arms: Comparison of approaches based on regulation theory," in *Advanced Robot Control*, Springer, 1991, pp. 190–206.

[35] A. De Luca and B. Siciliano, “Regulation of flexible arms under gravity,” *Robot. Autom. IEEE Trans.*, vol. 9, no. 4, pp. 463–467, 1993.

[36] J. H. Yang, F. L. Lian, and L. C. Fu, “Nonlinear adaptive control for flexible-link manipulators,” *Robot. Autom. IEEE Trans.*, vol. 13, no. 1, pp. 140–148, 1997.

[37] M. Isogai, F. Arai, and T. Fukuda, “Modeling and vibration control with neural network for flexible multi-link structures,” in *Robotics and Automation, 1999. Proceedings. 1999 IEEE International Conference on*, 1999, vol. 2, pp. 1096–1101.

[38] D. E. Torfs, R. Vuerinckx, J. Swevers, and J. Schoukens, “Comparison of two feedforward design methods aiming at accurate trajectory tracking of the end point of a flexible robot arm,” *Control Syst. Technol. IEEE Trans.*, vol. 6, no. 1, pp. 2–14, 1998.

[39] F. C. K. Cheung, E. H. K. Fung, and T. P. Leung, “A two-switching surface variable structure control scheme for a flexible manipulator,” *American Control Conference, Proceedings of the 1995*, vol. 1. pp. 830–836 vol.1, 1995.

[40] R. Caracciolo, D. Richiedei, A. Trevisani, and V. Zanotto, “Robust mixed-norm position and vibration control of flexible link mechanisms,” *Mechatronics*, vol. 15, no. 7, pp. 767–791, Sep. 2005.

[41] L. Zhang and J. Liu, “Optimal trajectory control of flexible two-link manipulator based on PDE model,” in *Decision and Control (CDC), 2012 IEEE 51st Annual Conference on*, 2012, pp. 4406–4411.

[42] S. J. Qin and T. A. Badgwell, “A survey of industrial model predictive control technology,” *Control Eng. Pract.*, vol. 11, no. 7, pp. 733–764, 2003.

[43] X. Chen, Q. Li, and S. Fei, “Constrained model predictive control in ball mill grinding process,” *Powder Technol.*, vol. 186, no. 1, pp. 31–39, 2008.

[44] T. Perez and G. C. Goodwin, “Constrained predictive control of ship fin stabilizers to prevent dynamic stall,” *Control Eng. Pract.*, vol. 16, no. 4, pp. 482–494, 2008.

[45] L. G. Bleris, P. D. Vouzis, M. G. Arnold, and M. V Kothare, “A co-processor FPGA platform for the implementation of real-time model predictive control,” in *American Control Conference, 2006*, 2006, p. 6–pp.

[46] M. Morari, M. Baotic, and F. Borrelli, “Hybrid systems modeling and control,” *Eur. J. Control*, vol. 9, no. 2, pp. 177–189, 2003.

[47] N. P. W. B. DUNBAR and R. FRANZ, “Online control customization via optimization, based control,” *Software-Enabled Control Inf. Technol. Dyn. Syst.*, p. 149, 2003.

[48] K. Zmeu and E. Shipitko, “Predictive controller design with offline model learning for flexible beam control,” in *Physics and Control, 2005. Proceedings. 2005 International Conference*, 2005, pp. 345–350.

[49] M. Hassan, R. Dubay, C. Li, and R. Wang, “Active vibration control of a flexible one-link manipulator using a multivariable predictive controller,” *Mechatronics*, vol. 17, no. 6, pp. 311–323, 2007.

[50] L. Bossi, C. Rottenbacher, G. Mimmi, and L. Magni, “Multivariable predictive control for vibrating structures: An application,” *Control Eng. Pract.*, vol. 19, no. 10, pp. 1087–1098, 2011.

[51] X. ZHANG, C. SHAO, S. LI, D. XU, and A. G. ERDMAN, "ROBUST H∞VIBRATION CONTROL FOR FLEXIBLE LINKAGE MECHANISM SYSTEMS WITH PIEZOELECTRIC SENSORS AND ACTUATORS," *J. Sound Vib.*, vol. 243, no. 1, pp. 145–155, May 2001.

[52] C. Trautman and D. Wang, "Experimental H∞ control of a single flexible link with a shoulder joint," *Robotics and Automation, 1995. Proceedings., 1995 IEEE International Conference on*, vol. 1. pp. 1235–1241 vol.1, 1995.

[53] M. Karkoub and K. Tamma, "Modelling and μ-synthesis control of flexible manipulators," *Comput. Struct.*, vol. 79, no. 5, pp. 543–551, Feb. 2001.

[54] P. Li, L. Cheng, Y. Y. Li, and N. Chen, "Robust control of a vibrating plate using μ-synthesis approach," *Thin-Walled Struct.*, vol. 41, no. 11, pp. 973–986, Nov. 2003.

[55] R. J. Theodore and A. Ghosal, "Robust control of multilink flexible manipulators," *Mech. Mach. Theory*, vol. 38, no. 4, pp. 367–377, Apr. 2003.

[56] Y. Li, G. Liu, T. Hong, and K. Liu, "Robust control of a two-link flexible manipulator with neural networks based quasi-static deflection compensation," *American Control Conference, 2003. Proceedings of the 2003*, vol. 6. pp. 5258–5263 vol.6, 2003.

[57] R. Vidoni, A. Gasparetto, and M. Giovagnoni, "A method for modeling three-dimensional flexible mechanisms based on an equivalent rigid-link system," *J. Vib. Control* , vol. 20 , no. 4 , pp. 483–500, Mar. 2014.

[58] E. Barjuei, P. Boscariol, A. Gasparetto, M. Giovagnoni, and R. Vidoni, "Control Design for 3D Flexible Link Mechanisms Using Linearized Models," in *Advances on Theory and Practice of Robots and Manipulators SE - 21*, vol. 22, M. Ceccarelli and V. A. Glazunov, Eds. Springer International Publishing, 2014, pp. 181–188.

[59] P. Boscariol, A. Gasparetto, and R. Vidoni, "Planning continuous-jerk trajectories for industrial manipulators," in *ASME 2012 11th Biennial Conference on Engineering Systems Design and Analysis*, 2012, pp. 127–136.

[60] P. Boscariol and A. Gasparetto, "Model-based Trajectory Planning for Flexible-link Mechanisms with Bounded Jerk," *Robot. Comput. Manuf.*, vol. 29, no. 4, pp. 90–99, Aug. 2013.

[61] P. Boscariol and V. Zanotto, "Design of a controller for trajectory tracking for compliant mechanisms with effective vibration suppression," *Robotica*, vol. 30, no. 01, pp. 15–29, 2012.

[62] M. T. Mason, "Compliance and force control for computer controlled manipulators," *Syst. Man Cybern. IEEE Trans.*, vol. 11, no. 6, pp. 418–432, 1981.

[63] T. Fukuda, "Flexibility control of elastic robotic arms," *J. Robot. Syst.*, vol. 2, pp. 73–88, 1985.

[64] B. C. Chiou and M. Shahinpoor, "Dynamic stability analysis of a one-link force-controlled flexible manipulator," *J. Robot. Syst.*, vol. 5, no. 5, pp. 443–451, 1988.

[65] F. Matsuno and K. Yamamoto, "Dynamic hybrid position/force control of a flexible manipulator," in *Robotics and Automation, 1993. Proceedings., 1993 IEEE International Conference on*, 1993, pp. 462–467.

[66] M. Svinin M and M. Uchiyama, “Contribution to inverse kinematics of flexible robot arms,” *JSME Int. journal. Ser. C, Dyn. Control. Robot. Des. Manuf.*, vol. 37, no. 4, pp. 755–764, 1994.

[67] I. Payo, V. Feliu, and O. D. Cortázar, “Force control of a very lightweight single-link flexible arm based on coupling torque feedback,” *Mechatronics*, vol. 19, no. 3, pp. 334–347, Apr. 2009.

[68] J. Borowiec and A. Tzes, “Force control for flexible robots using neural networks,” *American Control Conference, 1999. Proceedings of the 1999*, vol. 3. pp. 1950–1954 vol.3, 1999.

[69] L.-Y. Liu and H.-C. Lin, “Tip-contact force control of a single-link flexible arm using feedback and parallel compensation approach,” *Robotica*, vol. 31, no. 05, pp. 825–835, 2013.

[70] P. Boscariol, A. Gasparetto, and V. Zanotto, “Model Predictive Control of a Flexible Links Mechanism,” *J. Intell. Robot. Syst.*, vol. 58, no. 2, pp. 125–147, 2010.

[71] M. Giovagnoni, “A Numerical and Experimental Analysis of a Chain of Flexible Bodies,” *J. Dyn. Syst. Meas. Control*, vol. 116, no. 1, pp. 73–80, Mar. 1994.

[72] R. Vidoni, A. Gasparetto, M. Giovagnoni, and P. Boscariol, “A novel 3D equivalent rigid link system approach for flexible-link mechanisms: formulation and comparison with the floating frame of reference approach,” in *Proceedings of the ECCOMAS Thematic Conference on Multibody Dynamics*, 2011, pp. 1–13.

[73] A. Gasparetto, “ACCURATE MODELLING OF A FLEXIBLE-LINK PLANAR MECHANISM BY MEANS OF A LINEARIZED MODEL IN THE STATE-SPACE FORM FOR DESIGN OF A VIBRATION CONTROLLER,” *J. Sound Vib.*, vol. 240, no. 2, pp. 241–262, Feb. 2001.

[74] R. Caracciolo, D. Richiedei, and A. Trevisani, “Design and experimental validation of piecewise-linear state observers for flexible link mechanisms,” *Meccanica*, vol. 41, no. 6, pp. 623–637, 2006.

[75] R. Vinter, *Optimal control*. Springer Science & Business Media, 2010.

[76] “https://www.wikipedia.org/.” .

[77] B. D. O. Anderson and J. B. Moore, *Optimal control: linear quadratic methods*. Courier Corporation, 2007.

[78] J. Richalet, A. Rault, J. L. Testud, and J. Papon, “Model predictive heuristic control: Applications to industrial processes,” *Automatica*, vol. 14, no. 5, pp. 413–428, 1978.

[79] C. R. Cutler and B. L. Ramaker, “Dynamic matrix control?? A computer control algorithm,” in *joint automatic control conference*, 1980, no. 17, p. 72.

[80] J. M. Maciejowski, *Predictive Control: With Constraints*. Prentice Hall, 2002.

[81] N. O. Ghahramani and F. Towhidkhah, “Constrained incremental predictive controller design for a flexible joint robot,” *ISA Trans.*, vol. 48, no. 3, pp. 321–326, Jul. 2009.

[82] D.-W. Gu, P. H. Petkov, and M. M. Konstantinov, “Robust Control of a Flexible-Link Manipulator,” in *Robust Control Design with MATLAB®*, Springer, 2013, pp. 367–399.

[83] K. Glover, “A Tutorial on Hankel-Norm Approximation,” in *From Data to Model SE - 2*, J. Willems, Ed. Springer Berlin Heidelberg, 1989, pp. 26–48.

[84] S. Skogestad and I. Postlethwaite, *Multivariable feedback control: analysis and design*, vol. 2. Wiley New York, 2007.

[85] D. McFarlane and K. Glover, “A loop-shaping design procedure using H∞ synthesis,” *Autom. Control. IEEE Trans.*, vol. 37, no. 6, pp. 759–769, 1992.

[86] K. Glover and D. McFarlane, “Robust stabilization of normalized coprime factor plant descriptions with <e1>H</e1>∞-bounded uncertainty,” *Automatic Control, IEEE Transactions on*, vol. 34, no. 8. pp. 821–830, 1989.

[87] K. Zhou, J. C. Doyle, and K. Glover, *Robust and Optimal Control*. Prentice Hall, 1996.

[88] S. Tøffner-Clausen, P. Andersen, J. Stoustrup, and H. H. Niemann, “A new approach to mu-synthesis for mixed perturbation sets,” in *Proceedings of the 3rd European Control Conference, Roma*, 1995, pp. 147–152.

[89] J. Doyle and A. Packard, “Uncertain Multivariable Systems from a State Space Perspective,” *American Control Conference, 1987*. pp. 2147–2152, 1987.

[90] P. M. Young, M. P. Newlin, and J. C. Doyle, “μ analysis with real parametric uncertainty,” *Decision and Control, 1991., Proceedings of the 30th IEEE Conference on*. pp. 1251–1256 vol.2, 1991.

[91] D.-W. Gu, P. H. Petkov, and M. M. Konstantinov, *Robust Control Design with MATLAB® (Advanced Textbooks in Control and Signal Processing)*. Secaucus, NJ, USA: Springer-Verlag New York, Inc., 2005.

[92] T. Jiang, J. Liu, and W. He, “Boundary control for a flexible manipulator based on infinite dimensional disturbance observer,” *J. Sound Vib.*, vol. 348, pp. 1–14, 2015.

[93] B. Siciliano and L. Villani, *Robot force control*, vol. 540. Springer Science & Business Media, 2012.

[94] K. Richter and F. Pfeiffer, “A flexible link manipulator as a force measuring and controlling unit,” in *Robotics and Automation, 1991. Proceedings., 1991 IEEE International Conference on*, 1991, pp. 1214–1219.

[95] S. D. Eppinger and W. P. Seering, “Three dynamic problems in robot force control,” *Robotics and Automation, IEEE Transactions on*, vol. 8, no. 6. pp. 751–758, 1992.

[96] W. D. Fisher and M. S. Mujtaba, “Hybrid position/force control: a correct formulation,” *Int. J. Rob. Res.*, vol. 11, no. 4, pp. 299–311, 1992.

[97] F.-Y. Hsu and L.-C. Fu, “Intelligent robot deburring using adaptive fuzzy hybrid position/force control,” *Robotics and Automation, IEEE Transactions on*, vol. 16, no. 4. pp. 325–335, 2000.

[98] S. Abdolshah and G. Rosati, “First Experimental Testing of a Dynamic Minimum Tension Control (DMTC) for Cable Driven Parallel Robots,” in *Cable-Driven Parallel Robots SE - 17*, vol. 32, A. Pott and T. Bruckmann, Eds. Springer International Publishing, 2015, pp. 239–248.

[99] L. L. Cone, “SKYCAM-AN AERIAL ROBOTIC CAMERA SYSTEM,” *Byte*, vol. 10, no. 10, p. 122, 1985.

[100] G. Rosati, P. Gallina, and S. Masiero, "Design, Implementation and Clinical Tests of a Wire-Based Robot for Neurorehabilitation," *Neural Systems and Rehabilitation Engineering, IEEE Transactions on*, vol. 15, no. 4. pp. 560–569, 2007.

[101] S. Kawamura, H. Kino, and C. Won, "High-speed manipulation by using parallel wire-driven robots," *Robotica*, vol. 18, no. 01, pp. 13–21, 2000.

[102] J. J. German, K. W. Jablokow, and D. J. Cannon, "The cable array robot: theory and experiment," *Robotics and Automation, 2001. Proceedings 2001 ICRA. IEEE International Conference on*, vol. 3. pp. 2804–2810 vol.3, 2001.

[103] A. B. Alp and S. K. Agrawal, "Cable suspended robots: feedback controllers with positive inputs," *American Control Conference, 2002. Proceedings of the 2002*, vol. 1. pp. 815–820 vol.1, 2002.

[104] X. Diao and O. Ma, "Vibration analysis of cable-driven parallel manipulators," *Multibody Syst. Dyn.*, vol. 21, no. 4, pp. 347–360, 2009.

[105] P. Gallina and G. Rosati, "Manipulability of a planar wire driven haptic device," *Mech. Mach. Theory*, vol. 37, no. 2, pp. 215–228, 2002.

[106] D. E. Kirk, *Optimal Control Theory: An Introduction*. Dover Publications, 2004.